Pulsed Transcranial Ultrasound Stimulation and Its Applications in Treatment of Focal Cerebral Ischemia and Depression

A Thesis

Submitted to the Faculty

of

Drexel University

by

Hangdao Li

in partial fulfillment of the

requirements for the degree

of

Doctor of Philosophy

March 2018

DEDICATIONS

To My Parents

Acknowledgements

I would like to express my gratitude for my advisor, Dr. Peter A. Lewin for everything he has done for me during my stay in Drexel. His long-lasting enthusiasm in research always inspires me and his hands-off but supportive management taught me how to plan and stick to my project effectively. I would also like to thank him for patiently revising my manuscript and teaching me how to write scientifically.

I would like to thank Dr. Shanbao Tong for his guidance throughout my seven years of research in Neural Engineering Lab of Shanghai Jiao Tong University. I cannot imagine completing this journey without his mentoring. He has been not only supporting me with everything I need in my research, but also teaching me how to work and think scientifically. I would also like to thank Dr. Tong for providing me the opportunity to have a wonderful experience in Drexel University on the Dual-PhD program.

I would also like to thank Dr. Junfen Sun for all his help in the pTUS studies. His inspiring suggestion in the experiments and scrupulous revision of the manuscript has contributed substantially to this thesis. I would also like to thank Dr. Shengtian Li and his lab for their cooperation, without which the work presented in chapter 4 might be impossible to be completed in time.

Over this long journey of PhD, I always feel lucky to have the most wonderful and helpful lab-mates anyone could hope for. I want to thank each one of you, especially Dr. Hongyang Lu, Dr. Lin Cheng, and Dr. Qi Liu, etc., for making this seven-year experience a wonderful and unforgettable one. Also thank Xiaoliu Zhang, Daqu Zhang, Wen Jin and Jie Yang for the assistance in the experiments.

Last but not the least, I would like to thank my parents and family. My parents have always been supportive of every decision I made in these years. They gave me the courage to pursue a PhD and let me devote myself to this course without worries from home. I want to thank my sister and adorable niece for making me always feel cared for and loved by my family. Special thanks go to Yue Cao for always standing by my side and understanding me whenever I needed help or comforting. It has been a blessing to have you to share every moment with, no matter it is sweet, exciting, or it is frustrating, stressful during pursuit of the PhD. Thank you and I love you.

Table of Contents

List of Tables

List of Figures

Abstract

Pulsed Transcranial Ultrasound Stimulation and Its Applications in Treatment of Focal Cerebral Ischemia and Depression

Hangdao Li

Advisor: Peter A. Lewin, PhD & Shanbao Tong, PhD

The aims of this thesis were to investigate the therapeutic effects of pulsed transcranial ultrasound stimulation (pTUS) on focal cerebral ischemia and depression, respectively, in rodent models.

Neurological and psychiatric disorders, such as Parkinson's disease, epilepsy, Alzheimer's disease, stroke (vascular disorder that results in neurological defects), depression, and etc., present an increasing challenge and a substantial social and economic burden for an aging and stressed population. However, conventional treatments, especially pharmacologic interventions, have significant limitations, such as nonspecific effects, insufficient tailoring to the individual, adverse effects such as drowsiness, weight gain and nausea, or inadequate uptake into the brain due to the blood-brain-barrier (BBB). In contrast, neuromodulation techniques have gained more attention, which are able to enhance or inhibit the neural activities in specific cortex, such as motor, somatosensory or other areas related to cognition. Neuromodulation thus could potentially restore the disrupted neural network due to neurological disorders. Capitalizing on its noninvasiveness, high precision (in the scale of mm) and penetration depth (several centimeters), low-intensity (typically <1 W/cm^2 spatial-peak-pulse-average intensity-I_{SPTA}) low-frequency (typically <1MHz), pulsed transcranial ultrasound stimulation (pTUS) has been emerging as a promising therapeutic tool for neurological and psychiatric disorders. This thesis provided the first in-vivo demonstrations that pTUS might serve as neuroprotective preconditioning of ischemic brain injury and treatment of depression. Additionally, it also proposed a novel optical imaging-based technique to characterize the neuromodulatory effect of pTUS, which facilitates the parameter optimization of therapeutic pTUS in practice.

Both suppressive and excitatory pTUS are applied in this thesis. The corresponding pTUS parameters were: (a) suppressive pTUS (or $pTUS_S$): I_{SPPA} = 8W/cm^2, frequency (f) = 0.5 MHz, pulse repetition frequency (PRF) = 100 Hz, and duty cycle (DC) =5%, and (b) excitatory pTUS (or $pTUS_E$): I_{SPPA} = 8W/cm^2, f = 0.5MHz, PRF = 1.5 kHz, and DC = 60%, respectively. Before the therapeutic experiments, the neuromodulatory effects of both $pTUS_S$ and $pTUS_E$ were examined using laser speckle imaging(LSCI) and multispectral reflectance imaging (MSRI) in aspect of the neurovascular responses. Specifically, this thesis consists of:

(1) Study on the neurovascular response to pTUS. Compared with other methods, such as pTUS-triggered motor response and visual evoked potentials (VEP), optical imaging allows to measure the neurovascular change at high spatiotemporal resolution (in the scale of μm and ms), including cortical suppression without evoked output. LSCI and MSRI were used to monitor the primary somatosensory response (Chapter 2) to hind limb electrical stimulation before, immediately, and 1 h after 5-min application of $pTUS_S$ and $pTUS_E$, respectively. Several indicators, including *Response Index*, *Peak Response*, *Latency* and *Response Duration*, were derived from optical images to characterize the neuromodulatory effects of pTUS on primary somatosensory cortex. Our results showed that $pTUS_S$ could suppress the primary somatosensory cortex across all rats whereas $pTUS_E$ only presented excitatory effects in 5 out of 11 rats. The neuromodulatory effects of pTUS were correlated with the baseline cortical excitability. The results showed that: (i) pTUSs could serve in investigating cognitive function by silencing the neurons in the target region; (ii) $pTUS_E$ exposure should be treated with caution due to individual differences in neuromodulatory effects, which were associated with the initial brain state of rats; and (iii) optical imaging was useful in evaluating the pTUS neuromodulatory effects.

(2) Neuroprotection of preconditioning pTUS. By applying suppressive pTUS, it was investigated whether the severity of stroke could be minimized or alleviated by prior exposure to ultrasound stimulation (Chapter 3). Preconditioning was supposed to increase the tolerance of brain to subsequent ischemic insult. It can potentially be used to prevent the perioperative stroke in patients undergoing cardiovascular surgeries with a series of complications. Considering the noninvasiveness and safety of ultrasound, pTUS may provide a novel preconditioning method. To test the effectiveness of

preconditioning pTUS, rats were randomly assigned to control (n=12) and preconditioning pTUS (pTUS-PC) groups (n=14). The pTUS-PC animals received ultrasound stimulation before the induction of photothrombotic stroke, whereas control animals were handled identically except the ultrasound stimulation. The cerebral blood flow was monitored using LSCI in both groups during stroke induction, as well as 24 hours and 48 hours after stroke, respectively. Also, infarct volumes and edema were measured at 48 hours after euthanatizing the rats. Results showed that pTUS-PC rats had smaller ischemic volume during stroke induction, as well as 24 hours and 48 hours after the stroke than the controls. Moreover, the pTUS-PC group showed lower volume of brain edema than the control group.

(3) Antidepressant-like effect by pTUS. The potential antidepressant-like effects of pTUS were further investigated in a rat model of depression with excitatory pTUS. Stimulating the left prefrontal cortex (PFC) by TMS has been clinically used for depression treatment, it was thus hypothesize that $pTUS_E$ on PFC would act similarly with TMS and result in antidepressant-like effect. To test this hypothesis, pTUS was applied for 2 weeks daily to the left PFC of depressed rats induced by 48-hour restraint. The long-term (3 weeks) efficacy of the depression model as well as the antidepressant-like effects of pTUS were investigated with a group of behavioral tests. In addition, the hippocampal BDNF was measured by western blot to study the mechanisms underlying antidepressant-like effects of pTUS. The safety of long-term (2 weeks) pTUS was assessed by histologic analysis. Results showed that 48-hour-restraint stress could stably lead to at least 3-week reduction of exploratory behavior and protracted anhedonia, whereas $pTUS_E$ treatment could successfully reverse the depression-like phenotypes and promote the BDNF expression in the left hippocampus. In addition, H& E staining of brain tissues confirmed the safety of the long-term pTUS treatment.

In conclusion, the results in this work suggested that pTUS could serve as preconditioning of perioperative stroke and therapeutics for depression. Additionally, the results also demonstrated that optical neurovascular imaging could measure the neuromodulatory effect of pTUS. This study documented more evidence that pTUS is a promising tool for basic neuroscience and therapeutic applications.

KEY WORDS: Neurological and psychiatric disorders, brain stimulation, pulsed ultrasound stimulation, neurovascular imaging, preconditioning, stroke, depression.

Chapter 1: Introduction

The aims of this thesis were to investigate the therapeutic effects of pulsed transcranial ultrasound stimulation (pTUS) on focal cerebral ischemia and depression, respectively, in rodent models. Additionally, this work also aimed to propose a novel optical imaging-based technique to characterize the neuromodulatory effect of pTUS, which facilitates the parameter optimization of therapeutic pTUS in practice.

1.1 Background and motivation

1.1.1 Neurological and psychiatric disorders

Neurological and psychiatric disorders, such as Parkinson's disease, epilepsy, Alzheimer's disease, stroke (vascular disorder that results in neurological defects), depression, and etc., present an increasing challenge and a substantial social and economic burden for an aging and stressed population [1]. These two types of diseases are often termed together as brain disorders [2] because they are considered to share similar mechanisms [3]. Preclinical and clinical evidence strongly suggested that abnormal development of cerebral neurons and malfunctions of brain circuits significantly contribute to the pathogenesis of various neurological and psychiatric disorders [4]. For example, Parkinson’s disease is characterized by tremor at rest, rigidity, akinesia (or bradykinesia) and postural instability [5]. Its pathological features include degeneration of dopaminergic neurons in the substantia nigra pars compacta coupled with intracytoplasmic inclusions known as Lewy bodies [6]. Similarly, spontaneous motor seizures that occur in mesial temporal lobe epilepsy, which is the most common form of human epilepsy, are a consequence of hyper-excitability of dentate granule cells, resulting from alterations of circuitry due to hippocampal sclerosis [7,8].

Based on the exampled pathogenesis of brain disorders above, ideal therapies should selectively target the specific brain dysfunction with minimal or no adverse effects. However, conventional treatments, especially pharmacologic interventions, have significant limitations, such as nonspecific effects,

insufficient tailoring to the individual, and adverse effects, e.g. drowsiness, weight gain or nausea [9]. In addition, the uptake of drugs into the brain is impeded by the blood-brain-barrier (BBB) [10] as shown in ***Figure 1.1***. Therefore, the effectiveness of drug treatment is limited in many brain diseases [11–13]. Other treatments, such as physical therapy and cognitive-behavioral treatment are also alternatives for neurological and psychiatric disorders [14,15]. However, the efficacy of them depends to a large extent on the expertise of the therapist and the patient's cooperation.

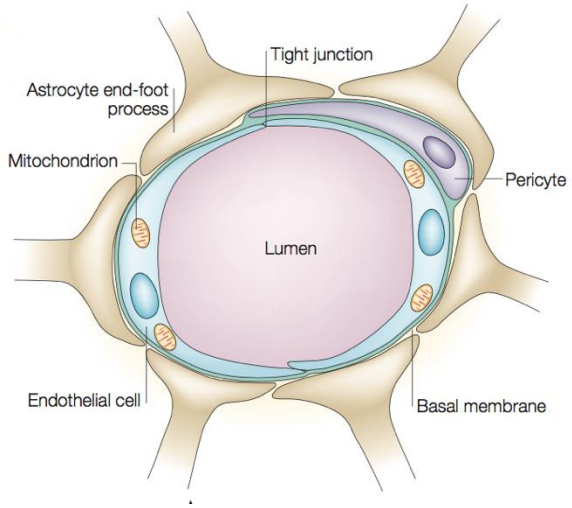

Figure 1.1 Schematic illustration of a brain capillary and the blood–brain barrier (BBB). BBB consists of three cellular elements, including endothelial cells, astrocyte end-feet and pericytes. Brain capillary endothelial cells and pericytes are surrounded by a basal membrane. Tight junctions between the cerebral endothelial cells form a diffusion barrier, which selectively impedes the influx of most compounds from the blood to the brain. This figure is edited based on the figure cited from [10].

1.1.2 Review of neuromodulation techniques

By contrast, neuromodulation techniques have gained more attention as they are able to specifically and selectively enhance or inhibit neural activities such as motor, sensory and cognitive functions, and thus could guide cortical plasticity to restore adaptive equilibrium in a disrupted neural network resulting from neurological disorders [16]. In 1986, Garrett Alexander, along with Mahlon DeLong and Peter Strick

introduced the segregated circuit hypothesis, which suggested that symptoms of many neurological and psychiatric diseases might be associated with dysfunction in specific cortical-basal ganglia brain circuits [17]. Later, DeLong et al. found that Parkinson's disease resulted from excessive activity of the subthalamic nucleus (STN) neurons and inactivation of the STN by lesions improved the parkinsonian motor disturbances [18] (see ***Figure 1.2a&b***). These findings shed lights on understanding of human neural networks, paving the way for brain modulation to be used in neurological and psychiatric disorders.

Soon thereafter, electrical deep brain stimulation (DBS) was introduced as a modulatory approach to the brain circuits in Parkinson's disease when a French neurosurgeon, Alim-Louis Benabid took the courageous step of implanting a wire that input continuous electrical current inside a human brain in 1987 [19] (see ***Figure 1.2c***). And it turned out to be very effective in suppressing tremor. Additionally, it allowed therapists to individualize the settings by programming the stimulation parameters [20].

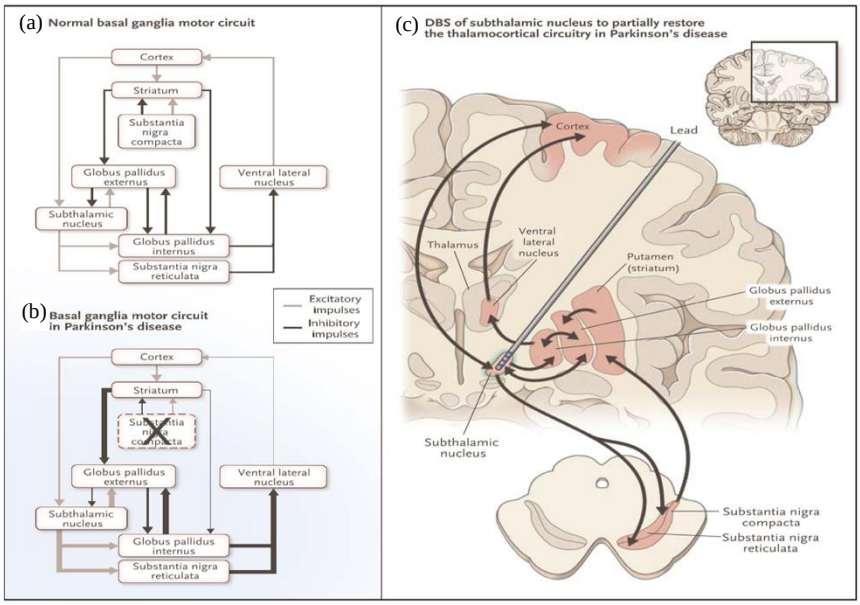

Figure 1.2 The Models Showing Changes of Basal Ganglia Circuitry in Parkinson's Disease and The Deep-Brain Stimulation (DBS) Based on the Models. (a) The group of brain circuits called basal ganglia as they behave in the normal condition. Dark arrows indicate inhibitory activity, and lighter arrows excitatory activity. (b) The changes of circuits as a result of Parkinson's disease. When the substantia nigra degenerates, the physiological output is changed across the entire circuit. There are particular changes in the rate and pattern of cellular activity in the globus pallidus internus and substantia nigra reticulata that lead to inhibition in the thalamus and the cortex. Thicker lines indicate

increase of activity, and thinner lines show the decrease. (c) Basal ganglia circuitry can be altered by DBS in the subthalamic nucleus. Areas referred to in a and b are shaded in red. Electrical stimuli convert the physiology in the box model to restore the output from the thalamus to the cortex, approximating that of normal basal ganglia. This figure is edited from REF. [29].

Since then, DBS has been extensively used to treat essential tremor [21], dystonia [22], epilepsy [23], obsessive-compulsive disorder [24], depression [25], Alzheimer's disease [26] and Tourette's syndrome [27]. However, this technique has several limitations. Current can spread into unintended brain regions, causing side effects. Most commonly, the implantation of electrodes into brain is associated with high risks of complications, such as infections, foreign body reactions and cerebrospinal fluid leak [28,29]. Therefore, DBS therapy is usually the last choice when all other treatments are not applicable or failed. Nevertheless, with the emergence of DBS, we have entered the era of human brain modulation.

Other neuromodulation approaches, such as repetitive transcranial magnetic stimulation (rTMS) and transcranial direct current stimulation (tDCS) are appealing due to their noninvasive nature. In the last two decades, these noninvasive brain stimulation (NIBS) techniques have made remarkable contributions to neuroscience, as well as treatment of neurological and psychiatric disorders [30,31].

The development of repetitive magnetic stimulation could be traced back to 1831, when a series of experiments conducted by Faraday led to the discovery of electromagnetic induction [32]. More than 150 years later, Barker et al. found that the magnetic coil, when placed on the human scalp over the motor cortex, could induce current flow and neural activation in the targeted cortex and elicit movements of the contralateral limbs [33]. Transcranial magnetic stimulation (TMS; ***Figure 1.3a***) induce currents in the brain via the principle of electromagnetic induction [34]. Single pulses of induced current with sufficient magnitude could only depolarize neurons transiently, but when applied repetitively (known as rTMS), they can decrease or increase cortical excitability depending on the parameters of stimulation, even after the stimulation period [35,36].

The concept of noninvasive brain stimulation with the use of weak direct currents dated back to around AD 47 in the application of electric torpedo fish to the affected regions to treat headaches and pain. Then the systematic investigation of tDCS began in the 1960s on animal models [37,38]. Recently, the growing

attention in noninvasive brain stimulation by TMS has revitalized the tDCS technique[39]. In 2000, Nitsche, M.A. et al. reported in their study [40] that tDCS could change the excitability of the human motor cortex. The setup used in this work consisted of a battery-driven stimulator delivering weak (⩽1 mA) currents between a pair of saline-soaked surface sponge electrodes, with one placed on the scalp over the motor cortex and the other over a reference location (***Figure 1.3b***). The results showed that anodal stimulation produced excitation whereas cathodal stimulation induced inhibition.

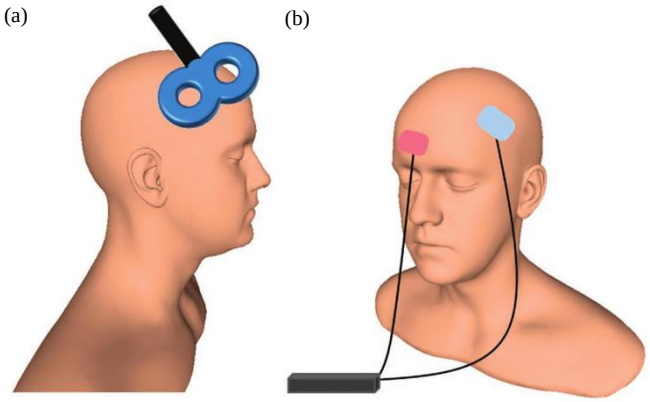

Figure 1.3 Schematics of NIBS setups. (a) A typical figure-eight TMS coil placed on the scalp (over dorsolateral prefrontal cortex here). (b) Bipolar tDCS electrodes, with one over dorsolateral prefrontal cortex and the other one as reference over the contralateral supraorbital region. This figure was edited from REF. [16]

There is growing evidence that support the clinical use of NIBS in various neurological disorders: modulation of epileptic activity in the targeted cortical area (focal epilepsy) [41]; restoration of adaptive equilibrium in a disrupted network, guiding plasticity to improve behavioral outcomes (stroke) [42,43], modulation of functional connectivity both within and between neuronal networks (depression) [44]and suppression of plastic changes associated with chronic pain [45–47]. However, sham-controlled clinical trial evidence is still insufficient to endorse the wide application of these techniques, despite the current encouraging findings [9].

Except for the modalities above, other brain stimulation techniques also exist. For example, surgical invasive neuromodulation techniques that are (pending) on the market include vagus nerve stimulation (VNS) [48][49], implanted electrocortical stimulation (IES) and epidural cortical stimulation (ECS) [50]; other minimally or noninvasive brain stimulation methods include cranial electrotherapy stimulation (CES) [51], and trigeminal nerve stimulation (TNS) [52].

Noninvasive brain stimulation techniques have advantages in safety over the invasive ones such as DBS, whose limitations were discussed in previous sections. However, these techniques also have their limitations. For example, tDCS and rTMS have poor spatial precision. The typical focus of rTMS is several centimeters in diameter, and it cannot target deeper structures unless stimulating more proximal tissue. Additionally, the penetration of TMS is minimal, unless using an H-coil, which has an even larger focus than traditional coils [53]. Therefore, a noninvasive brain stimulation technique that overcomes these limitations would be extremely desired in neuroscience research and treatment of neurological and psychiatric disorders.

1.1.3 Pulsed transcranial ultrasound stimulation (pTUS)

In recent years, low-intensity (typically<1W/cm^2 spatial-peak-temporal-average intensity-I_{SPTA}) low-frequency (typically <1MHz) pulsed transcranial ultrasound stimulation (pTUS) has been emerging as a promising neuromodulation tool and therapeutics for neurological and psychiatric disorders [54,55]. Compared with deep brain stimulation (DBS) [56], pTUS works in a noninvasive and safe way. It also has better precision (in the scale of mm) and penetration depth (several centimeters) than the noninvasive transcranial magnetic stimulation (TMS) [42] or transcranial direct current stimulation (tDCS) [40],.

1.1.3.1 Construction and characterization of pTUS waveforms

Ultrasound acoustic waves generated by mechanical vibrations with acoustic frequency above the normal range of human hearing (20 kHz). Unlike electrical currents or magnetic fields, ultrasound can travel longer distances with minimal loss in soft biological tissues and can be transmitted and focused across solid structures [57]. As shown in ***Figure 1.4***, the pTUS waveforms are produced by an immersion-type ultrasound transducer operating at a low frequency (<1MHz). Two identical function generators are

used to generate pulsed signals or tone bursts. Before activating the transducer, the pulse signals are amplified using a radio frequency (RF) amplifier. Additionally, a custom-designed acoustic collimator made of plexiglass is coupled to the ultrasound source so that the target is confined to the area of interest.

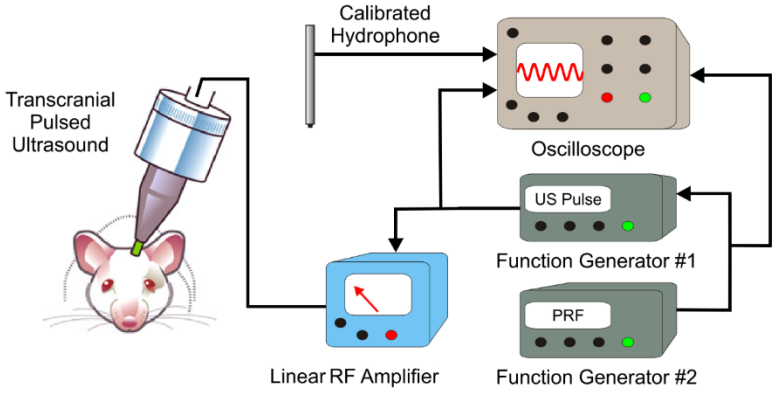

Figure 1.4 Illustration of the pTUS system. This figure was modified from REF. [54]

The ultrasound field distribution is measured using a calibrated hydrophone mounted on the 3D ultrasound intensity measurement system, which consists of a water tank and a three-dimensional motor-driven manipulator stage to hold and move the hydrophone for scanning.

An important quantity of the field is the intensity which is defined as the power carried by sound waves per unit area in a direction perpendicular to that area. The instantaneous intensity I(t) can be calculated using Eq. (1.1), assuming the acoustic wave is plane.

$$\mathrm{I(t)} = \frac{p^2(t)}{\rho c}, \tag{1.1}$$

where p(t) is the instantaneous acoustic pressure amplitude, ρ is the density of the medium and c is the velocity of sound in the medium.

Two average intensities, i.e., the spatial-peak temporal-average intensity (I_{SPTA}) and the spatial-peak pulse-average intensity (I_{SPPA}), are commonly used. To calculate these two quantities, the pulse intensity integral (PII) is first calculated using Eq. (1.2):

$$\mathrm{PII} = \int \mathrm{I(t)}\,\mathrm{dt} = \int \frac{p^2(t)}{\rho c}\mathrm{dt} = \frac{p_{rms}^2}{\rho c}\mathrm{TBD}, \tag{1.2}$$

where p_{rms} is the effective pressure amplitude and TBD is Tone-burst-duration, or pulse duration.

Then the $\mathrm{I_{SPPA}}$ was defined as:

$$I_{SPPA} = \frac{\mathrm{PII}}{TBD}, \tag{1.3}$$

As the ultrasound waveform is usually assumed sinusoidal, thus approximately $\mathrm{p}_{rms} = \frac{\sqrt{2}}{2}\mathrm{p}_{peak}$. Therefore $\mathrm{I_{SPPA}}$ could be approximately calculated using Eq. (1.4).

$$\mathrm{I_{SPPA}} = \frac{\mathrm{PII}}{TBD} \approx \frac{p_{rms}^2}{\rho \mathrm{c}} = \frac{p_{peak}^2}{2\rho \mathrm{c}}, \tag{1.4}$$

$\mathrm{I_{SPTA}}$ was defined as:

$$I_{SPTA} = I_{SPPA} \times DC = I_{SPPA} \times \mathrm{TBD} \times \mathrm{PRF} = \mathrm{PII} \times \mathrm{PRF}, \tag{1.5}$$

where PRF is the pulse repetition frequency, and DC is the duty cycle.

1.1.3.2 Development of pTUS

Making use of these characteristics, as well as its safety, ultrasound has a long history and wide applications in biomedical imaging [58]. Last two decades have witnessed the deepening understanding of how ultrasound waves interact with biological tissues, as well as major technological breakthroughs in the development of approach for accurately focusing ultrasound into a small region of interest in the brain through the intact skull [59,60]. These advancements have led to broad and new applications of ultrasound. First, high-intensity (typically exceeding 500 W/cm^2) focused ultrasound (HIFU) brain surgery to treat movement disorders [61,62], in which the ultrasound is used to irreversibly ablate pathological tissue. Secondly, ultrasound with low intensity (under 1W/cm^2) has been extensively investigated in improving drug delivery to brain by reversible disruption of blood brain barrier (BBB) in order to treat neurological disorders [63–65].

In contrast to the high-intensity applications of focused ultrasound, low-intensity pulsed ultrasound was first shown to be able to directly stimulate brain circuits through its non-thermal effects in pilot study by Tyler et al. a decade ago [66]. The first demonstration of ultrasonic effects on excitable tissues could be traced back to the 1920s [67] when Harvey showed that ultrasound stimulation could influence the neuromuscular activity of frog and turtle. Later groundbreaking work by Fry and colleagues demonstrated that ultrasound transmitted through a cranial window could reversibly suppress the visual evoked potentials (VEPs) in cats [68]. However, compared with clinically widespread diagnostic imaging and therapeutic applications, neural stimulation by ultrasound was only pursued by only a small number of relatively scattered research groups after these pioneering studies by Harvey and Fry [67,68] . In particular, much of these studies were done in the 1970s and 1980s in Moscow, by Gavrilov et al., examining ultrasound effects on peripheral receptors underneath the skin and in the auditory system of both animals and humans [69–71].

Then two pioneering in-vitro studies reported in 2008 that low-intensity ultrasound pulsation could directly elicit action potentials and stimulate synaptic transmission in localized brain circuits [66,72]. These findings have sparked a new wave in the area of ultrasound neuromodulation. The last few years witnessed a considerable number of studies on both excitation and suppression of central nervous system in response to ultrasound stimulation with different ultrasound parameters, experimental models and conditions [73]. In the landmark study in 2010, Tufail et al. first demonstrated in-vivo noninvasive transcranial stimulation of motor cortex and hippocampus using pulsed ultrasound [54]. This work was followed by a group of in-vivo studies in anesthetized rodent and rabbit models, examining the excitatory and inhibitory effects of ultrasound stimulation on different brain areas, by looking into the induced motor activities, evoked potentials, microelectrode recordings and fMRI signals [74–81].

More recently, researchers have applied pTUS to non-human primates and humans towards the clinical translation of this promising technique [82]. Hameroff et al. reported an early pTUS study on human subjects, applying a low-intensity high-frequency (8MHz) ultrasound imaging probe to the scalp area overlying the frontal-temporal cortex [83]. This study reported improved mental state after receiving ultrasound stimulation. To explore specific neuromodulatory effects induced by pTUS, Deffieux et al

applied low-intensity ultrasound to the frontal eye field (FEF) of Macaque Rhesus monkeys during a visual task [84]. They found that pTUS (320 kHz) significantly modulated anti-saccade latencies in the contralateral visual field and reduced eye movements. Their recent follow-up study demonstrated that the neuromodulatory effects of pTUS could be assessed in real time in awake behaving monkeys by recording neuronal discharge [85]. This non-human primate study of specific pTUS neuromodulation was later followed up by Tyler and Yoo teams, who applied pTUS to human primary somatosensory cortex (S1) and observed the modulation of somatosensory evoked potentials (SEP), as well as the behavioral response [86–89]. Additionally, Lee et al. stimulated the human primary visual cortex (V1) and resulted in the perception of phosphene and associated evoked potentials, which also revealed a network involved in visual and higher-order cognitive processes [90].

A considerable number of studies, including those mentioned above, have also been making efforts to improve the pTUS technique in its stability, accuracy and spatial specificity. Firstly, some studies investigated the characterization of ultrasound field transmitted through the animal or human skull, providing a better understanding of inter-subjects variations due to the different cranial and neural anatomy [55,78,91–93]. Secondly, researchers introduced image guidance into pTUS, allowing precise placement of transducers [94–97], which is of importance in pTUS applications requiring longitudinal treatment at the same target. At the same time, there are also researchers working on ultrasound transducer design to achieve higher spatial resolution and transmission efficacy of pTUS [98–102].

1.1.3.3 Applications of pTUS

Capitalizing on the noninvasiveness, exquisite spatial selectivity and capability of penetration of pTUS, a few studies have reported its uniqueness of applications in neurosciences and clinical therapeutics. For example, Dallapiazza et al. demonstrated that it was feasible to use pTUS for selective brain mapping in large-brain animals and humans [103]. Downs and colleagues reported that ultrasound stimulation could enhance performance of complex cognitive tasks, specifically decision-making in monkeys [104]. More intriguingly, Lee et al used pTUS as a stimulation modality to perform brain-to-brain interface (BBI) in humans [105].

At the same time, there have also been increasing interests in the neuroprotective effect of pTUS neuromodulation on the central nervous system (CNS) [106]. Hakimova et al. applied suppressive ultrasound stimulation to a rodent model of mesial temporal lobe epilepsy and demonstrated that pTUS was able to inhibit recurrent seizures and improve behavioral outcomes [107]. Another study reported that repeated ultrasound stimulation could remove amyloid-β (Aβ) peptide, which is implicated in the pathogenesis of Alzheimer's disease (AD), and restored memory function in an AD mouse model [108]. It suggested that isolated pTUS could serve as a noninvasive method with therapeutic potential in AD, without using therapeutic agent such as anti-Aβ antibody. In particular, our previous study [109] investigated pTUS's neuroprotective effect on stroke in a rat model of distal middle cerebral artery occlusion (dMCAO). The results showed reduced infarct volume and improved behavioral performance after receiving pTUS. These findings provided evidence that pTUS is a unique non-invasive neuromodulation technique in the treatment of acute ischemic stroke.

1.1.4 Motivation

Inspired by previous studies on therapeutic pTUS, this thesis focuses on the neuroprotection of pTUS preconditioning in focal cerebral ischemia and the therapeutic effect on depression. The rationales for these applications are to be introduced in Section 3.1 and Section 4.1, respectively. Briefly, it has been proposed that preconditioning could reduce brain metabolism and render the neurons more tolerant to ischemia [110]. By contrast, it also was reported that promotion of neuronal activity in target brain regions (e.g. left prefrontal cortex) might alleviate depression [111]. Thus, it was conjectured that suppressive pTUS might serve as a preconditioning method to protect brain from subsequent ischemic injury, whereas excitatory pTUS might alleviate depression. The corresponding pTUS parameters were: (a) suppressive pTUS (or $pTUS_S$): I_{SPPA} = 8W/cm^2, frequency (f) = 0.5 MHz, pulse repetition frequency (PRF) = 100 Hz, and duty cycle (DC) =5%, and (b) excitatory pTUS (or $pTUS_E$): I_{SPPA} = 8W/cm^2, f = 0.5MHz, PRF = 1.5 kHz, and DC = 60%, respectively. These parameters were chosen because they have been suggested as suppressive and excitatory, respectively, both in experiments [75][109] and in theory [112]. Before applying pTUS, it is necessary to characterize the neuromodulatory effect of different pTUS parameters to facilitate the parameter optimization of therapeutic pTUS in practice.

1.2 Aims of the study

Based on the review above, the specific aims of this work are as follows:

Specific Aim 1: to assess the neuromodulatory effect of both excitatory and suppressive pTUS parameters that will be used in the following experiments.

The working hypothesis of this aim is that pTUS could modulate the cortical excitability in response to hind limb electrical stimulation, and functional optical imaging could be used to study the neuromodulatory effects of pTUS. It is of interest to study the neuromodulatory effects of different ultrasonic parameters. Optical imaging allows for mapping of neural activity with high spatial and temporal resolution. Therefore, two widely adopted techniques, i.e., laser speckle contrast imaging (LSCI) and multispectral reflectance imaging (MSRI), will be used to monitor the neural modulation by pTUS. This study allows us to optimize the sonication parameters in the treatment of neurological diseases.

Specific Aim 2: to explore whether the severity of stroke can be minimized or alleviated by preconditioning pulsed transcranial stimulation.

Aim 2A: to investigate whether 1-hour pTUS preconditioning could delay and alleviate hemodynamic compromises during photochemically induced focal ischemia in rats;

Aim 2B: to examine whether rats receiving pTUS preconditioning show better outcomes from ischemia 24 hours and 48 hours after photothrombolic ischemic injury

The working hypothesis of this aim is that 1) the cerebral blood flow of rats receiving pTUS preconditioning would drop more slowly and end with a higher level than control animals; 2) the blood supply to the infarcted region of brain would be improved in pTUS preconditioned rats at 24 and 48 hour after phothothrombosis compared with control rats and the infarct volumes and brain edema at 48 hour would be less than the preconditioning group.

Using laser speckle contrast imaging technique, intraoperative monitoring of cerebral blood flow has been previously realized in rat stroke model [113]. This study will examine whether the pTUS preconditioning could alleviate the damage in the subsequent focal cerebral ischemia from the

hemodynamic perspective as well as histological analysis. This work will provide experimental evidence for the use of pTUS preconditioning in perioperative stroke, which has great potential in clinical applications.

Specific Aim 3: to study the antidepressant-like effects of pTUS on depression in a 48-hour-restraint rat depression model.

The working hypothesis of this aim is that two-week daily pTUS treatment could alleviate depression-like symptoms, such as anhedonia, reduced exploratory and despair behavior in a rat depression model by 48-hour restraint.

A large body of evidence has demonstrated the involvement of brain-derived neurotrophic factor (BDNF) in the pathophysiology of depression and its alleviation [114,115]. On the other side, recent animal studies demonstrated that pTUS, which increased neuronal activity with appropriate parameters, could elevate BDNF expression in hippocampus [54] and significantly promote the neural proliferation in the dentate gyrus of the dorsal hippocampus [116]. These findings suggest an intriguing hypothesis that pTUS might be able to alleviate depression symptoms by promoting the BDNF level and neurogenesis. Thus, this study will for the first time test this hypothesis by applying pTUS to a rat depression model and investigate its antidepressant-like effects using a group of behavioral tests.

1.3 Contribution and novelty

This thesis provides the first in-vivo demonstrations that pTUS might serve as the early protection of ischemic stroke and treatment of depression. The contributions include: 1) characterizing the modulation of cortical excitability by pTUS with different sonication parameters using multi-modal neuroimaging techniques; 2) demonstrating pTUS preconditioning could mitigate the subsequent injury due to focal cerebral ischemia in the rodent model; 3) showing that pTUS on prefrontal cortex (PFC) has antidepressant-like effects in a rat depression model.

The novelty of this study is as follows:

1) Innovative approach by using optical imaging techniques to study the pTUS neuromodulation. Based on review of current tools for assessing pTUS neuromodulation (see Section 2.1), this thesis proposed that optical imaging techniques, i.e., laser speckle contrast imaging (LSCI) and multi-spectral reflectance imaging (MSRI), could be used to characterize the neuromodulatory and therapeutic effects of pTUS from the hemodynamic perspective. This imaging-based approach allows mapping the changes of cortical excitability induced by pTUS with higher spatial resolution (in the scale of μm) than the current electro-neurophysiological methods [117].

2) Noninvasive and precise therapeutics based on the novel neuromodulation technique, i.e., pTUS. This thesis for the first time investigated whether pTUS has preconditioning effect on a rat brain ischemia model and whether it could alleviate depression-like symptoms in a rat depression model. Based on the noninvasiveness and precision of pTUS, these pilot studies showed the potential of pTUS in treatment of neurological disorders.

1.4 Outline

This chapter first describes neurological and psychiatric disorders and then reviews their treatment from pharmaceuticals to brain stimulation techniques before introducing pTUS as a promising therapeutic agent for its unique neuromodulatory effects. Based on the above review, the detail aims, contributions and novelty of the thesis are proposed. Next, using optical neuroimaging techniques, Chapter 2 characterizes neuromodulatory effects of different pTUS parameters to be used in Chapter 3 and Chapter 4, where suppressive pTUS serves as preconditioning against subsequent focal cerebral ischemia while excitatory pTUS is used to alleviate depression-like syndromes in rats, respectively. Finally, Chapter 5 summarizes the findings and discusses the mechanisms underlying therapeutic and neuromodulatory effects of pTUS. The future work of pTUS technique is also envisioned.

Chapter 2: Assessing the Neuromodulatory Effects of Different Mode of pTUS Using Optical Neurovascular Imaging

This chapter proposes an optical imaging-based approach to assess the modulation of cortical excitability by pTUS and evaluate the neuromodulatory effects of pTUS parameters to be used in following studies. Specifically, two optical imaging techniques, i.e., laser speckle contrast imaging and multispectral reflectance imaging, were used to monitor the activity of primary somatosensory cortex elicited by hind limb electrical stimulation before, immediately after (< 1minute), and 1 h after 5-min application of pTUS with recognized excitatory and suppressive parameters. The suppressive and excitatory parameters are used in Chapter 3 and Chapter 4, respectively. Additionally, several imaging derived indicators are proposed to characterize the neuromodulatory effects that pTUS might have on primary somatosensory cortex. To study the influence of cortical excitability at baseline on neuromodulatory effects of pTUS, the correlation between them was analyzed.

2.1 Introduction

The excitatory and suppressive effects of pTUS on neural activity are of interest because of the potential biomedical applications (such as enhancing cognitive function and treating neurological disorders). Specifically, modification of the pTUS exposure parameters, such as frequency, intensity, pulse repetition frequency (PRF), duty cycle (DC) and Tone-burst-duration permits introduction of both excitation and suppression neuromodulatory effects, i.e., up- and down-regulating neural activity [6–9]. These features of pTUS were applied in treatment of neurological diseases especially those caused by disturbed neural activity [74,109,118] . For instance, the outcome of the experiments in [109] where excitatory pTUS delivered at 500 kHz at the spatial-average-temporal-average intensity (I_{SATA}) level of 86 mW/cm^2 and PRF of 1.5 kHz appeared to act in neuroprotective mode when applied immediately (< 1minute) after stroke in rats. Additionally, suppressive pTUS (690 KHz at I_{SPTA} of 130 mW/cm^2, 100 Hz PRF and 5% DC) could serve as a therapy for abnormal hyper-excitability of neurons in epilepsy [74].

Previous studies have made efforts to examine the dual neuromodulatory effects of pTUS experimentally and theoretically, but are still insufficient to fully understand the influence of pTUS on neural activity, such as the spatial and temporal changes of cortical excitability under both excitatory and suppressive pTUS. For instance, Kim et al. [119] examined a range of ultrasound parameters (frequency of 350-650 kHz at I_{SPPA} of 4-14 W/cm^2, DC of 30-100%, PRF of 0.1-2.8 kHz and SD of 150-400 ms) for neurostimulation by measuring the motor response. But they were unable to assess the neuromodulatory effects of pTUS in brain areas that yield no observable behavioral outputs, such as primary somatosensory cortex. Also, it is unfeasible to assess suppressive pTUS when there is not a motor response. By contrast, Yoo et al. studied the suppressive effects of pTUS on the visual cortex by detecting the decrease of visual evoked potentials (VEP) [75]. However, VEP lacks in spatial resolution of the associated neural activity as it is obtained using only a few subdermal EEG electrodes (e.g., two electrodes in [75]), which could limit its characterization of neuromodulatory effects in terms of spatial pattern of cortical excitability changes. From the theoretical perspective, Plaksin et al. proposed an intramembrane cavitation model for ultrasound-induced neuromodulation [120] that was subsequently extended to predict excitatory and suppressive ultrasonic stimulation at single-neuron and network levels [112]. The model agreed well with recent experimental results in [75] and [119]. Nevertheless, it is difficult to use this theoretical model to reveal spatial and temporal changes of cortical excitability due to the complexity of brain structures.

Real-time optical imaging allows mapping the neural activity with higher spatial resolution (in the scale of μm) than the current electro-neurophysiological methods [117]. For instance, laser speckle contrast imaging (LSCI) has been widely adopted to non-invasively image cerebral blood flow (CBF), whereas multispectral reflectance imaging (MSRI) is able to obtain dynamic and relative changes in cortical metabolic rate of oxygen ($CMRO_2$) [121] (the principles of LSCI and MSRI are briefly introduced in the Section 2.2.1 as well). These imaging techniques may serve as potential approaches to evaluate the neuromodulatory effects because CBF and $CMRO_2$ are both the hemodynamic and metabolic response of corresponding brain areas to functional stimulation, and have been regarded as manifestations of cortical excitability. Optical imaging of the brain activity elicited by hind-limb electrical stimulation was already reported [122]. In the experiments in [122], LSCI and MSRI were simultaneously applied to obtain CBF and $CMRO_2$ changes, respectively, under functional electrical stimulation.

Based on the review above, we propose to characterize the neuromoulatory effects of pTUS by concomitantly using optical imaging. Specifically, LSCI and MSRI were employed to monitor the activity of primary somatosensory cortex in live animal model (11 rats) under electrical stimulation to the hind-limb before, immediately after (<1 minute), and 1 h after 5-min exposure to pTUS with two well-recognized sets of excitatory and suppressive parameters ($pTUS_E$ and $pTUS_S$, respectively). These two sets of parameters were to be used Chapters 3 and 4 to investigate the therapeutic properties of pTUS. The corresponding pTUS parameters were: (a) suppressive pTUS (or $pTUS_S$): I_{SPPA} = 8 W/cm^2, frequency (f) = 0.5 MHz, pulse repetition frequency (PRF) = 100 Hz, and duty cycle (DC) = 5%, and (b) excitatory pTUS (or $pTUS_E$): I_{SPPA} = 8 W/cm^2, f = 0.5 MHz, PRF = 1.5 kHz, and DC = 60%, respectively. Also, several indicators, such as *Response Index*, *Peak Response*, *Latency* and *Response Duration* were derived to characterize the neuromodulatory effects of pTUS.

2.2 Methods

2.2.1 Experimental System

The experimental system is shown in

Figure 2.1a. The setup included pulsed signal generators, optical imaging modules and electrical stimulation system. Two identical function generators (AFG3022B, Tektronix, USA) were used to generate pulsed signals or tone bursts (***Figure 2.2b***). Before activating the transducer, the pulse signals were amplified using a radio frequency (RF) amplifier with adjustable gain (Custom designed, HGX100, Nanjing, China). The transducer was mounted using custom-designed adapters onto the manipulator arms of the stereotaxic frame (Model 68006, RWD Life Science Inc. Shenzhen, China), allowing precise (to within 0.1 mm) control of the transducer. As shown in

Figure 2.1a and ***Figure 2.2b***, the pTUS waves were produced by an immersion-type ultrasound transducer (V301-SU, Olympus NDT, Waltham, USA) operating at 0.5 MHz, which was consistent with our previous study [109]. A custom-designed acoustic collimator (7 mm diameter output aperture) made of plexiglass was coupled to the ultrasound source so that the target brain area confined to the region of interest (see

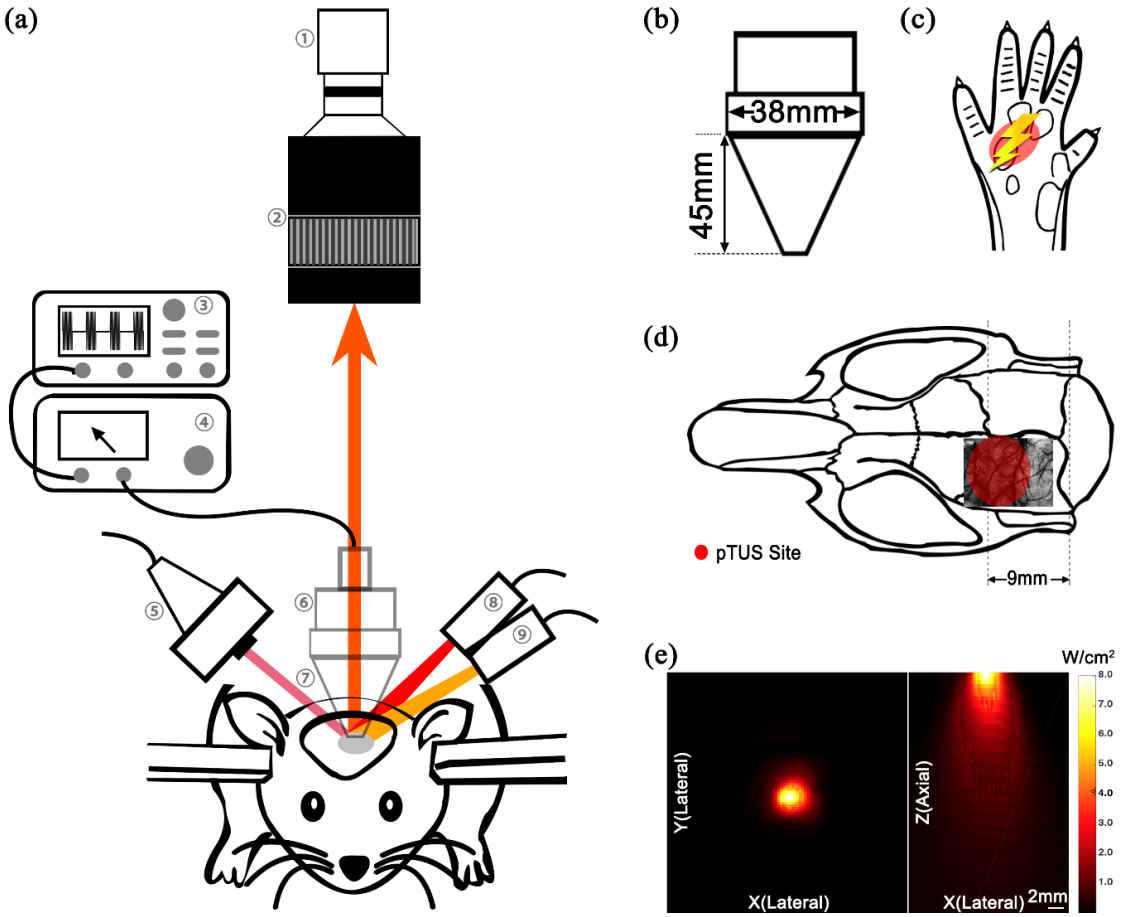

Figure 2.1b, ***d*** and ***e***).

Figure 2.1 Overview of the experimental system and pTUS parameters. (a) Schematic of the entire experimental system. The transducer was illustrated translucently as it would be removed after ultrasound stimulation to avoid interference with the optical modules. Magenta light beams represented the optical path of 780-nm whereas red and orange beams represented the optical paths of 635 and 590-nm LED, respectively. Components: ①CCD Camera, ②Camera Lens, ③Function Generator (X2), ④RF Amplifier, ⑤780nm Laser Diode, ⑥Ultrasound Transducer, ⑦Acoustic Collimator, ⑧635-nm LED ⑨590-nm LED. (b) Dimension of the transducer and collimator used in the study. (c) Illustration of the electrical stimulation on hind limb of the rat. (d) The location and areas of ultrasound stimulation on the brain. A cerebral blood flow image obtained by laser speckle contrast imaging is overlaid on the skull. (e) Lateral (Left) and axial (Right) acoustic spatial-peak pulse-average intensity (I_{SPPA}) maps.

As non-contact optical imaging techniques, LSCI and MSRI provides two-dimensional CBF and oxygenation information, respectively, with high spatial (in the scale of μm) and high temporal resolution (in the scale of ms). The optical imaging system included a 780 nm laser diode (10 mW, L780P010,

Thorlabs, USA), two light-emitting diodes (590 nm, 100 mW, M590L3 and 635 nm, 400 mW, M635L3 respectively, Thorlabs), a CMOS camera (12bit, acA2040-180km, Basler, Ahrensburg, Germany) and a camera lens (Nikon AF-S VR Micro-Nikkor, 105mmf/2.8G IF-ED, Tochigi, Japan). The system was positioned by the holders mounted on the optical table.

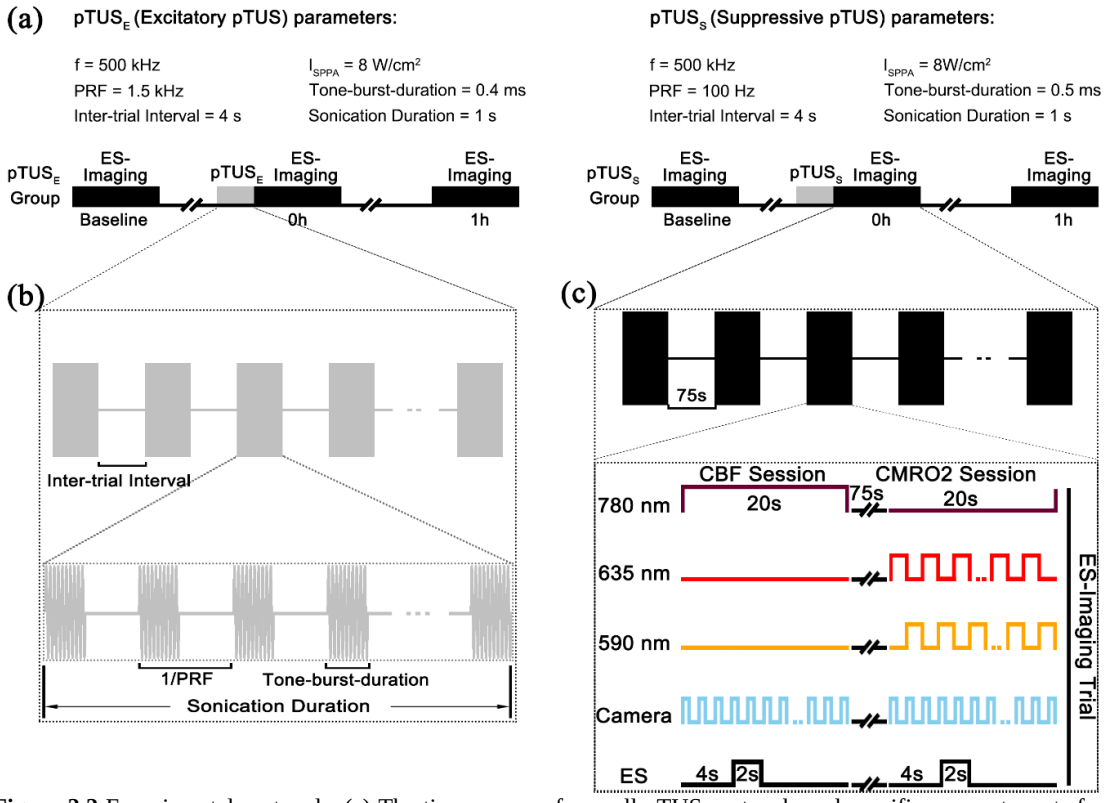

Figure 2.2 Experimental protocols. (a) The time course of overall pTUS protocols and specific parameter sets for both pTUS$_E$ and pTUS$_S$ groups. (b) Illustration of pTUS sequences. (c) Illustration of one ES-imaging trial. Logic voltage levels symbolizes the working flow of the ES-imaging system, with high level representing 'on' and low level representing 'off'.

Principles and intraoperative monitoring techniques of LSCI and MSRI have been well documented [123,124]. Briefly, the contrast value *K* was defined and estimated by temporal laser speckle contrast analysis (tLASCA) [125] using Eq. (2.1) after the registration of the raw images [126].

$$K^2 = \frac{\sigma^2}{\langle I \rangle^2}, \tag{2.1}$$

where σ and $\langle I \rangle$ are the temporal standard deviation and the temporal average of the speckle intensity (i.e., grayscale at each speckle), respectively. As K^2 has been shown to be inversely proportional to the CBF velocity [127], the mapping of $1/K^2$ represents the distribution of CBF.

According to Ref. [128], the relative change in $CMRO_2$ ($rCMRO_2$), can be calculated from the relative CBF (rCBF or ΔCBF), concentration of total hemoglobin ([HbT]) and deoxy-hemoglobin ([HbR]) using the equation:

$$1 + rCMRO_2 = \left(1 + \frac{\Delta CBF}{CBF_0}\right)\left(1 + \gamma_R \frac{\Delta[HbR]}{[HbR]_0}\right)\left(1 + \gamma_T \frac{\Delta[HbT]}{[HbT]_0}\right)^{-1}, \tag{2.2}$$

where the subscript '0' indicates the baseline values, and the coefficients γ_R and γ_T are vascular weighting constants (assumed to be 1 for simplification as suggested by [121], which tested the assumed γ_R and γ_T ranging from 0.5-2 and found they did not substantially influence the calculated $CMRO_2$ response), and [HbT] consists of [HbR] and concentration of hemoglobin ([HbO]). Changes in HbR and HbT, i.e., $\Delta[HbR]$ and $\Delta[HbT]$, respectively, at each pixel were solved using the modified Beer Lambert Law applied to each pixel:

$$\ln\left(\frac{I(0)}{I(t)}\right) = l(\varepsilon_{HbR}\Delta[HbR] + \varepsilon_{HbO}\Delta[HbO]), \tag{2.3}$$

where $\ln\left(\frac{I(0)}{I(t)}\right)$ is the attenuation at each wavelength, I(0) and I(t) are the measured reflectance intensities at baseline and the time t, ε_{HbR} and ε_{HbO} are the molar extinction coefficients for HbR and HbO, respectively, and l is the differential pathlength factor.

Two wavelengths, 590 nm and 635 nm, were selected according to ***Figure 2.3b*** to calculate the changes of [HbR] (i.e., $\Delta[HbR]$) and [HbO] (i.e., $\Delta[HbO]$). Specifically, 590 nm is close to an isosbestic point whereas absorption coefficients of HbO and HbR are significantly different at 635 nm. Thus, [HbT]

could be readily obtained from the reflectance intensities under 590 nm. Combined with [HbT], [HbO] and [HbR] could be calculated using the data at 635 nm.

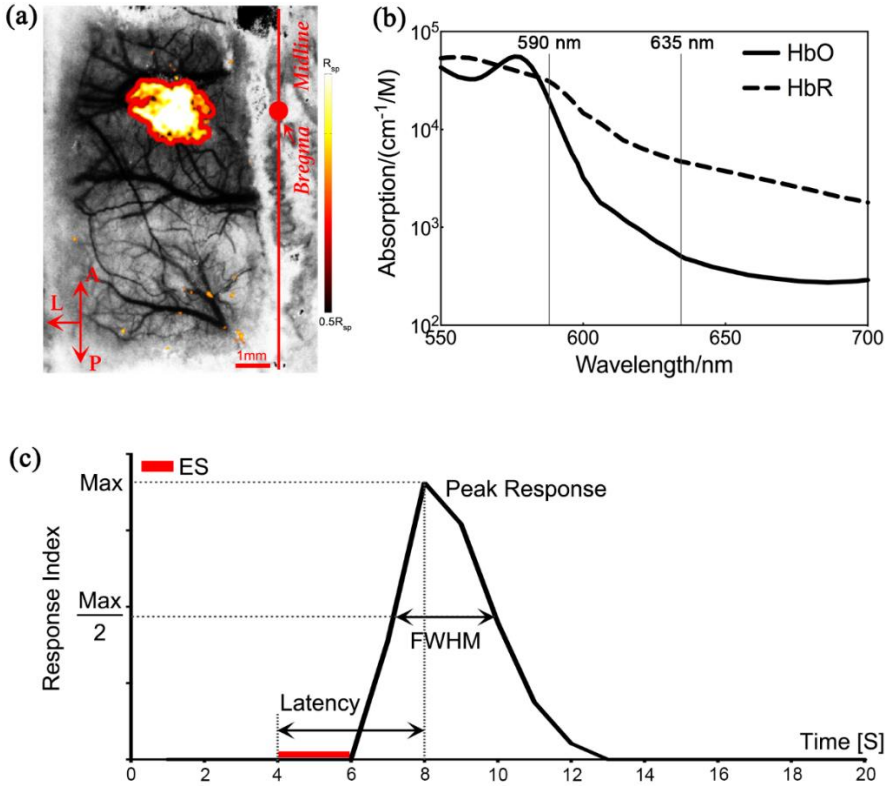

Figure 2.3 Illustration of defined indicators and MSRI principles. (a) ES induced functional activation overlaid on an CBF images obtained by LSCI on the left hemisphere of a rat. The red contour represents calculated response area. (b) Molar absorption coefficients of HbO and HbR. Vertical black thin lines indicate the wavelengths of LEDs used in this study. (c) Illustration of imaging-based indicators, i.e., *Peak Response*, *Latency*, and *Response Duration* (i.e., *FWHM*), defined for both CBF and $CMRO_2$ results.

2.2.2 Animal Preparation

All animal experiments in this study were approved by the Animal Care and Use Committee of Shanghai Jiao Tong University. Twelve adult male Sprague-Dawley rats (320 ±20g, Slac Laboratory Animal Co. Ltd., Shanghai, China) were used in this study. The sample size was determined using the methods in [129] so it yielded statistical power greater than 80%. The imaging cranial window was

prepared 12 hours before the first imaging session. Each rat was anesthetized with an intraperitoneal injection of 7% chloral hydrate (5 ml/kg). During the surgery, the rats were constrained in a stereotaxic frame and the rectal temperature was monitored and maintained at 37±0.2℃ with a heating pad and a direct current (DC) control module (FHC Inc., Bowdoinham, USA). All procedures were performed under standard sterile precautions. After being shaved, the rat's scalp was incised along the midline and the exposed tissues were carefully cleaned with a scalpel to expose the skull. A 3.0 mm (horizontal) × 5.0 mm (vertical) cranial window centered at 0.5 mm posterior, 1.5 mm lateral to the bregma over the left hemisphere was then thinned by a high speed (about 10000 rpm) dental drill (Strong 90 Micro Motor, Saeshin Precision, Korea) with Ø 1.4 mm steel burr until the cortical vessels were clearly visible. The rats were then caged with sufficient supply of food and water for 12 hours to eliminate the influence of the anesthetics.

2.2.3 Experimental Design

2.2.3.1 Experimental protocols

The overall experimental protocols are shown in ***Figure 2.2a***. During the experiment, rats were anesthetized with isoflurane (5% initial and 1% for maintenance) in accordance with the anesthetic protocols in previous studies [128][109] and mounted on the stereotaxic frame. Cranial windows were filled with mineral oil for optimal image quality. First, the baseline Electrical Stimulation (ES)-imaging block before ultrasound stimulation was performed and followed by a 15-minute resting time. Next, the selected region of cortex was stimulated with either excitatory or suppressive pTUS ($pTUS_E$ and $pTUS_S$, respectively). After pTUS, '0h' and '1h' ES-imaging blocks were performed immediately (<1 minute) and 1 hour after pTUS, respectively. The ES and pTUS were repeated on the same animal with the other set of pTUS parameter after 24 hours. For example, if the rat was first stimulated with the $pTUS_E$ then it would be stimulated by the $pTUS_S$ after 24 hours, or vice versa. The order of $pTUS_E$ and $pTUS_S$ was randomly applied to avoid the possible influence of the adaptation. Rats were put back to home cages with free access to food and water after measurements.

2.2.3.2 pTUS parameters

It was proposed to monitor the neuromodulatory effects of pTUS with parameters suggested as excitatory and suppressive, respectively [73,74, 111] by LSCI and MSRI. Specifically, animals were exposed to ultrasound stimulation for 5 min (in comparison with the experiment in [75]) with parameters: (a) $pTUS_S$: I_{SPPA} = 8W/cm^2, frequency (f) = 0.5MHz, pulse repetition frequency (PRF) = 100 Hz, and duty cycle (DC) =5%, and (b) $pTUS_E$: I_{SPPA} = 8W/cm^2, f = 0.5MHz, PRF = 1.5 kHz, and DC = 60%, respectively. The exposure condition for $pTUS_S$ was selected according to the suppressive parameters well examined in studies [74,75]. Similarly, the $pTUS_E$ parameters were based on our previous study using excitatory pTUS to protect brain from ischemic injury [109]. Additionally, in the future work, we plan to expand this study to investigate a series of parameters in order to optimize the selection of excitatory/suppressive parameters.

Since the peak pressures were the same for both $pTUS_E$ and $pTUS_S$, their I_{SPPA} could be considered identical. This acoustic intensity I_{SPPA} was approximately 8 W/cm^2 according to Eq. (1.4).

For both $pTUS_E$ and $pTUS_S$, a 1s single sequence as described above was repeated 60 times at a 4s interval. This way to deliver ultrasound stimulation was based on the experience from study [109] in order to minimize the accumulation of potential thermal effect. The stimulation site and protocols are shown in ***Figure 2.1 d*** and ***Figure 2.2b***, respectively. Additionally, the ultrasound field distribution is illustrated in ***Figure 2.1e*** and the details of measurement are described in the section ***1.1.3.1***.

2.2.3.3 Electrical stimulation (ES)-imaging block

As illustrated in ***Figure 2.2c***, each ES-imaging block consisted of 10 repeated trials with an inter-trial interval of 75 s. Each ES-imaging trial contained a 20s CBF imaging session and a 20s $CMRO_2$ imaging session, and the interval in between was also 75 s. In each session, hind-paw electrical stimulation was applied from the 4th to the 6th second. Specifically, during hind-paw stimulation, electrical pulses of 1.5 mA were applied for 2 ms at 5 Hz using a programmable stimulator (YC-2, Cheng Yi, China) with two needle electrodes inserted subcutaneously into the right hind paw as shown in ***Figure 2.1c***.

The protocols used for imaging and electrical stimulation were designed according to the study [128]. During CBF imaging, the cortex was illuminated by coherent light from the 780 nm laser diode powered by a drive module (LDC220C, Thorlabs). During the $CMRO_2$ session, the cortex was illuminated by amber (590 nm) and red (635 nm) LEDs, which were powered alternatively at the frequency of 40 Hz to obtain reflected images under both wavelengths in one session. In both imaging sessions, the reflected images (480×640 pixels, $4.65\ \mu m/pixel$) were captured by the CMOS camera at 40 fps for 20 s through the lens system.

2.2.4 Imaging Data preprocessing

All collected images were processed with MATLAB (Ver. 2016a, MathWorks, Natick, MA, USA). CBF were mapped as $1/K^2$ using Eq. (2.1). The relative change of CBF compared with baseline (rCBF) was used to quantify the ES-induced changes of CBF. Similarly, the relative $CMRO_2$ ($rCMRO_2$) was calculated using Eqs. (2.2) and (2.3). To improve the signal-to-noise ratio (SNR), the rCBF and $rCMRO_2$ were averaged across all trials over 20 samples from each (1sec interval). In addition, according to [130], a spatial 2D Gaussian filter of size 5×5 with standard deviation 3 was applied to further improve the SNR.

To comprehensively understand the influence of pTUS on sensory response to hind-limb ES, an indicator called *Response Index* (*RI*) was defined in Eq. (2.4), which may collectively reflect the overall response area and response amplitude at each time point. Specifically, as illustrated in ***Figure 2.3a***, the *Response Area* (in red) was defined as the region with rCBF or $rCMRO_2$ greater than 50% of the *Spatial Peak Response* (R_{sp}). The R_{sp} was calculated by averaging the largest ten rCBF or $rCMRO_2$ values in the frame. Then RI was defined as the summation of rCBF or $rCMRO_2$ within the response area.

$$\mathrm{RI} = \sum_{i=1}^{M}\sum_{j=1}^{N} rVal(i,j) * \mathbb{I}(rVal(i,j) \geq 0.5 * R_{sp}) , \tag{2.4}$$

where rVal(i, j) indicates the value of rCBF or $rCMRO_2$ respectively at the (i, j) pixel, $\mathbb{I}(\cdot)$ is the indicator function which equals 1 or 0 when $(\cdot)$ is true or false, respectively, and R_{sp} is the *Spatial Peak Response* that has been defined above.

As shown in ***Figure 2.3c***, according to [130], a few more indicators were defined based on RI: 1) *Peak Response* as the maximum of RI among all 20 time points; 2) *Latency* as the time to reach the *Peak Response* after the ES onset; 3) *Full Width at Half Maximum* (*FWHM*) or *Response Duration* as the duration when *Response Index* stayed above half the *Peak Response.*

To study the influence of cortical excitability at baseline on neuromodulatory effects of pTUS, the correlation between them was analyzed. The pTUS induced relative changes of *Peak Response*, defined as Δ_{PR}

$$\Delta_{PR} = \frac{PR_0 - PR_{baseline}}{PR_{baseline}} \times 100\%, \tag{2.5}$$

was used to represent the neuromodulatory effects of pTUS, where PR_0 is the *Peak Response* immediately after pTUS and $PR_{baseline}$ is the *Peak Response* at baseline.

2.2.5 Statistical analysis

All statistical analysis was carried out with SPSS software (Ver.24.0, SPSS Inc., Chicago, USA). Mauchly's test was used to test the sphericity, i.e., the homogeneity of variances. Once the sphericity was confirmed, repeated measures analysis of variance (ANOVA) was performed to compare *Peak Response*, *Latency* and *FWHM* at baseline, 0 h and 1 h after pTUS (Baseline, 0 h and 1h group, respectively) for both rCBF and $rCMRO_2$, respectively. Once an overall significant difference existed, post hoc tests using the Bonferroni correction were then performed to obtain pair-wise comparisons among the three groups. Significance level was set at $p < 0.05$, and all data were expressed as mean ± S.D.

2.3 Results

One of the twelve rats died from surgery failure in anesthesia before the experiment and was thus excluded from the rest procedures and data analysis. ***Figure 2.4a*** and illustrated qualitatively how CBF and $CMRO_2$ responses were influenced by different pTUS, whereas the rest subfigures in ***Figure 2.4*** and presented the *Peak Response*, *Latency* and *Response Duration* of each rat at different time moment, respectively.

2.3.1 Effects of pTUS on the CBF response to hind-limb electrical stimulation

Figure 2.4a showed the strongest response of CBF during the 20s ES-Imaging process overlaid on the corresponding LSCI images over the left hemisphere. Corresponding thresholds were calculated and applied to the CBF responses. In total, 5 out of 11 rats receiving $pTUS_E$ showed enhanced response (See left ***Figure 2.4b***). The top two rows of ***Figure 2.4a*** demonstrated distinct cortical CBF response to $pTUS_E$ in two typical rats. By contrast, the CBF decreased in the rat receiving $pTUS_S$ and slightly recovered after 1 h (row 3 in ***Figure 2.4a***). This outcome was consistent among all $pTUS_S$ rats (See ***Figure 2.4b*** (right)).

As already noted the sphericity of all data was confirmed, the repeated measures ANOVA was performed. As shown in ***Figure 2.4b*** and ***Figure 2.4c***, the *Peak Response* and the *Latency* in $pTUS_E$ group had no significant difference at baseline, 0 h and 1h ($F(2, 20) = 1.723$, $p = 0.204$ and $F(2, 20) = 3.177$, $p = 0.063$, respectively). However, in contrast to the $pTUS_E$ group, the *Peak Response* and the *Latency* in $pTUS_S$ group differed significantly at baseline, 0 h and 1h ($F(2, 20) = 10.659$, $p = 0.001$ and $F(2, 20) = 12.759$, $p < 0.001$, respectively). *Post hoc* tests using the Bonferroni correction revealed that *Peak Response* diminished significantly from baseline to 0h and 1h after $pTUS_S$ (3372 ± 584 (baseline) *vs* 1283 ±304 (0h), $p = 0.015$; 3372 ± 584 (baseline) *vs* 1461 ± 340 (1h), $p = 0.022$, respectively). Meanwhile, the *Latency* increased significantly from baseline to 0h and 1h after $pTUS_S$ (3.27 ± 0.14s (baseline) *vs* 4.00 ±0.19s (0h), $p = 0.036$; 3.27 ± 0.14s (baseline) *vs* 4.55 ± 0.25s (1h), $p = 0.003$, respectively, see ***Figure 2.4c*** (right)). The repeated measures ANOVA also showed that the *Response Duration* (i.e., *FWHM*) differed significantly in $pTUS_E$ rats at baseline, 0 h and 1h ($F(2, 20) = 4.979$, $p = 0.018$, ***Figure 2.4d***). *Post hoc* tests revealed that $pTUS_E$ elicited a slight increase in *Response Duration* from baseline to 0 h after pTUS (1.55 ± 0.16 s vs 2.36 ±0.31 s, $p = 0.127$) though under the significance level. However, the *Response Duration* at 1h was significantly higher than that of baseline (1.55 ± 0.16 s to 2.64 ±0.34 s, $p = 0.029$). By contrast, $pTUS_S$ group did not show significant difference in *Response Duration* at baseline ($F(2, 20) = 2.360$, $p = 0.120$).

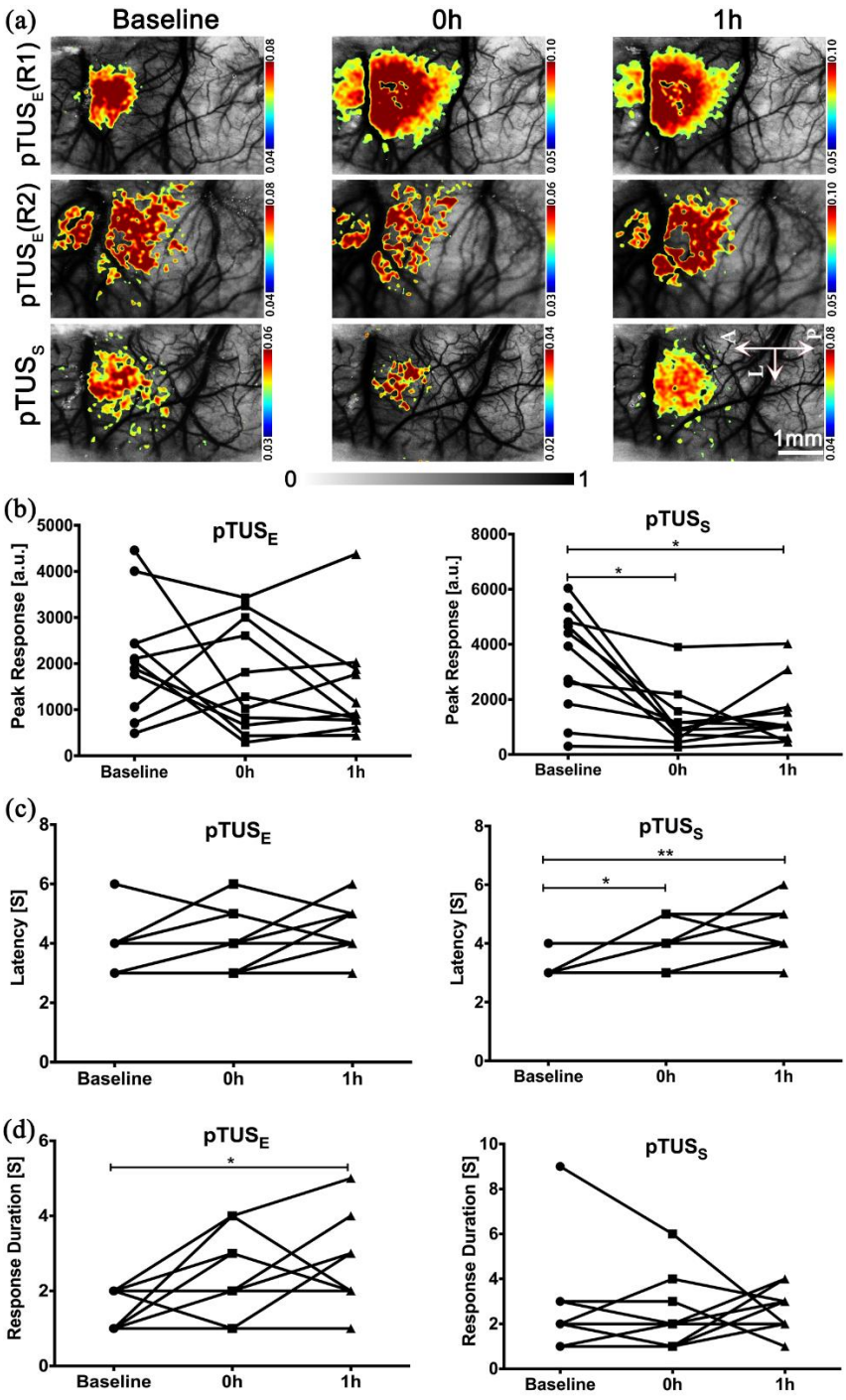

Figure 2.4 Cerebral blood flow (CBF) responses to hind-limb electrical stimulation before and after $pTUS_E$ and $pTUS_S$, respectively. (a) The strongest response of CBF during the 20s ES responses overlaid on the corresponding CBF images obtained by LSCI on the left hemisphere for three typical rats. Corresponding thresholds were calculated and applied to CBF response images. The scale bar represents 1 mm that applies to all images. "A", "L" and "P" denote the anterior, left and posterior directions, respectively. (b)-(d) Individual changes of *Peak Response*, *Latency* and *Response Duration* (i.e., *FWHM*), respectively, before pTUS (Baseline), 0 h and 1 h after ultrasound stimulation,

including both $pTUS_E$ and $pTUS_S$. Noted that in (b), each line represents one rat, while in (c) and (d), some lines overlap each other, as the corresponding *Latency* or *Responding Duration* for those rats are the same in the unit of second. "*" denotes $p < 0.05$, and "**" denotes $p<0.01$.

2.3.2 Effects of pTUS on the $CMRO_2$ response to hind-limb electrical stimulation

The $CMRO_2$ was similarly analyzed and compared between two groups at different time points (***Figure 2.5a***). The results of $CMRO_2$ were similar to those of CBF. Only the same 5 out of the 11 rats showed increased response to $pTUS_E$ (see the two typical rats in the first two rows in ***Figure 2.5a*** and the individual response in ***Figure 2.5b*** (left)). $pTUS_S$ also showed high consistency of suppression in aspect of *Peak Response* of $CMRO_2$ across all rats (***Figure 2.5b*** (right hand side)). The $CMRO_2$ response decreased at 0h and then recovered at 1h after $pTUS_S$ (see the results for a typical rat in the third row of ***Figure 2.5a***).

Repeated measures ANOVA of *Peak Response*, *Latency* and *Response Duration* (i.e., *FWHM*) in $pTUS_E$ rats did not show significant difference at baseline, 0 h and 1h after $pTUS_E$ (*Peak Response*: $F(2, 20) = 2.793$, $p = 0.085$; *Latency*: $F(2, 20) = 2.737$, $p = 0.089$; and *Response Duration*: $F(2, 20) = 0.645$, $p = 0.535$). By contrast, the *Peak Response* and the *Latency* in $pTUS_S$ rats differed significantly at selected time points (*Peak Response*: $F(2, 20) = 7.139$, $p = 0.005$ and *Latency*: $F(2, 20) = 9.556$, $p = 0.001$). *Post hoc* tests revealed that pTUSs induced a significant decrease of the *Peak Response* of $CMRO_2$ immediately (4821 ± 901(baseline) vs 2050 ± 400 (0h), $p = 0.013$) but marginal change at 1h (4821 ± 901(baseline) vs 2118 ± 568 (1h), $p = 0.079$). It is also worthy of noting that *Latency* showed a significant increase at 1h after $pTUS_S$ (2.64 ± 0.15 s (baseline) vs 3.27 ± 0.20 s (1h), $p = 0.006$).

In line with CBF results, ***Figure 2.5d*** illustrated that *Response Duration* of $CMRO_2$ in $pTUS_S$ group did not show significant difference by ANOVA ($F(2, 20) = 1.443$, $p = 0.260$).

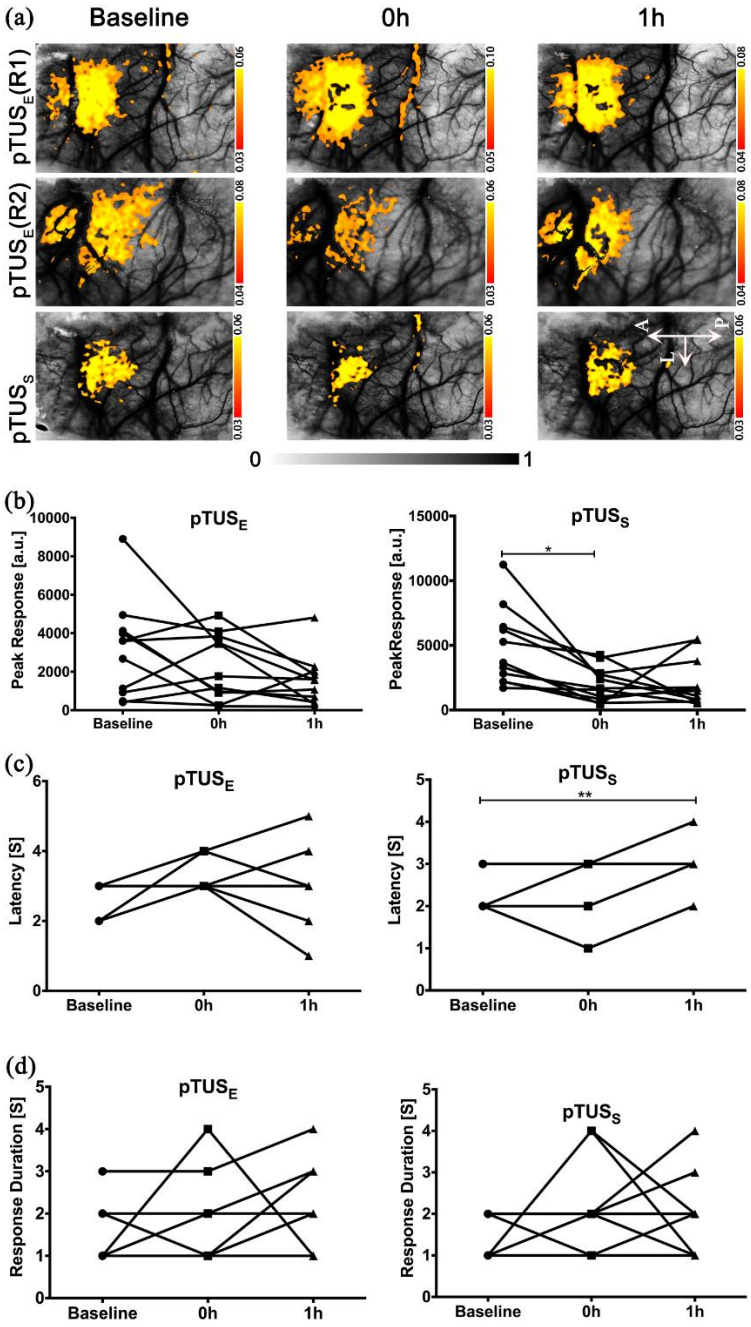

Figure 2.5 Cortical metabolic rate of oxygen ($CMRO_2$) responses to hind-limb electrical stimulation before and after excitatory and suppressive pTUS, respectively. (a) The strongest response of $CMRO_2$ during the 20s ES responses overlaid on the corresponding CBF images. Corresponding thresholds were calculated and applied to CMRO2 images. The scale bar represents 1 mm that applies to all images. "A", "L" and "P" denote the anterior, left and posterior directions, respectively. (b)-(d) Individual changes of Peak Response, Latency and Response Duration (i.e., FWHM), respectively, at baseline, 0 h and 1 h after pTUS, for both $pTUS_E$ and $pTUS_S$. Noted that in (b), each

line represents one rat, while in (c) and (d), some lines overlap each other, as the corresponding Latency or Responding Duration for those rats are the same in the unit of second. "*" denotes $p < 0.05$, and "**" denotes $p<0.01$.

2.3.3 Correlation between neuromodulatory effects of pTUS and cortical excitability at baseline

As shown in ***Figure 2.6a***, the changes of *Peak Response* (Δ_{PR}) induced by $pTUS_E$ immediately after stimulation (0 h) showed negative correlation with baseline *Peak Response* in CBF results (Pearson r = -0.67, p = 0.025), whereas $CMRO_2$ result showed marginal and negative correlation between them (see ***Figure 2.6c***, Pearson r = -0.56, p = 0.075).

For pTUSs, CBF results at 0 h also showed negative correlation between neuromodulatory effects (Δ_{PR}) and baseline *Peak Response* (see ***Figure 2.6b***, Pearson r = -0.66, p = 0.028). However, as shown in ***Figure 2.6d***, it demonstrated no correlation between neuromodulatory effects (Δ_{PR}) and baseline *Peak Response* in $CMRO_2$. As illustrated in ***Figure 2.7***, the CBF and $CMRO_2$ at 1 h after pTUS showed similar correlation between neuromodulatory effects and baseline *Peak Response* with that at 0 h.

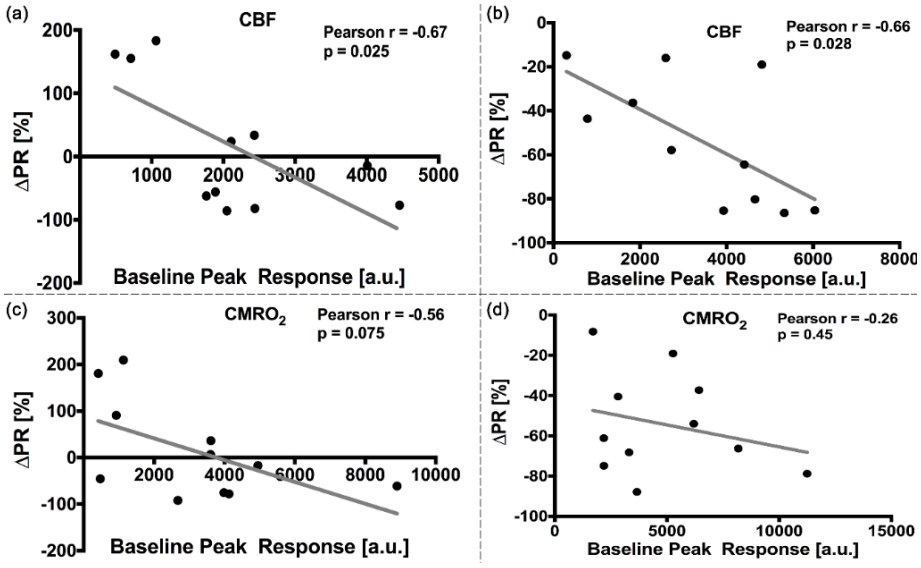

Figure 2.6 Correlation between neuromodulatory effects of pTUS (Δ_{PR}) at 0h after ultrasound stimulation and baseline Peak Response in aspects of CBF (a, b) and CMRO2 results (c, d) for $pTUS_E$ (a, c) and $pTUS_S$ (b, d), respectively.

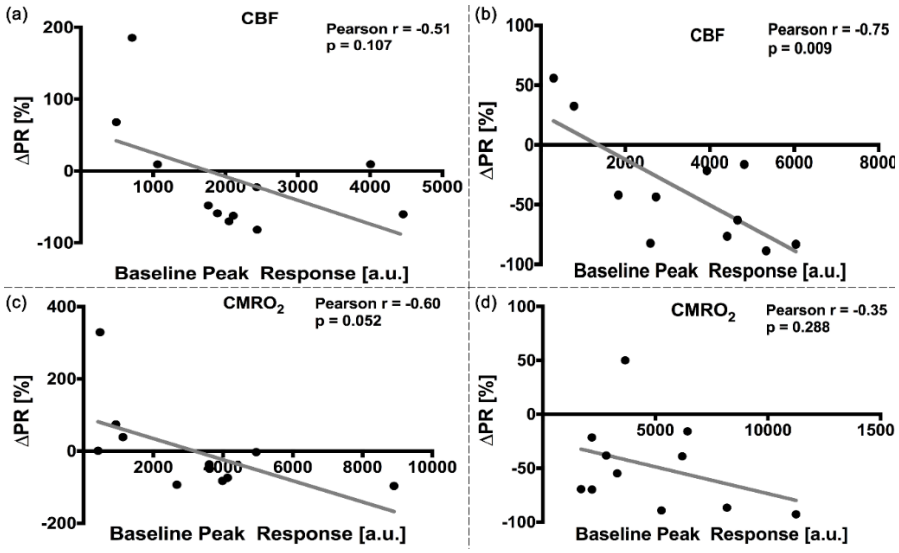

Figure 2.7 Correlation between neuromodulatory effects of pTUS (Δ_{PR}) at 1h after ultrasound stimulation and baseline *Peak Response* in aspects of CBF (a, b) and $CMRO_2$ results (c, d) for $pTUS_E$ (a, c) and $pTUS_S$ (b, d), respectively.

2.4 Discussion

In this study, the applicability of optical imaging for characterization of the excitatory and suppressive neuromodulation on primary somatosensory cortex by pTUS was examined. The hemodynamic response was considered as the manifestation of cortical (de-)activation. Increase of response amplitude and/or decrease of latency was used as an indicator to reflect the enhanced cortical excitation [131].

The results presented indicate that ultrasound exposure of the somatosensory cortex with excitatory and suppressive pTUS resulted in different end-points of the hemodynamic response to hind-limb ES. Specifically, analyzing the CBF response, it was determined that *Response Duration* was increased significantly 1 h after $pTUS_E$. In contrast, *Peak Response* and *Latency* did not show significant difference at either 0 h or 1h after $pTUS_E$. However, further examination showed that the *Peak Response* (either CBF or $CMRO_2$) only increased in 5 out of 11 rats, indicating a subject-dependent effect of $pTUS_E$. On the other hand, $pTUS_S$ treatment significantly decreased the amplitude of *Peak Response* and increased the *Latency* of CBF response in all animals. In agreement with the CBF results, $CMRO_2$ not only show

suppressive effects of $pTUS_S$ with lower *Peak Response* and longer response *Latency*, but also a subject-dependent effect of $pTUS_E$.

As noted earlier, the existence of biological variety in individual rats receiving $pTUS_E$ on primary somatosensory cortex cannot be dismissed. Similar variety effects on $pTUS_E$ in motor cortex had already been reported in other studies [77,78,132]. For instance, Younan et al. [78] reported a failure rate of ~40% in obtaining motor response after treating rats with $pTUS_E$. Such a difference in responses between $pTUS_S$ and $pTUS_E$ exposure might be explained by the 'NICE' model proposed by Plaksin and his colleagues [133]. According to this model, the cortex consists of one type of excitatory regular spiking (RS) pyramidal neurons and two types of inhibitory interneurons (i.e., low-threshold spiking (LTS) neuron and fast spiking (FS) neuron). As the LTS (low-threshold spiking) excitation threshold (in terms of I_{SPPA}) is usually much lower than that for FS or RS neurons, it is conceivable that the LTS neurons can be selectively excited with ultrasound intensity below the neurons' excitation threshold of the RS or FS. Assuming that the ultrasound stimulation is sufficiently high to activate all types of neurons (RS, LTS and FS), the net outcome might not result in "excitation" unless more than 75% neurons activated are of RS type [133]. Consequently, with the same I_{SPPA} of $pTUS_E$ and $pTUS_S$ (~8 W/cm^2 in this study), the suppressive effect for $pTUS_S$ is more likely to be achieved than the excitatory effect for $pTUS_E$. In practice, the variance of skull thickness would lead to different ultrasound attenuation, and thus individual rats may be unresponsive, or the neural activity of stimulated area was even suppressed to the given intensity of the $pTUS_E$. Additionally, as the intensity is an important variable to determine the threshold for neuromodulatory effects, parameters with different amplitude need to be examined to reveal the role amplitude plays in the neuromodulatory effects.

Further, as suggested in Section 2.3.3, the individual differences might be associated with the cortical excitability, as represented by *Peak Response*, at baseline, especially for $pTUS_E$. Specifically, rats with high cortical excitability before pTUS, i.e., baseline *Peak Response*, are more likely to be unresponsive or even suppressed (negative Δ_{PR}) to $pTUS_E$. This might serve as a protective mechanism to avoid over excitation, which could lead to excitotoxicity and cell death [134]. In the case of $pTUS_S$, the *Peak Response* change (Δ_{PR}) also showed significant negative correlation with baseline *Peak Response* before

pTUS in CBF results; however, such a negative correlation was not observed in analysis of the $CMRO_2$ results. This inconsistence may suggest that the neuromodulatory effect reflected by $CMRO_2$ has more complicated dependence on initial brain state due to the complexity of neurovascular coupling [135]. Both $pTUS_E$ and $pTUS_S$ show baseline state-dependent neuromodulatory effects, as also demonstrated in tDCS [35,136–138], which may explain the high rate of hemodynamic irresponsiveness to $pTUS_E$.

A failure rate as high as 40% in Younan et al.'s study [78] might compromise the applications of $pTUS_E$ in probing brain function or clinical translations. In the present study, optical imaging-based indicators provided direct physiologic evidence for the subject-dependent effects of $pTUS_E$ and permitted to achieve reliable perturbation of neuronal activity that is indispensable in studying the role of a specific neural circuit. The results of the experiments also suggest that interpretation of experimental results should be very guarded when using the $pTUS_E$ neuromodulation. It is likely that individualized pTUS, similarly to the individualized treatment when using TMS, should be used in pre-clinical practice to ensure consistent neuromodulation effects, especially for $pTUS_E$.

The results of this study also suggest that $pTUS_S$ may serve as a reliable neuronal silencing/suppressing technique to study the advanced cognitive function, considering its consistent suppression effect on cortical excitability across all rats. It is already established that the techniques for reversible and selective silencing of neuronal activity, for example, localized cooling, pharmacological agents and genetically encoded approaches, are useful in investigating the role of a specific neuronal population in brain [139].

Finally, the difference in the response of the cortex to electrical stimulation was also observed in both $pTUS_E$ and $pTUS_S$ experiments at 1 h after the ultrasound exposure. Similar observations were also reported by Yoo et al. [75], where $pTUS_S$ (tone burst duration = 0.5 ms, PRF=100 Hz, and I_{SPPA} = 6.4 W/cm^2 for 7-8 s) reduced VEP P30 at 2 min after stimulation, which would last for about 7 min. These results might be associated with the establishment of excitatory (AMPA) and inhibitory ($GABA_A$) synaptic connections [140] as well as synaptic plasticity [141]. However, it is not adequate to attribute the observation to the long-lasting effects of pTUS as unknown physiologic factors might also operate during this period.

2.5 Chapter conclusion

The objective of this chapter was to examine how different pTUS exposures influence the cortical excitability in response to functional electrical stimulation. Two types of ultrasound stimulation were investigated, i.e., suppressive and excitatory pTUS. The animal model (rat) was used and optical imaging techniques were employed to extract the relevant data. It was shown that pTUSs exposure down-regulated the excitability of primary somatosensory cortex in all 11 animals whereas $pTUS_E$ demonstrated the excitatory effects in only 5 rats.

Further, the results demonstrated that: (i) pTUSs could serve as a tool in investigating cognitive function by silencing the neurons in the target region; (ii) $pTUS_E$ exposure should be treated with caution due to the biological variability (e.g., animals' skull thickness and baseline cortical excitability); (iii) the response to pTUS was correlated with the initial brain state or the baseline cortical excitability of rats; and (iv) optical imaging is useful in assessing the pTUS neuromodulatory effects, especially for regions, such as primary somatosensory cortex that yield no observable behavior outputs.

As mentioned before, $pTUS_S$ and $pTUS_E$ are to be used as preconditioning for focal cerebral ischemia and treatment of depressionin subsequent Chapter 3 and Chapter 4, respectively.

Chapter 3: Pulsed TUS Preconditioning May Mitigate Focal Cerebral Ischemia in Rats

3.1 Introduction

Perioperative stroke remains one of the most serious complications induced by cardiovascular procedures [142], such as coronary artery bypass grafting [143] or carotid endarterectomy [144], resulting in increased (5.2%) rate of disability and mortality after surgery [145]. Clinically, preconditioning methods, which could increase tolerance of brain to subsequent ischemic injuries with a small dose of non-injury stimuli, have gained attention as perioperative stroke presents serious complications in patients undergoing cardiovascular surgeries [146,147]. Several neuroprotective preconditioning methods have been reported, including exposure to spreading depression [148–150], brief ischemia [151], hypoxia [152], immune activation [153], hypoperfusion [154], hyperthermia [155] and inhalation of volatile anesthetics [156]. However, due to the toxic nature and dose-dependent effects of these stimulations, preconditioning could cause unpredictable brain damage or fail to trigger the protection mechanism [157]. All these methods, as already pointed out in [157], suffer from a clinical drawback that the accurate dosage of the drugs is difficult to determine due to biological difference in subjects. Furthermore, the precise mechanisms underlying preconditioning-induced neuroprotection are still unclear, though a few reports attributed them to down-regulation of brain metabolism [110,158,159] or modulation of inflammatory pathways [160,161].

As introduced in the Chapter 1, pTUS has emerged as a promising technique for neuromodulation and treatment of neurological diseases [54,55,108,109]. This is because ultrasound in addition to being a nonionizing modality can be applied in a noninvasive and safe manner with appropriate choice of exposure parameters. For instance, it has been previously observed that 500 kHz pTUS applied at the intensity level of 86 mW/cm^2 I_{SATA} (spatial-average temporal-average intensity) and pulse repetition frequency (PRF) of 1.5 kHz is neuroprotective when applied immediately after focal brain ischemia in rats [109]. The neuroprotection after ischemic brain injury might benefit from neuromodulation via changes of brain metabolism [162]. It has been proposed that therapeutic hypothermia and ischemic

preconditioning to reduce brain metabolism could render neural tissue more tolerant to ischemia [110]. Also, ultrasound stimulation was reported to activate anti-inflammatory pathways [163–166]. In particular, the experiment in [164] indicated that preconditioning of kidneys using ultrasound could prevent renal ischemia-reperfusion injury by activating the splenic cholinergic anti-inflammatory pathway. Based on the above review, it was hypothesized that preconditioning by exposing neural tissue to suppressive pulsed transcranial ultrasound may mitigate the effects of focal cerebral ischemia or ischemic brain injury.

To test the hypothesis, both photothrombotic stroke model and laser speckle contrast imaging (LSCI) were integrated into pTUS experimental setup, which facilitated to intraoperatively monitor the spatiotemporal dynamics of cerebral blood flow (CBF) changes before and after ischemic stroke. As already indicated above, the primary somatosensory cortex of the rat brain was exposed to pTUS before the induction of photothrombotic stroke [167]. The photothrombosis model allowed targeting any cortical areas of interest in a reproducible and non-invasive manner. Li et al. [168] reported that the early reduction of CBF was highly correlated to the severity of ischemic brain injury, and thus could serve as a prognostic marker of stroke [169]. On the other side, LSCI has been widely adopted for CBF imaging non-invasively with high spatiotemporal resolution [127], in the scale of a few μm and ms. Therefore, CBF was recorded by LSCI at various time points to study the influence of pTUS on cerebral hemodynamics during and after the photothrombosis induction. By utilizing CBF imaging and histologic analysis of brain slices, we assessed the ischemic tolerance induced by pTUS preconditioning, and its neuroprotective effect up to 48 hours after photothrombosis.

3.2 Methods

3.2.1 Experimental system

The experimental system is shown in ***Figure 3.1a***. The setup included pTUS generators, photothrombosis induction system and LSCI module. The transducer of pTUS and the 532 nm (typically used wavelength for photoactivation) laser diode (Model: 13216-620, Forward Optoelectronics Co. Ltd., Shanghai, China) were mounted using custom-designed adapters onto the manipulator arms of the

stereotaxic frame (Model 68006, RWD Life Science Inc. Shenzhen, China), allowing precise (< 0.1 mm) control of the pTUS and photothrombosis induction on the brain. An iris diaphragm was connected to the 532nm laser diode to generate 1.5-mm diameter beam. The 780nm laser diode (L780P010, Thorlabs, USA), CMOS camera (DCC1545M, Thorlabs, USA) and a camera lens (60mm f/2.8G ED, Nikon, Japan) of the LSCI system were positioned by the holders mounted on the optical table. A band-pass filter (780 ±10nm, FL780-10, Thorlabs, USA) was positioned between the CMOS camera and lens to exclude light outside 780 nm wavelength of imaging laser.

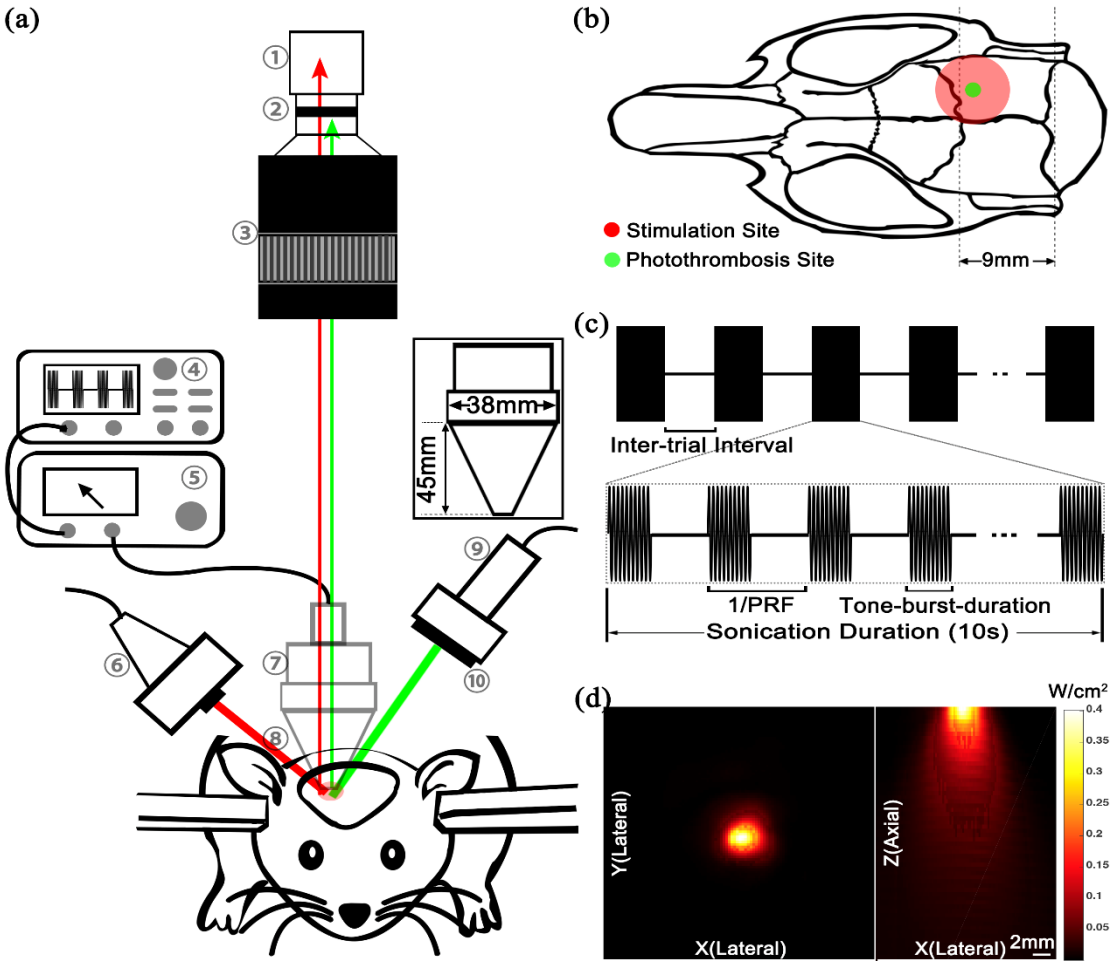

Figure 3.1 Overview of the experimental system and pTUS parameters. (a) Schematic of the entire experimental system. The transducer was illustrated translucently as it would be removed after ultrasound stimulation to avoid interference with camera and 532-nm laser modules. Red and green light beams represented the optical path of 780-nm and 532-nm lasers, respectively. Components: ①CCD Camera, ②Band-pass Filter, ③Camera Lens, ④Function

Generator (X2), ⑤RF Amplifier, ⑥780nm Laser Diode, ⑦Ultrasound Transducer, ⑧Acoustic Collimator, ⑨ 532nm Laser Diode, ⑩Iris Diaphragm. (b) The location and areas of ultrasound stimulation and illumination by the 532-nm laser. (c) Parameters for the pTUS, where inter-trial interval was 10 s, PRF equaled to 100 Hz and Pulse Duration was 0.5 ms. (d) Lateral (Left) and axial (Right) acoustic spatial-peak-temporal-average intensity (I_{SPTA}) maps.

As shown in ***Figure 3.1a***, the pTUS waves were produced by an immersion-type ultrasound transducer (V301-SU, Olympus NDT, Waltham, USA) operating at 0.5 MHz, which was chosen based on the study in [109]. Two identical function generators (AFG3022B, Tektronix, USA) were used to generate pulsed signals or tone bursts (***Figure 3.1c***). Before activating the transducer, the pulse signals were amplified using a radio frequency (RF) amplifier with adjustable gain (Custom designed, HGX100, Nanjing, China). As shown in the inset panel in ***Figure 3.1a***, a custom-designed acoustic collimator (7 mm diameter output aperture) made of plexiglass was coupled to the ultrasound source so that the stimulated brain regions of the rats were confined to the area of interest (see ***Figure 3.1b***).

The hemodynamic changes were assessed by LSCI. Fundamentals and intraoperative monitoring techniques of LSCI have been well documented [113,123] (also see Eq. (2.1)).

3.2.2 Ultrasound field measurement and simulation

The measurement and simulation of ultrasound field was done at the Ultrasound & Wound Healing Lab of Drexel University. Specifically, the ultrasound field distribution was measured using a calibrated hydrophone (TC4038-1, Teledyne RESON A/S, Slangerup, Denmark) mounted onto the 3D ultrasound intensity measurement system (Model ASTS-01, NTR Systems Inc., Seattle, WA, USA) (see ***Figure 3.1d***). The finite element analysis (FEA) was performed using COMSOL software to verify the measured ultrasound field and investigate how the collimator interfered with the ultrasound transmission.

As shown in ***Figure 3.2***, the results of the FEA are consistent with the measured ultrasound field illustrated in ***Figure 3.1d***, in both distribution and I_{SPTA} amplitude of the ultrasound thereby verifying the results of measurements. Specifically, the simulated I_{SPTA} is 578 mW/cm^2 whereas the measured I_{SPTA} is 402 mW/cm^2. Additionally, compared with the measured distribution of free ultrasound field, FEA also

suggested that the collimator not only increased the spatial resolution of ultrasound output, but also boosted the amplitude of ultrasound (on the order of 4) due to the reflection and interference inside it.

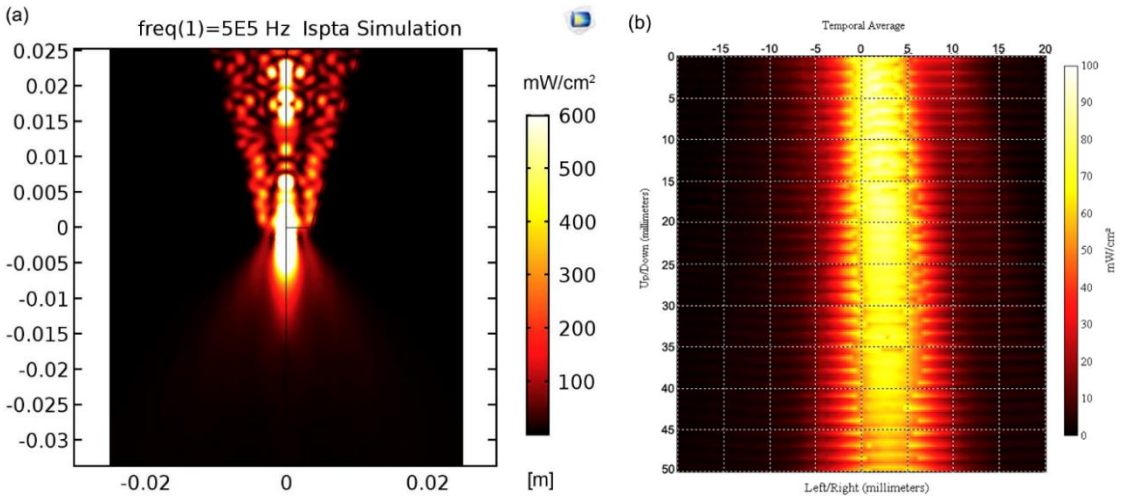

Figure 3.2 (a) Results of the FEA are consistent with the measured ultrasound distribution. (b) Acoustic distribution of free ultrasound field without collimator.

3.2.3 Animal preparation

All animal experiments in this study were approved by the Animal Care and Use Committee of Shanghai Jiao Tong University. Twenty-six adult male Sprague-Dawley rats (320 ± 20g, Slac Laboratory Animal Co. Ltd., Shanghai, China) were randomly assigned to pTUS-PC group (n = 14) or control group (n = 12). The sample size was determined using the methods in [129] so it yielded statistical power of 80%. The imaging cranial window was prepared 24 hours earlier. Each rat was anesthetized with an intraperitoneal injection of 7% chloral hydrate (5 ml/kg). During the surgery, the rats were constrained in a stereotaxic frame and the rectal temperature was monitored and maintained at 37 ± 0.2 ℃ with a heating pad and a direct current (DC) control module (FHC Inc., Bowdoinham, USA). All procedures were performed under standard sterile precautions. After being shaved, the rat's scalp was incised along the midline and the exposed tissues were carefully cleaned with a scalpel to expose the skull. A 10.0 mm (horizontal) × 8.0 mm (vertical) cranial window centered at 3.5 mm posterior to the bregma was then

thinned by a high speed (about 10000 rpm) dental drill (Strong 90 Micro Motor, Saeshin Precision, Korea) with ∅ 1.4 mm steel burr until the cortical vessels were clearly visible. The rats were then caged with sufficient supply of food and water for 24 hours to eliminate the influence of the anesthetics.

3.2.4 pTUS preconditioning and photothrombotic stroke experiments

After 24-hour recovery, all rats were anesthetized with isoflurane (5.0% initial and 1% to 1.5% for maintenance) and mounted on the stereotaxic frame. Then the pTUS-PC group was exposed to ultrasound treatment for 60 min so as to compare with the experiments in [109]. Also, based on the sonication parameters that have been proved suppressive both experimentally [74,75] (also see the Chapter 2) and theoretically [112], the pTUS parameters used in this work were: I_{SPTA} = 402 mW/cm^2, frequency (f) = 0.5 MHz, pulse repetition frequency (PRF) = 100 Hz, and duty cycle (DC) =5%.

The ultrasound exposure was software-controlled: A 10s single sequence, i.e., 1000 tone burst was repeated 180 times at 10s intervals and delivered to the rat cortex before the induction of photothrombotic stroke. The stimulation site and the protocols are shown in ***Figure 3.1b*** and ***Figure 3.1c***, respectively. The control group was handled identically to the pTUS-PC group, with the exception of the ultrasound stimulation; the animals were also administrated with isoflurane to rule out the potential influences of anesthetics.

Next, both control and pTUS treated cohorts underwent the same photothrombotic procedures to regionally occlude cortical surface vessels over the right primary hind-limb somatosensory cortex. Briefly, Rose Bengal dye (80 mg/kg, Sigma-Aldrich Co. LLC., St. Louis, Missouri) was injected intravenously into the tail vein. Photoactivation was initiated by illumination at the selected location using the 532 nm laser for 10 min. The 532 nm laser beam and the center of acoustic collimator were located at 1.3 mm posterior and 3.0 mm lateral to the bregma over the right hemisphere, referring to *The Rat Brain in Stereotaxic Coordinates* [170]. Laser speckle images were acquired for half an hour at 1 minute intervals, starting right before the illumination. At each time point the cerebral blood flow was assessed by collecting 320 images (640 × 640 pixels, 4.65 μm/pixel) at 50 fps (exposure: 5 ms). The rats were then sent back to their home cages with sufficient supply of food and water. At 24 and 48 hours after the photothrombosis, CBF was also evaluated in anesthetized rats before the rat was euthanized for the

histologic analysis as well as the infarct volume and brain swelling.

3.2.5 LSCI (laser speckle contrast imaging) data processing

It was shown previously that cerebral blood flow within the ischemic core in photothrombosis model fell between 20% and 30% of the baseline [171]. Therefore, to characterize the size of ischemic core, ischemic areas R_{20}, R_{25} and R_{30} were defined as areas with CBF decreasing to less than 20%, 25% and 30% of the baseline level, respectively. The spatiotemporal development of cerebral ischemia as ascertained in each individual animal was subsequently determined. Similarly, the 'ischemic core', defined by R_{20}, R_{25} or R_{30}, at 24 and 48 hrs after photothrombosis was calculated. At every time point, the mean value of cerebral blood flow in the unaffected contralateral hemisphere was used as the corresponding baseline.

3.2.6 Histological analysis

All rats were euthanized 48 hours after the photothrombosis. The brains were then carefully removed and sectioned coronally into six 2-mm thick slices with brain matrices (Model 68710, RWD Life Science Inc., Shenzhen, China). All brain slices were stained using 2% 2,3,5- triphenyltetrazolium chloride (TTC, Sigma-Aldrich Co. LLC, St. Louis, Missouri, USA) at 37 ℃ for 15 minutes in the dark. ImageJ (Ver. 1.49, National Institutes of Health) was used to determine the ischemic areas of the contralateral hemisphere (C_i), ipsilateral hemisphere (I_i), and the non-ischemic ipsilateral hemisphere (N_i) in the i^{th} slice on both sides. The infarction volume (V) was calculated using Eq. (3.1) [172]:

$$\mathrm{V}\ (\%) = 100 \times \sum_i \left(\left(\frac{I_i - N_i}{I_i} \right) C_i \right) / (2 \sum_i C_i). \tag{3.1}$$

In addition, the cerebral edema after focal stroke was also measured by assessing the change in the affected hemisphere (CIH) compared with the contralateral hemisphere in each brain slice [173]:

$$\mathrm{CIH}\ (\%) = 100 \times \left(\frac{\sum (I_i - C_i)}{\sum C_i} \right). \tag{3.2}$$

3.2.7 Statistical analysis

All statistical analysis was carried out with SPSS software (Ver. 24.0, SPSS Inc., Chicago, USA). One-sample Kolmogorov-Smirnov test was used to test the normal distribution of the results. Once the normal distribution was confirmed, two-tailed unpaired Student's t-test was used to compare R_{20}, R_{25} and R_{30} at each time point, infarct volume and brain edema for the two groups respectively. Recovery from 24 to 48 hr in each group was analyzed by two-tailed paired Student's t-test. The correlation between R_{20}, R_{25}, R_{30} and infarct volumes was then tested with regression analysis. Significance level was set at $p < 0.05$, and all data were expressed as mean $\pm$ S.D.

3.3 Results

3.3.1 Delayed and alleviated hemodynamic compromise during photothrombosis

Two-dimensional CBF images demonstrated the development of ischemia during and immediately after photothrombosis (***Figure 3.3a***). Compared with the control group, the pTUS-PC group (top images) showed that the ischemia affected area was smaller than the one observed in the sham (control) group (the 2nd row of images). It was also noted that substantial ischemia did not appear in the pTUS-PC group until four minutes after light exposure, while ischemia was observable at the first minute after the photothrombosis was induced in the control group. Such a cohort difference was consistent among all rats**.**

Quantitative analysis of the ischemic areas R_{20}, R_{25}, and R_{30} also confirmed that the ultrasound treatment delayed (by approximately 3 minutes) and alleviated hemodynamic compromise in the pTUS-PC group. First, R_{25} (0.24 ± 0.30 mm^2 vs. 0.66 ± 0.57 mm^2, $p=0.037$) and R_{30} (0.51 ± 0.52 mm^2 vs. 1.27 ± 0.90 mm^2, $p=0.02$) were significantly less in the pTUS-PC group than that in the control group at the 3rd minute. R_{20} also exhibited the same trend, though with a marginal significance (0.09 ± 0.14 mm^2 vs. 0.24 ± 0.25 mm^2, $p=0.079$), which may be attributed to the high variance or small size of the samples. These results concurred with the later and weaker development of ischemia in the pTUS-PC group in aspect of CBF change (***Figure 3.3a***). The pTUS-PC group also presented a slower (see ***Figure 3.3b***) increase of ischemic areas in comparison with the control group during the formation of thrombosis. As

a result, the pTUS-PC group had significantly lower ischemic areas in the post-photothrombosis stage from the 10th to the 30th minute (***Figure 3.3b***), indicating the protective effects of the preconditioning ultrasound treatment.

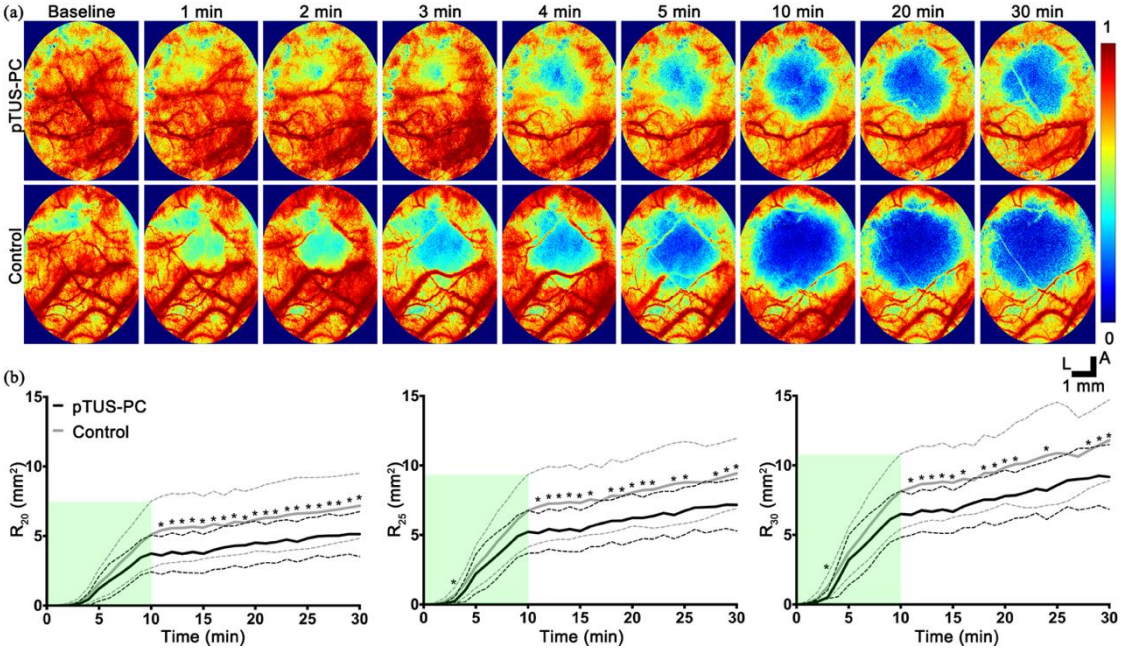

Figure 3.3 Progression of ischemia induced by photothrombosis. (a) CBF images of the ipsilateral hemisphere cortex before (baseline) and 1, 5, 10, 20 and 30 min after illumination initiation. "A" and "L" denote the anterior and left directions, respectively. (b) Changes of R20, R25 and R30 over 0 to 30 min in each group. The translucent green bar represents the period of illumination of 532-nm laser. R20, R25 and R30 were defined as areas where CBF declined to less than 20%, 25% and 30% of their baseline values, respectively. "pTUS-PC" represents the transcranial ultrasound preconditioning group. "*" denotes the statistical significance of $p < 0.05$. Thick lines represent the mean measures for the two groups respectively, and error bars indicate standard deviation of the mean.

3.3.2 Improved CBF restoration 24 and 48 hours after photothrombosis

Six rats that did not survive within the 48 hours after the operation of photothrombosis model were excluded in the following analysis. Specifically, two rats died in pTUS-PC group (one died within 24 hr and the other one died between 24 and 48 hr), whereas four died in control group (two died within 24 hr and the other two died between 24 and 48 hr).

CBF images (***Figure 3.4a***) at either 24 hr or 48 hr were significantly different between two groups, so were the CBF changes from 24hr to 48hr. At either time point, lesion area in pTUS-PC group was significantly smaller than that of control group except the R_{20} at 24hr (***Figure 3.4b*** and ***Table 3.1***, R_{20}@24hr: 10.58 ± 0.92 mm^2, n=13 (pTUS-PC) vs 13.94 ± 1.48 mm^2, n=10 (Control), p=0.058; R_{25}@24hr: 14.01 ± 0.96 mm^2, n=13 (pTUS-PC) vs 17.85 ± 1.51 mm^2, n=10 (Control), p=0.036; R_{30}@24hr: 16.68 ± 1.02 mm^2, n=13 (pTUS-PC) vs 20.79 ± 1.58 mm^2, n=10 (Control), p=0.033; R_{20}@48hr: 8.76 ± 1.36 mm^2, n=12 (pTUS-PC) vs 13.97 ± 1.12 mm^2, n=8 (Control), p=0.014; R_{25}@48hr: 11.45 ± 1.31 mm^2, n=12 (pTUS-PC) vs 17.13 ± 1.05 mm^2, n=8 (Control), p=0.006; R_{30}@48hr: 13.67 ± 1.30 mm^2, n=12 (pTUS-PC) vs 19.50 ± 1.11 mm^2, n=8 (Control), p=0.005). And pTUS-PC rats also showed significant recovery in all CBF measures while controls group did not (***Figure 3.4c*** and ***Table 3.1*,** **pTUS-PC Group:** R_{20}: 8.76 ± 1.36 mm^2 (48hr) vs 10.58 ± 0.92 mm^2 (24hr), p=0.009; R_{25}: 11.45 ± 1.31 mm^2 (48hr) vs 14.01 ± 0.96 mm^2 (24hr), p=0.001; R_{30} : 13.67 ± 1.30 mm^2 (48hr) vs 16.68 ± 1.02 mm^2 (24hr), p=0.001; **Control Group:** R_{20} : 13.97 ± 1.12 mm^2 (48hr) vs 13.94 ± 1.48 mm^2 (24hr), p=0.243; R_{25} : 17.13 ± 1.05 mm^2 (48hr) vs 17.85 ± 1.51 mm^2 (24hr), p=0.097; R_{30} : 19.50 ± 1.11 mm^2 (48hr) vs 20.79 ± 1.58 mm^2 (24hr), p=0.050).

Table 3.1 Ischemic areas of control and pTUS-PC groups at 24 h and 48 h.

	Groups	R_{20} (mm^2)	R_{25} (mm^2)	R_{30} (mm^2)
24 h	Control	13.94 ± 1.48	17.85 ± 1.51	20.79 ± 1.58
	pTUS-PC	10.58 ± 0.92	14.01 ± 0.96	16.68 ± 1.02
48 h	Control	13.97 ± 1.12	17.13 ± 1.05	19.50 ± 1.11
	pTUS-PC	8.76 ± 1.36	11.45 ± 1.31	13.67 ± 1.30

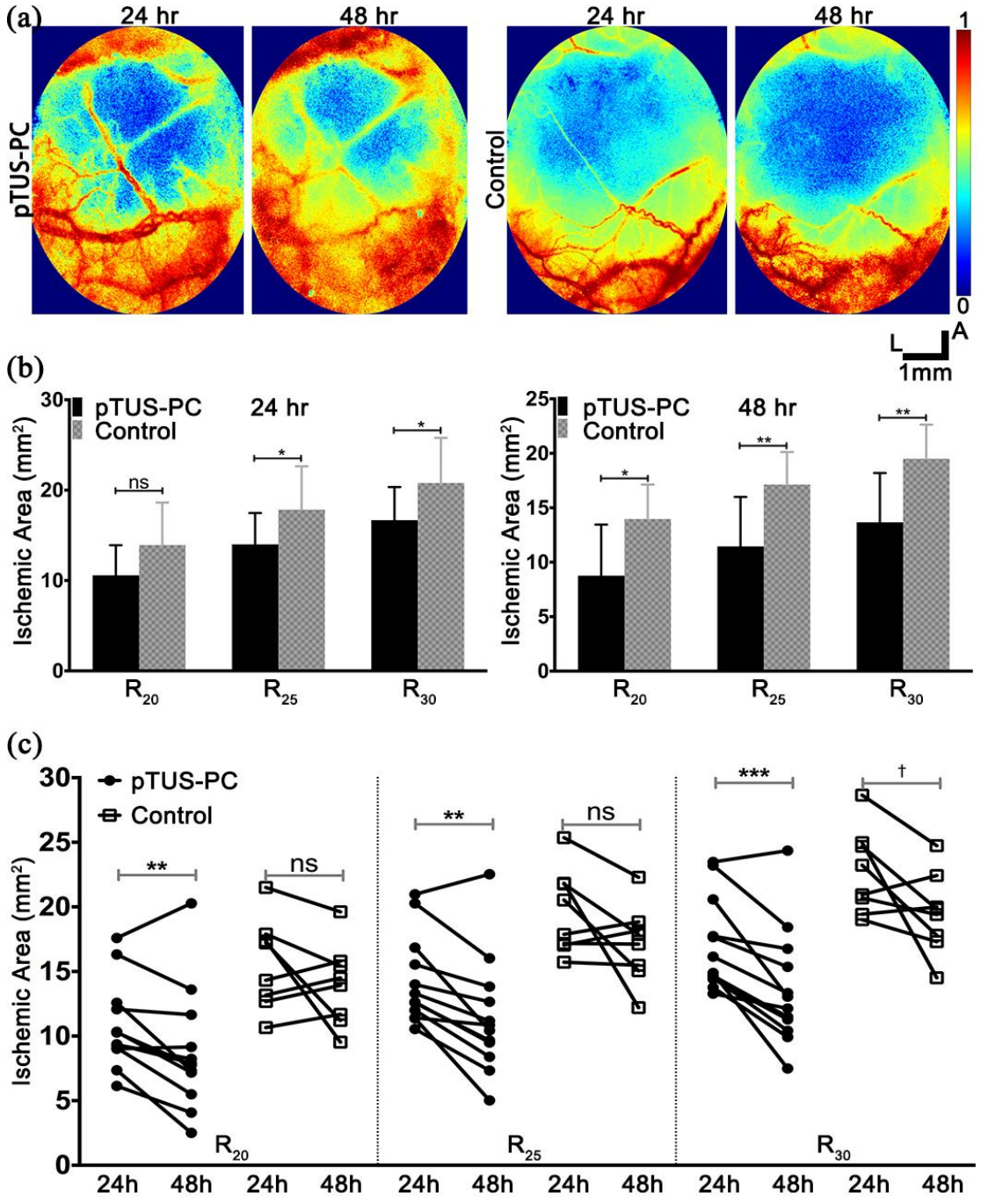

Figure 3.4 The changes of ischemic areas at 24 and 48 hr. (a) CBF images at 24 and 48 hr of the same areas as those in ***Figure 3.3*** (a). (b) R_{20}, R_{25} and R_{30} in each group at 24 and 48 hr. (c) Changes of R_{20}, R_{25} and R_{30} between 24 (left) to 48 hr (right) linked by line for each rat in each group. "ns" denotes no statistical significance ($p>0.05$), "*" denotes $p < 0.05$, "**" denotes $p<0.01$, "***" denotes $p<0.001$ and "†" denotes marginal significance. Note that the actual p-values for R20, R25 and R30 are 0.0087, 0.0012 and 0.0006, respectively, while the p-values reported in main text were approximated to 3 decimal places.

3.3.3 Improved histological outcomes – infarct volume and brain edema

The infarct volume and brain edema were determined using the TTC-stained brain sections as shown in ***Figure 3.5b***. Animals subjected to ultrasound preconditioning had significantly lower infarct volumes than those of control animals (1.770 ±0.169%, n=12 vs. 3.215 ±0.401%, n=8, p=0.0014; ***Figure 3.5a(i)***). Likewise, the pTUS-PC group also had significantly lower ipsilateral brain hemisphere volumes, i.e., alleviated brain edema, compared with the control group (6.658 ±1.183%, n=12 vs. 12.48 ±1.386%, n=8, p=0.005; ***Figure 3.5a(ii)***).

To validate the R_{20}, R_{25}, and R_{30} as indicators of ischemia severity, we examined their correlation with the corresponding infarct volumes at 48 hr in both groups. In line with [168], all ischemic area measures (R_{20}, R_{25}, and R_{30}) showed close correlation with infarct volumes at 48 hr (R_{30} - see ***Figure 3.5c***; Pearson r = 0.58, p = 0.01 for R_{20} and Pearson r = 0.59, p = 0.01 for R_{25}).

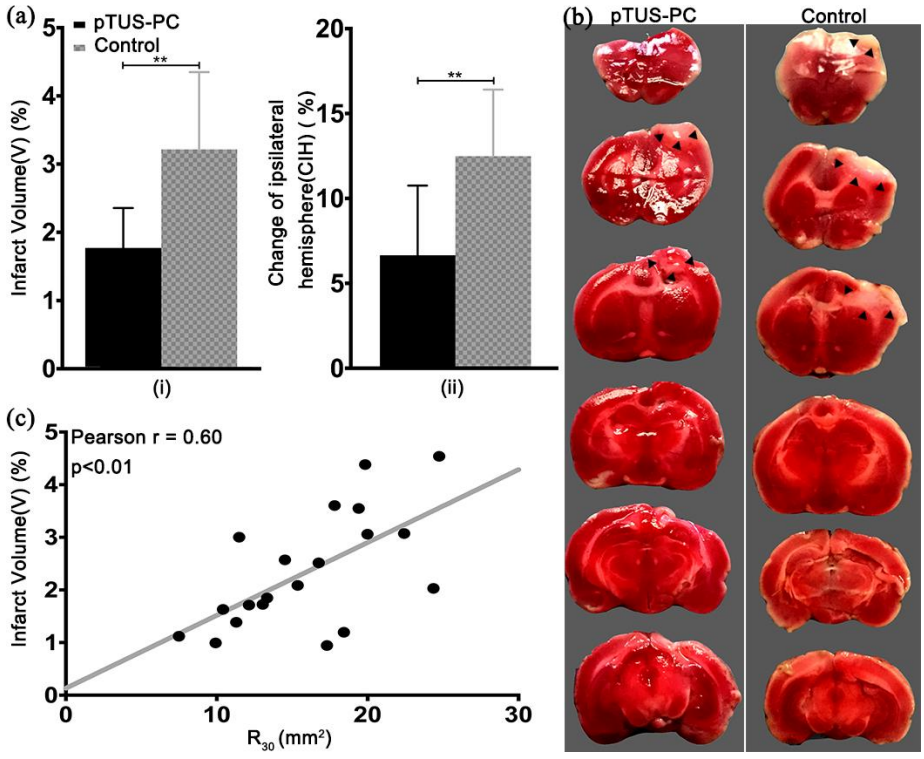

Figure 3.5 Histological outcomes. (a) Infarct volumes (i) and Ipsilateral hemisphere volumes (ii) in each group. "**" denotes p<0.01. (b) Representative brain sections in each group. (c) Correlation between R_{30} at 48 hr and the corresponding infarct volumes.

3.4 Discussion

Rats exposed to pTUS before the ischemic stroke had exhibited lower infarct and edema volume than the controls, implying that pTUS preconditioning could be neuroprotective; specifically, it is able to delay and reduce hemodynamic compromise. Furthermore, CBF during and after photothrombosis was studied using LSCI to reveal the mechanisms of preconditioning pTUS. LSCI-based indicators R_{20}, R_{25} and R_{30} were used to assess the development of the ischemia core, and results showed that preconditioning pTUS exposure delayed and decreased the hemodynamic compromise. LSCI proved to be an effective tool for assessing the severity of ischemia at different time points, i.e., 24 hr and 48 hr.

Our experiments provided the first in-vivo demonstration that pTUS preconditioning could assuage subsequent focal cerebral ischemia, and such neuroprotection was associated with the alleviated infarctions and CBF restoration. It is plausible that such an improved blood supply to penumbra could rescue these neurons from subsequent necrosis [174].

Nevertheless, the underlying mechanisms of the neuroprotection induced by ultrasound exposure are still insufficiently clarified; in this context, it had been noted that angiogenesis and anti-inflammation are often suggested as the two possible mechanisms for neuroprotection by the ultrasound exposure.

However, several experiments [175,176] suggested that low intensity (I_{SPTA} = 151-193 mW/cm^2 in study [175] and I_{SPTA} = 300 mW/cm^2 in study [176]), pulsed (PRF =7.1kHz in study [175] whereas PRF was not provided in [176]) ultrasound delivered at the frequency of 1.875 MHz [175] or 1MHz [176] could promote the angiogenesis, with a repetitive ultrasounic exposure up to 14 days. Similarly, effective anti-inflammatory pTUS required up to hours of (24 hours in [164]) application. Thus, neither angiogenesis nor anti-inflammatory mediators are likely to be the underlying mechanisms for neuroprotection due to the relatively short (1 hour) sonication time in this experiment.

On the other hand, based on the CBF manifestation (see sections ***3.3.1*** and ***3.3.2***), the neuroprotection of pTUS was likely to be related to the release of endothelial nitric oxide (NO) and metabolic depression. Indeed, ultrasound (e.g., 2.5 MHz, 2 MPa peak pressure in [177] and 1.05-MHz, 0.35-1.3 MPa in study [178]) has been reported to be capable of promoting the formation and release of endothelial nitric oxide

(NO) within several (15 and 2 in [177] and [178], respectively) minutes of sonication. Hence, the improved blood supply observed here (see section 3.1 and 3.2) might be associated with the production of endothelial NO, which could alleviate the development of thrombus by promoting tissue perfusion and preventing the platelet adhesion [179–182]. Unfortunately, the level of cellular NO was not directly measured during the experiment.

Also, metabolic depression resulting from non-ultrasound preconditioning (e.g., due to hypoxia and deep hypothermia (<25℃), as used in clinical practice during high-risk surgeries such as coronary artery bypass) has been proposed as a possible mechanism for neuroprotection [110]. The results in [110] suggested that the brain tissue was more tolerant to ischemic events by suppressing the metabolic activity, which in turn protected neurons from the subsequent ischemic insults. In our experiment, suppressive pTUS was applied by referring to the sonication parameter in [112] and [75]. Since $pTUS_S$ could down-regulate brain metabolism within a relatively short period of time (e.g. ~9 sec [75]), it was speculated that neuroprotective pTUS preconditioning could promote the ischemic tolerance through metabolic depression of the brain.

Collectively, our results demonstrated that $pTUS_S$ preconditioning could alleviate ischemic lesions by promoting the CBF, however, this study did not deliver an unequivocal answer to the underlying mechanisms in the ultrasound-induced blood flow changes. Thus, as also underscored in the next chapter, further studies are needed to elucidate the mechanism(s) in the neuroprotection induced by pTUS preconditioning.

3.5 Chapter conclusion

In this chapter, it was demonstrated that preconditioning $pTUS_S$ could mitigate ischemic injury, in a synergistic manner, by reducing blood supply compromise, which is possibly mediated by anti-thrombosis of endothelial NO, or down-regulating brain metabolism. LSCI revealed the alleviated hemodynamic compromise and improved CBF (cerebral blood flow) restoration caused by the prior ultrasound exposure. These findings indicate that ultrasound treatment constitutes a potential noninvasive and novel procedure for patients with high risk of brain ischemia, for instance, patients undergoing

cardiovascular surgery or those with signs of subarachnoid hemorrhage or transient ischemic attack (TIA). Nevertheless, additional experiments are desirable to fully elucidate the underlying mechanisms before the clinical translations of pTUS.

Chapter 4: Antidepressant-like Effects in a Rat Depression Model by Low-frequency pTUS[1]

4.1 Introduction

Depression, also referred to as major depressive disorder or clinical depression, is a common mental disorder with devastating symptoms including depressed mood, loss of interest or pleasure, executive dysfunctions, psychomotor retardation, suicide ideation, and eating and sleep disturbances [183,184]. Globally, more than 300 million people of all ages suffer from depression [185]. In addition, depression is also a life-threatening disorder as American Association of Suicidology reported that depression is presented in at least 50% of all suicides. Currently, there are mainly three types of treatments: pharmaceutics, psychotherapy and physical therapy by brain stimulation. Despite the remarkable increase of antidepressant medications as the initial main treatments in depression, therapeutics are still plagued by inadequate response in 10-30% of depression patients, which are termed as medicine-resistant [186,187].

For those patients with medicine-resistant depression, brain stimulation methods have been utilized as alternative therapies, including electroconvulsive therapy (ECT), vagus nerve stimulation (VNS), deep brain stimulation (DBS), and transcranial magnetic stimulation (TMS) [188–191]. However, ECT may cause side effects on cognition, VNS and DBS needs invasive implant surgery and TMS has limitation in spatial resolution and lack of penetration depth[192].

As discussed in previous chapters, compared with transcranial direct current stimulation (tDCS) and TMS, pTUS is a promising non-invasive alternative with better spatial resolution and penetration depth for neuromodulation in both basic and clinical neurosciences. At low intensity, pTUS can both activate and suppress neuronal activity via non-thermal effects (see section 5.2 "*Mechanisms underlying neuromodulatory effects of pTUS*") without irreversible damage [193]. As for its potential applications,

[1] The work described in this chapter is from the collaboration with Dr. Shengtian Li's group, also with contributions from Daqu Zhang. She also measured the level of hippocampal BDNF by western blot and assessed the safety of 2-week pTUS by histologic analysis.

recent studies have reported therapeutic effects of pTUS in ischemic brain injury [194,195], epilepsy [196], and Alzheimer's disease [108,197]. Inspired by these encouraging results, Tsai hypothesized that pTUS might be a potential therapeutic strategy for depression [198]. However, it still needs solid experimental studies to test those hypotheses, thereby verifying whether pTUS could serve as treatment for depression.

A large body of evidence over the past decade has demonstrated the involvement of brain-derived neurotrophic factor (BDNF) in the pathophysiology of depression and its alleviation [114,115]. BDNF serves as a major neuronal growth factor in the brain, regulating neurogenesis, neuronal maturation and survival, as well as synaptic plasticity [199]. Depressed patients and suicide subjects have demonstrated decreased levels of BDNF in brain as well as blood [200,201], whereas depression treatment could reverse the reduction of BNDF [202]. Additionally, Sakata et al. reported that increased neuronal activity promoted activity-dependent BDNF expression, which in turn induced neuronal activity to maintain active brain functions [111,203]. Therefore, these findings suggested that: 1) any disruption in the activity-dependent BDNF expression would lead to decrease in neuronal activity, which could in turn induce depression; 2) promotion of neuronal activity and function in target brain regions might alleviate depression by increasing the activity- dependent BDNF (see ***Figure 4.1***) [204,205].

On the other side, recent animal studies demonstrated that pTUS, which increased neuronal activity with appropriately selected parameters, could elevate BDNF expression in hippocampus [54] and significantly promote the neural proliferation in the dentate gyrus of the dorsal hippocampus [116]. These findings suggest an intriguing hypothesis that pTUS might be able to alleviate depression symptoms by promoting the BDNF level and neurogenesis. Additionally, pTUS has been reported to induce temporary and reversible blood-brain barrier (BBB) disruption, which allows antidepressants to reach the targeted region of brain[64], thereby increasing the efficacy of pharmaceuticals to treat depression. Note that the study in this chapter investigated the therapeutic effects of pTUS without application of antidepressants.

Researchers have achieved antidepressant outcomes using brain stimulation techniques, e.g., TMS, by targeting specific brain circuits such as prefrontal cortex (PFC), hippocampus and other limbic structures in reward and affective circuitry [206]. Among these regions, pTUS could easily target and

stimulate PFC, without attenuation of ultrasound waves when penetrating brain tissues to reach deeper structures [54]. In addition, accumulating clinical evidence have demonstrated the efficacy and safety of TMS to the left PFC of depression patients [207]. Thus, pTUS was applied to the left prefrontal cortex (PFC) [208] to study its therapeutic effect on depression in a rodent model.

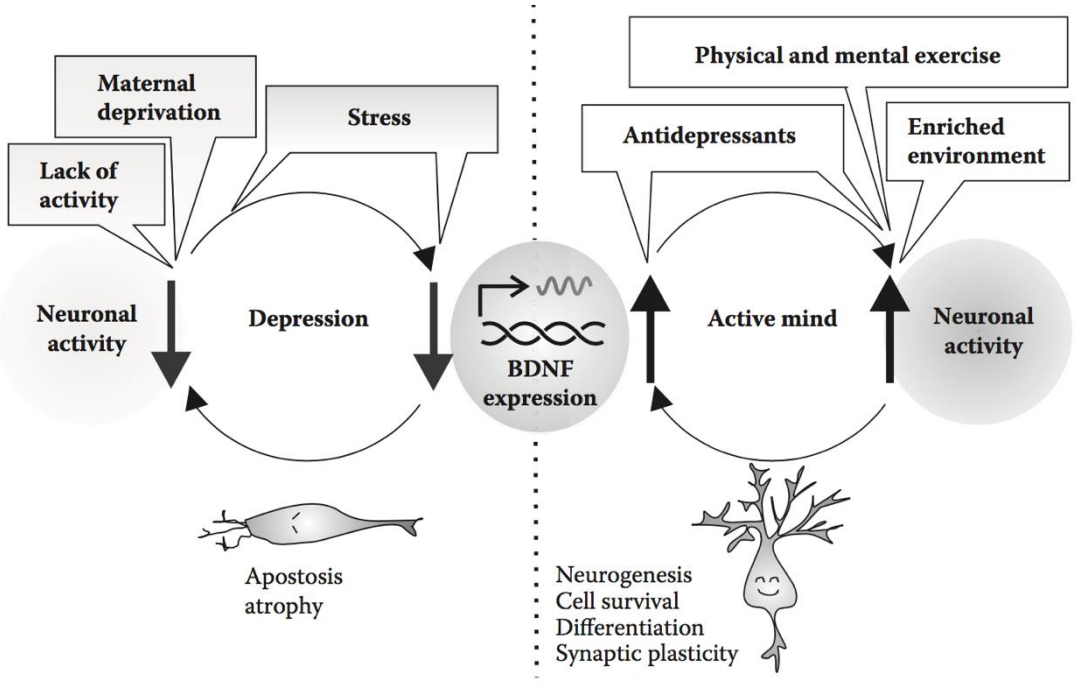

Figure 4.1 The role of activity-dependent BDNF plays in pathophysiology and treatment of depression. This figure was modified from REF. [205]

Based on the above review, this study, which was from the collaboration with Dr. Shengtian Li's group, also with contributions from my lab-mate, Daqu Zhang, aimed to investigate the potential antidepressant-like effects of pTUS in a 48-hour-restraint rat model. Making use of the created depression model and a set of behavioral tests, we investigated the antidepressant-like effects of pTUS in a controlled study where we applied pTUS to one groups. It was also examined whether the effect of the rat model lasted during treatment to exclude spontaneous remission. Additionally, Daqu Zhang measured the level of hippocampal BDNF by western blot, which is an analytical technique to separate and identify proteins,

to test hypothesized mechanisms underlying antidepressant-like effects of pTUS. Furthermore, she assessed the safety of 2-week pTUS by histological analysis.

4.2 Methods

4.2.1 Experimental Design

Figure 4.2 illustrated the animal grouping and protocols in the experiment. Before experiments, rats acclimated at cages for 10 days. Sucrose preference test (SPT), or pre-SPT hereafter was then performed in all rats to obtain the baseline of anhedonia before the restraint. Based on the pre-SPT results, rats were divided into three groups with similar distribution of sucrose preference index (*SPI)*, which is defined as:

$$SPI = \frac{Sucrose\ Consumption}{Total\ Fluid\ Consumption} \times 100\% \tag{4.1}$$

Next, these rats were assigned to: 1) Control group (N=16), which received sham pTUS without 48-hour-restraint, 2) Sham group (N=16), which received the restraint and sham pTUS, and 3) pTUS group (N=16), which received the restraint and pTUS (see ***Figure 4.2***).

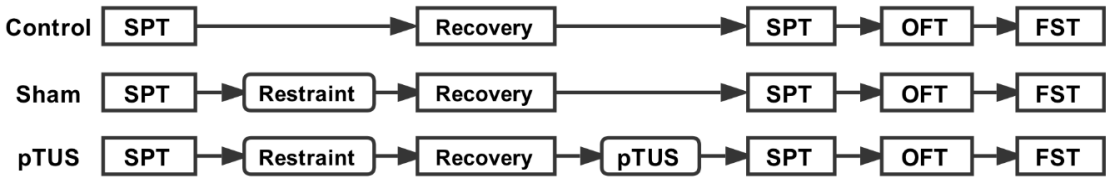

Figure 4.2 Grouping and experimental protocols of the study. The time taken for Restraint, recovery and pTUS was 48 hours, 1 week and 2 weeks, respectively. SPT: sucrose preference test; OFT: open field test; FST: forced swimming test.

Two restraint groups (Sham and pTUS groups) then received the 48-hour restraint as described in the following section "*Procedure of 48-hour restraint*", while the rest group (Control group) remained in their cages placed in a separated room. After the restraint, rats were put back to home cages with free

access to food and water to recover the weight. After one week, pTUS were applied to the pTUS group for two more weeks, while handling the rest groups identically without activating the transducer.

To investigate the antidepressant-like effects of pTUS as well as the long-term effect of the rat depression model, a set of behavioral tests were performed, including SPT, open field test (OFT) and forced swimming test (FST), which will be discussed in following sections. After that, all rats were sacrificed before examining the level of BDNF expression by western blotting analysis and assessing the safety of 2-week pTUS by H&E staining.

The experimental protocols were reviewed and approved by the Institutional Animal Care and Use Committee (IACUC), Shanghai Jiao Tong University, and every possible effort was made to minimize the number of animals used and their suffering.

4.2.2 Animal preparation

Six-week-old male Sprague-Dawley rats (200-250g) were purchased from Beijing Vital River Laboratory Animal Technology Co., Ltd (Beijing, China) and housed those of the same group in pairs in polycarbonate cages (420×260×200mm) with free access to food and water. Additionally, the room was set with a 12h reversed light/dark cycle (lights on at 9pm), temperature at 24-26℃ and relative humidity at 50-66%. The reversed light/dark cycle was set in order to conveniently conduct behavioral testing in rat's active (dark) phase at our daytime.

4.2.3 Rat depression model

In our initial preliminary studies, WKY rats were adopted as depression model but failed to demonstrate depression-like symptoms (see *Appendix* in the end of this chapter). Inspired by the work reported in [209], our lab created and validated a new rat depression model, which was then adopted in this study. Briefly, each rat was placed in a separate cylindrical container (60 to 65mm in diameter and 240mm in length) for 48 hours. The container was made of transparent plastic and was ventilated through side holes with a diameter of 1cm and intervals of 2cm. Based on the weight of rats, deformable plastic sheets of 1 mm to 3 mm thickness were put inside the container to tightly secure the rat while avoiding

injury. During the restraint, rats were able to move its head and anterior limb, but unable to turn around. The food and water supply were also deprived during the restraint.

4.2.4 pTUS system and parameters

The pTUS system was constructed as described in previous chapters. Briefly, as illustrated in ***Figure 4.3***, the system consisted of four major parts: (i) signal generator module (AFG3022B, Tektronix, USA), (ii) custom-designed radio frequency amplifier (HGX100, Nanjing, China), (iii) a single element immersion type planar transducer (V301, Olympus, USA), and (iv) a custom-designed acoustic collimator (7 mm diameter output aperture). The transducer was positioned precisely to the target area (left PFC, 3.5 mm anterior and 0.75 mm lateral to the bregma) [210] using the stereotaxic apparatus (brain stereotaxic, RWD, Shenzhen, China).

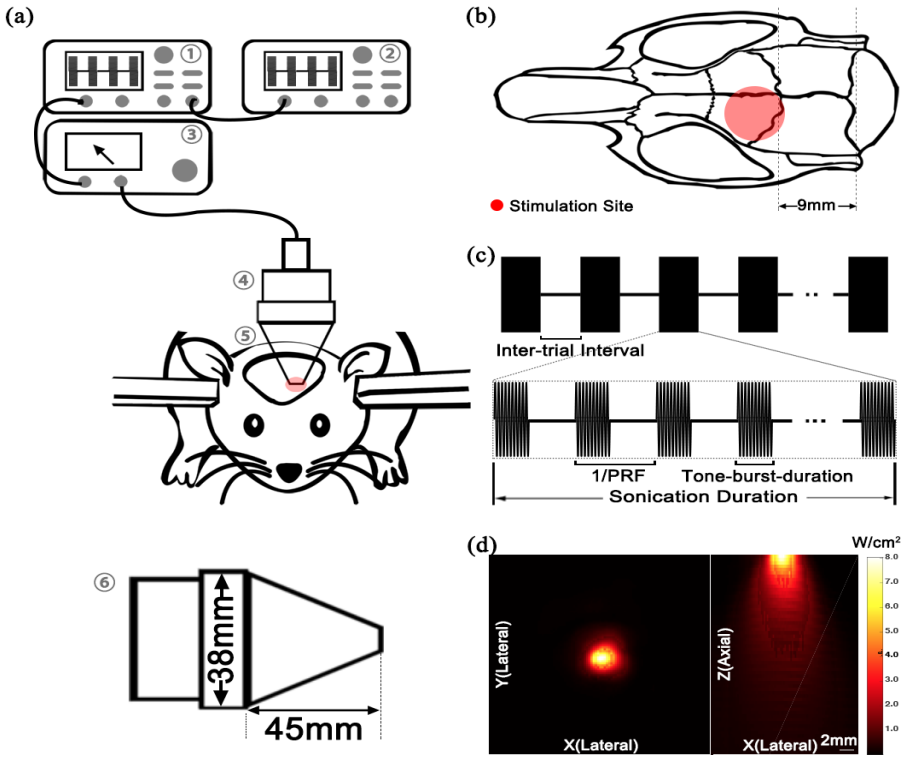

Figure 4.3 Overview of the experimental system and pTUS parameters. (a) Schematic of the pTUS system: 1 function generator #1, 2function generator #2, 3amplifier, 4transducer, 5acoustic collimator (d=7mm)and 6dimensions of the transducer and collimator. (b) The location and areas of ultrasound stimulation (left prefrontal cortex) on the brain. Illustration of the parameters for the pulsed TUS, i.e., acoustic intensities (AI), sonication duration (SD), tone burst

duration (TBD), and pulse repetition frequencies (PRF). The tone pulse was composed of several cycles' basic waves. (c) Parameters for the pTUS, where inter-trial interval was 4 s, PRF equaled to 1.5 kHz, tone-burst-duration was 0.4 ms and sonication duration was 400 ms. (d) Lateral (Left) and axial (Right) acoustic spatial-peak-pulse-average intensity (ISPPA) maps.

This study used the excitatory pTUS parameters ($pTUS_E$) as described in chapter 2. As shown in ***Figure 4.3***, each ultrasound pulse contained 200 sinusoidal waves corresponding to the tone burst duration (TBD) of 0.4 ms at the fundamental frequency of 0.5 MHz. For each trial, ultrasound pulses were repeated at pulse repetition frequency (PRF) of 1.5 kHz for a sonication duration (SD) of 400 ms. Such trial was then repeatedly applied to the left PFC of rats in pTUS group with intervals of 3s for 15 minutes on a daily basis. The pTUS treatment lasted for 2 weeks. During pTUS, rats were fixed on the stereotaxic apparatus and anesthetized by inhalation isoflurane (5% isoflurane for the initial, and 2% isoflurane for maintenance). The rest groups were handled identically to the pTUS group during these two weeks but without the ultrasound stimulation.

4.2.5 Behavioral tests

4.2.5.1 Sucrose preference test (SPT)

Before pre-SPT test, rats were trained to drink water with sucrose for two-day adaptation. During this period, rats were individually caged with two side-by-side bottles containing pure water (200ml) and 1% sucrose solution (200 ml) respectively. The position of sucrose solution and water was exchanged to avoid the side preference after 24 hours. After the sucrose adaptation, rats were deprived of water and food for 12 hours and then resume the sucrose solution and pure water supply. The fluid consumption was recorded 12 hours later, and then the sucrose and water bottles were exchanged, and the fluid consumption was recorded after another 12 hours. *SPI* was defined as the ratio of the *sucrose consumption* to the *total fluid consumption* (see Eq. (4.1)). Decline in *SPI* indicates the typical anhedonia symptom in depression.

4.2.5.2 Open field test (OFT)

OFT is commonly used to measure the exploratory behavior and general activity of animal in a novel environment. Each rat was individually and gently placed into the center of a square plexiglass box

(90×90×50 cm) to freely explore the chamber for 10 min. Its activities were recorded by ANY-maze (Stoelting, USA) and the number of its rearing was counted by an experienced technician who was blind to the experimental grouping. The box was cleaned after the OFT of each rat. OFT videos were analyzed by a technician in terms of *moving distance*, *time in center zone*, and *number of rearing*.

4.2.5.3 Forced swimming test (FST)

FST is used to assess the immobility of the animals in the water, as the measurement of their despair. This test consisted of two sessions. In the first session, rats were trained to discover the test without being scored in the first day. In the second session on the next day, the performance of FST was recorded with ANY-maze (Stoelting, USA) for further analysis. In each session, rats were placed individually into a transparent plexiglass cylinder (60 cm in height, 30 cm in diameter) for 5 min. The cylinder was filled with fresh water (25±1℃, 35cm in depth) and the swimming animal could not touch the bottom of the container with their posterior limbs or tails. Immobility was defined as the status in which animals floated in water with only occasional slight movements to keep their balance. The immobility time of each rat was measured from the average of two separate measures by a technician who was blind to the groups.

4.2.6 Statistical analysis

The statistical analysis was carried out with SPSS software (Ver. 24.0, SPSSS Inc., Chicago, USA). One-way ANOVA was used and nonparametric tests (Kruskal Wallis test) were applied if data did not pass the test of homogeneity of variances. Post hoc Mann-Whitney test and LSD test were performed after Kruskal Wallis test and One-way ANOVA, respectively, for group comparison. The level of statistical significance was set at p-value≤0.05. All data are expressed as mean ± S.E.M.

4.3 Results

4.3.1 Behavioral tests

4.3.1.1 Sucrose preference test

Nonparametric test was performed on the *SPI* of the three groups due to the lack of homogeneity of variances and the result is shown in ***Table 4.1***. The statistical analysis showed marginal difference in *SPI*

among groups (p=0.064, Kruskal Wallis Test) at the 24th hour. Post hoc analysis showed a significant decrease of the *SPI* in Sham group compared with Control group (72.77 ± 7.154% vs 89.90 ± 1.747%, p=0.042, Mann-Whitney), and a significant increase of the *SPI* in pTUS rats compared with Sham rats (88.84 ± 2.452% vs 72.77 ± 7.154%, p=0.046, Mann-Whitney). A similar trend was also found at the 12th hour (89.50 ± 2.059% vs 76.67 ± 5.837%, p=0.070, Control vs Sham; 76.67 ± 5.837% vs 87.47 ± 2.853%, p=0.132, Sham vs pTUS). One-way ANOVA on the *sucrose consumption* indicated a marginal group effect at the 12th hour (p=0.082). Post hoc analysis revealed a significant decrease of sucrose intake in Sham rats compared with Control (55.22 ± 4.195 g vs 40.68 ± 5.292 g, p=0.045) at the 12th hour, but pTUS rats showed only marginal increase of *sucrose consumption* compared with Sham rats (71.83 ± 7.546 g vs 53.58 ± 5.973 g, p=0.052) at the 24th hour.

Both *SPI* and *sucrose consumption* decreased in Sham group compared with the Control group, indicating anhedonia, which is a key symptom of depression [211], in the rat depression model without treatment. As expected, the anhedonia represented by the decrease in sucrose intake was alleviated by pTUS treatment.

4.3.1.2 Open field test

The trajectory of the movement of rats was illustrated in **Figure *4.4d***. Except for total *moving distance*, *rearing*, and *time in center zone*, the variability of these indicators within this period were also assessed according to [212]. The *moving distance* and *time in center zone* did not significantly change across groups (**Figure *4.4a*** and **Figure *4.4c***), while the *number of rearing* was affected by both restraint and pTUS. Specifically, Sham rats showed a significant decrease of *number of rearing* compared with Control (10.80 ± 0.751 vs 8.67 ± 0.599, p=0.029, One-way ANOVA, post hoc) during 2-4 minutes, whereas pTUS rats had a significantly greater *number of rearing* than the Sham rats (7.40 ± 0.550 vs 9.18 ± 0.671, p=0.022, One-way ANOVA, post hoc) during 9-10 minutes (**Figure *4.4b***). These results showed that pTUS could relieve the reduction of exploratory behavior due to restraint stress.

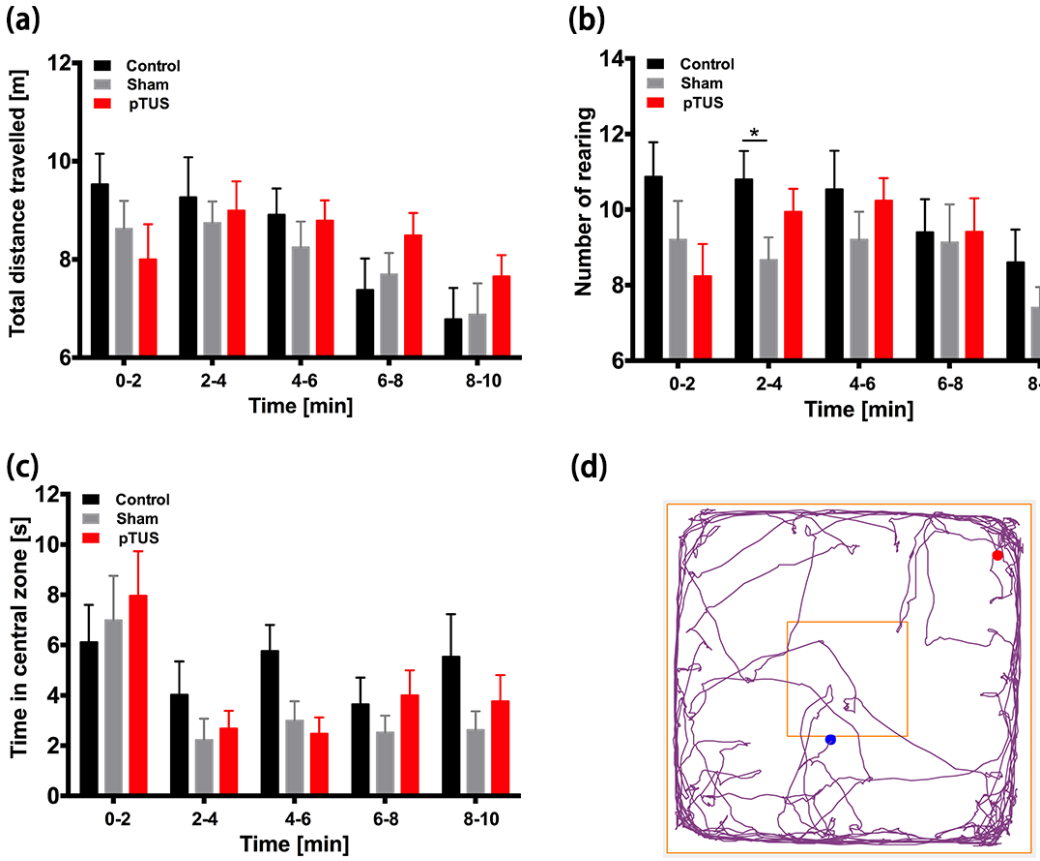

Figure 4.4 Results of open field test. (a) Distance travelled, (b) number of rearing (c) time in central zone in Control, Sham and pTUS groups. All these data were presented as Means ±S.E.Ms. * denotes p<.05, as revealed by LSD post hoc comparisons. (d) Trajectory of the rats' movement. The outer square represents the monitored field by camera and the inner square represents the central zone.

Table 4.1 Results of sucrose preference test. '*' denotes p<.05, as revealed by Mann-Whitney test compared with Sham subjects for SPI results and by LSD post hoc comparisons with Sham group for Sucrose consumption results.

		Control	Sham	pTUS
SPI (%)	12 hr	89.50 ± 2.059	76.67 ± 5.837	87.47 ± 2.853
	24 hr	89.90 ± 1.747*	72.77 ± 7.154	88.84 ± 2.452*
Sucrose consumption (g)	12 hr	55.22 ± 4.195*	40.68 ± 5.292	54.86 ±6.173
	24 hr	67.18 ±5.935	53.58 ± 5.973	71.83 ± 7.546

4.3.1.3 Forced swimming test

As shown in ***Figure 4.5***, neither restraint process nor pTUS treatment significantly altered the forced swimming performance.

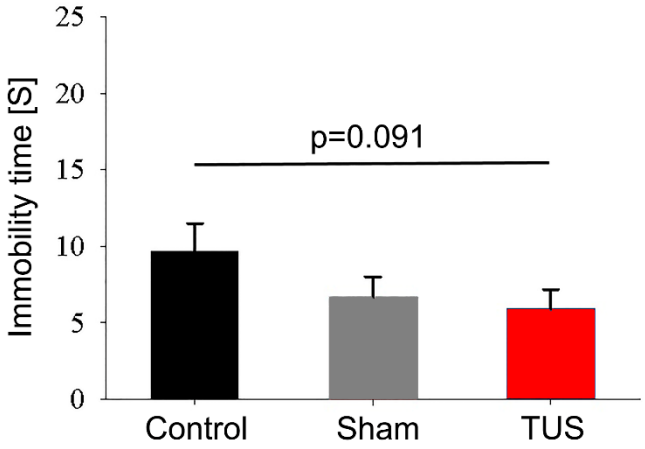

Figure 4.5 Results of forced swimming test.

4.3.2 Examination of BDNF level and the safety of 2-week pTUS

As mentioned in the Introduction, this part of the study was completed by Daqu Zhang. The methods and results were to be introduced in a journal paper submitted for publication as well as in Zhang's Master thesis.

Briefly, the BDNF levels of rats from three groups were examined using Western Blotting analysis whereas the safety of 2-week pTUS was investigated by hematoxylin and eosin (H&E) staining to detect potential tissue damage and hemorrhage in rat brains.

The Western Blotting analysis showed that two weeks' pTUS significantly increased the expression of BDNF in pTUS rats compared with Control and Sham ones. However, restraint stress only induced a marginal decrease of BNDF in Sham subjects compared with Control 3 weeks after the restraint.

4.4 Discussion

Current therapeutic strategies for depression suffer from several drawbacks, such as inadequate responses, side effects and high risks associated with implanting surgeries, and etc. Therefore, noninvasive physical therapies are highly desired. Transcranial ultrasound stimulation has been hypothesized to be an effective treatment for depression due to its ability to stimulate neuronal activity in a precise and non-invasive manner [198]. To test this hypothesis, pTUS was applied for 2 weeks on a daily basis to the prefrontal cortex of a 48-hour-restraint rat depression model. It was found that pTUS could reverse depression-like phenotypes manifested in the created model, such as anhedonia and reduced exploratory behavior, which would maintain during experiment without intervention as shown in the sham group.

This result suggested that although $pTUS_E$ failed to show excitatory effects consistently among rats in Chapter Chapter 2: , it could still manifest therapeutic effects on depression at a group level. As discussed in Chapter Chapter 2:, the lack of cortical excitation might be ascribed to subthreshold intensity of pTUS, which stimulates insufficient number of neurons to show cortical excitation. However, these subthreshold number of excited neurons might be sufficient to reverse the abnormal neuronal activities in the target brain area (i.e., left PFC in this study), thereby alleviating depression symptoms. In addition, the 2-week repeated stimulation might induce accumulative influence on neuronal activities.

Additionally, the left hippocampus showed an elevation of BDNF after pTUS. It has been proven that BDNF plays an important role in the survival, differentiation, and proliferation of neurons and the formation of new synapses [213], and elevation of hippocampal BDNF expression has also been reported in mice [54]. It was therefore speculated that the antidepressant effect of pTUS might operate by promoting the expression of BDNF and thereby protecting neurons from restraint stress. Interestingly, Western Blotting analysis demonstrated the increase in endogenous BDNF expression in the left hippocampal among the rats receiving pTUS on the left PFC. This might be associated with the prefrontal-hippocampal cortex pathway, which is a projection of neurons from hippocampal formation (defined here as the hippocampus, prosubiculum, and subiculum) to the PFC [214]. The activity of this pathway is highly sensitive to stress, which is a major precipitating factor for symptoms of depression, schizophrenia

and anxiety disorders [215,216]. Targeting this pathway, other brain stimulation techniques, e.g. DBS and ECT have shown promising outcomes in treatment of mental disorders [217].

In addition to the change of BDNF, depression is also associated with decrease in hippocampal neurogenesis. As it has been reported that pTUS as well as BDNF could promote hippocampal neurogenesis [116,218], it is worth investigating whether pTUS alleviated depression via promoting neurogenesis directly or indirectly by boosting BDNF expression. Therefore, more studies are needed to fully elucidate mechanisms underlying the antidepressant effect of pTUS.

Furthermore, H&E staining indicated no tissue damage or hemorrhage in the brain that have received 2-week ultrasonic stimulation (refer to H&E results in Daqu Zhang's mater thesis). This is consistent with most literature where low-intensity pTUS has been applied. For example, pTUS of I_{SPTA} at 6.3 W/cm^2 for sonication duration of 2s [75] or even continuous stimulation with I_{SPPA} of 2.9 W/cm^2 for 48 hours [219] did not show any tissue damage. However, it should be cautious when attempting to use higher intensity, as (unstable) cavitation induced by pTUS may result in hemorrhaging or BBB disruption, thus it should be carefully examined and controlled. For example, it has been reported that exposure to relatively high acoustic intensity (I_{SPPA} = 22.4 W/cm^2, I_{SPTA}=11.2 W/cm^2) may result in focal bleeding in the brain [119]. In our study, low intensity of pTUS (I_{SPPA} = 8 W/cm^2) was implemented for a short sonication duration (0.4 s) with intervals of 3s in each trial to prevent potential tissue damage.

Additionally, in our experiment, rats were divided into three groups as: 1) Control group (N=16), which received sham pTUS without 48-hour-restraint, 2) Sham group (N=16), which received the restraint and sham pTUS, and 3) pTUS group (N=16), which received the restraint and pTUS. In future work, we suggested to add another group, which receives pTUS on the other site, e.g., the right prefrontal cortex, to verify the region-specific therapeutic effects of pTUS. This design may also help understand the circuitry by which pTUS operate to alleviate depression.

4.5 Chapter conclusion

In this chapter, antidepressant-like effects, e.g., protracted anhedonia and increased exploratory activity, were found in depressive rats (a 48-hour-restraint depression model) that had received 2-week

pTUS on a daily basis. Additionally, the level of BDNF expression increased after pTUS. The safety of the long-term pTUS on brain tissues was also examined and no damage was found. To the best of our knowledge, this study is the first attempt to report the antidepressant-like effects of pTUS on the animal model, and the results suggest that pTUS might be a promising therapeutic strategy for depression. However, stimulation parameters, targeting of brain regions, and the underlying mechanisms etc. still need to be further studied for the clinical translation of this approach.

Appendix (Wistar Kyoto (WKY) model of depression)

The WKY strain was first developed as a normotensive control for the spontaneously hypertensive rat strain [220], but was later found to demonstrate depressive-like behaviors [221].

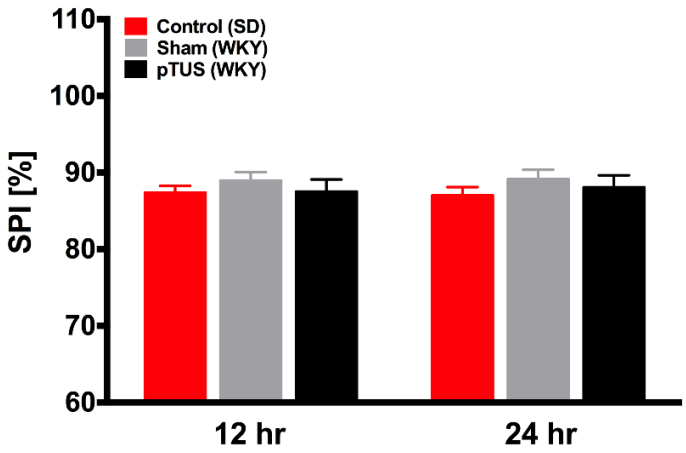

Figure S4.1 Results of Sucrose Preference Test in the preliminary study

However, as pointed out in [222], this model has high variability within the strain and might be subject to unstable behavioral responses. In our preliminary study, WKY rats were adopted as depression model and Sprague-Dawley rats as normal control. With a similar experimental design, the preliminary study showed that WKY rats failed to demonstrate depression-like symptoms as shown in ***Figure S4.1***, where SPI of Sham WKY and Control (SD) group did not differ significantly, indicating the absence of depression-like symptoms such as anhedonia in this model.

Chapter 5: Discussion and Future Work

This chapter summarizes the thesis and then discusses possible mechanisms underlying therapeutic effects of pTUS in stroke preconditioning and depression treatment. After that, I will review potential mechanisms underlying neuromodulatory effects of pTUS. And in the end, I make some comments on individualization of pTUS, system improvements, and possible future directions of the pTUS technique.

5.1 Summary of the thesis

Neurological and psychiatric disorders, such as Parkinson's disease, epilepsy, Alzheimer's disease, stroke (vascular disorder that results in neurological defects), and depression, and etc., present an increasing challenge and a substantial social and economic burden for an ageing and stressful population. However, conventional treatments, especially pharmacologic interventions, have significant limitations, such as nonspecific effects, insufficient tailoring to the individual, adverse effects, as well as inadequate uptake into the brain due to the blood-brain-barrier (BBB). By contrast, neuromodulation techniques have gained attention as they are able to selectively enhance or inhibit neural activities, thus could guide cortical plasticity to restore adaptive equilibrium in a disrupted neural network resulted from neurological disorders. Capitalizing on its noninvasiveness, high precision and penetration depth, low-intensity low-frequency pulsed transcranial ultrasound stimulation (pTUS) has been emerging as a promising therapeutic neuromodulation tool for neurological and psychiatric disorders. Therefore, utilizing its different neuromodulatory effects, i.e., suppression and excitation of neuronal activity, this thesis investigated the therapeutic effects of pTUS as preconditioning for focal cerebral ischemia and treatment of depression, respectively, in animal experiments. The results suggested that pTUS could serve as preconditioning for perioperative stroke (Chapter 3) and therapeutics for depression (Chapter 4). Before that, the neuromodulatory effects of pTUS parameters were also examined using multi-modal neuroimaging techniques, and it showed that optical neuroimaging could characterize the neuromodulatory effect of pTUS (Chapter 2), which is important when applying pTUS to basic and clinical neurosciences.

5.2 Mechanisms underlying neuromodulatory effects of pTUS

As mentioned earlier, explanation of the phenomenon in Chapter 2, where $pTUS_E$ and $pTUS_S$ influenced cortical excitability differently, needs deep understanding of the mechanisms underlying pTUS neuromodulation. However, despite of the promising outcomes by pTUS in the experimental studies, the mechanisms through which pTUS can influence neuronal activity still have not been fully elucidated. Several models have been proposed as candidates, among which the neuronal intramembrane cavitation excitation (NICE) model might be the most promising to explain the results in Chapter 2 as well as other studies on pTUS neuromodulation. Therefore, in this section I introduce the NICE model more specifically and review other models briefly for comparison.

5.2.1 NICE model

Due to its low intensity and pulsed nature, pTUS causes only minimal temperature elevation (typically <0.01 ℃) [54,57,109]. Thus, ultrasonic neuromodulation is believed to operate primarily by non-thermal (mechanical) mechanisms. Plaskin et al. proposed a unifying framework that provided a detailed predictive explanation for ultrasound-induced excitation and suppression effects on neural circuits. The core of this theory is the concept of intramembrane cavitation, or nanobubble formation within the bilayer cell membrane produced by ultrasonic pressure [223], inducing expansions and contractions of the space between two leaflets of the membrane (bilayer sonophores). As the local curvature of the membrane changes due to oscillations of nanobubbles (see **Figure *5.1***), the membrane capacitance as a function of curvature Z, according to the bilayer sonophore model, can be expressed as:

$$\mathrm{C_M}(\mathbf{Z}) = \frac{\mathrm{C_M}D}{a^2}\left[\boldsymbol{Z} + \frac{a^2 - \boldsymbol{Z} - \boldsymbol{Z}D}{2\boldsymbol{Z}}\, ln\left(\frac{2\boldsymbol{Z} + \boldsymbol{D}}{D}\right)\right], \tag{5.1}$$

where $\mathbf{Z} = \mathbf{Z}(t)$ is the membrane curvature and its relationship with driving ultrasound pressure is modeled by the Rayleigh-Plesset equation for bubble dynamics [224], $\mathrm{C_M}$ is the capacitance, D is the resting thickness of the membrane, and a is the radius of a round patch of membrane.

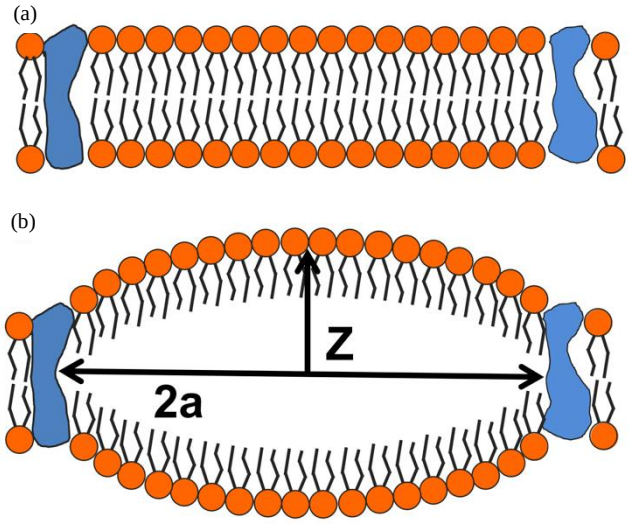

Figure 5.1 (a) Patch of membrane regions between two proteins. (b) Change in the local curvature of the membrane induced by intramembrane cavitation. This figure was edited based on the figure cited from REF. [237].

The NICE model modifies the H-H model to include the bilayer sonophore model by adding the capacitive current $\mathrm{I_C} = V_m \frac{dC_M}{dt}$, which is zero in the original H-H model (see the membrane equivalent circuit illustrated in **Figure *5.2***). The AP equation in the modified H-H model is:

$$\frac{dV_m}{dt} = -\frac{1}{\mathrm{C_M}}\left[V_m \frac{dC_M}{dt} + g_{Na}(V_m - E_{Na}) + g_k(V - E_k) + g_M(V_m - E_k) + g_L(V_m - E_L)\right], \tag{5.2}$$

where g_{Na}, g_k, g_M and g_L are the conductance of the sodium, delayed-rectifier potassium, and the leak channels, respectively, whereas E_{Na}, E_k, and E_L are the equilibrium potentials.

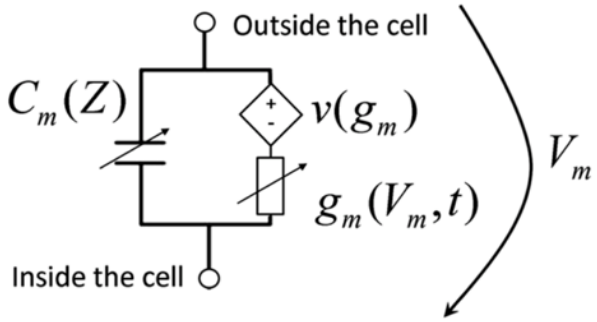

Figure 5.2 Illustration of the membrane equivalent circuit, which has a potential (V_m), time-varying capacitance (C_M) and H-H type ionic conductance (g_m) and source $v(g_m)$.

Taken together, the logically connected equations above constitute the NICE model, the solutions of which describe mathematically the generation of the AP by ultrasound.

Furthermore, Plaskin et al. extended the NICE model to different types of neurons and proposed cell-type selective mechanisms [112], which predictively theorize how ultrasonic pulses excite as well as suppress neural circuits [225]. Briefly, the cortex consists of one type of excitatory regular spiking (RS) pyramidal neurons and two types of inhibitory interneurons (i.e., low-threshold spiking (LTS) neuron and fast spiking (FS) neuron). The excitation threshold (in aspect of I_{SPPA}) for LTS is usually much lower than that for FS or RS neuron, thus, LTS neurons can be selectively activated for brain suppression with a stimulation below the thresholds for RS and FS neurons. When the stimulation is strong enough, all types of neurons (RS, LTS and FS) can be activated, however, the net outcome may not be of brain excitation unless more than 75% neurons are RS[112].

The predictions based on the NICE model were found to be both qualitatively and quantitatively consistent with the experimental data, ranging from rodents to humans. However, the predictions remain to be validated.

5.2.2 Continuum mechanics model

Considering the extracellular space as a continuous medium [226] with the presence of both cerebrospinal fluid (CSF) [227] and cell membranes in the brain, Tyler proposed the continuum

mechanics model to describe how ultrasound exerts mechanical interactions on tissues and their boundaries [228][229]. As illustrated in **Figure *5.3***, this model proposed that ultrasound influences neuronal activity through pressure-fluid-membrane actions in various mechanical effects, e.g., stable cavitation, acoustic streaming, acoustic radiation force, shear stress and Bernoulli effects, and etc. These fluid-mechanical effects stem from acoustic impedance mismatches between lipid bilayers, surrounding intracellular or extracellular fluids and cerebrovasculature.

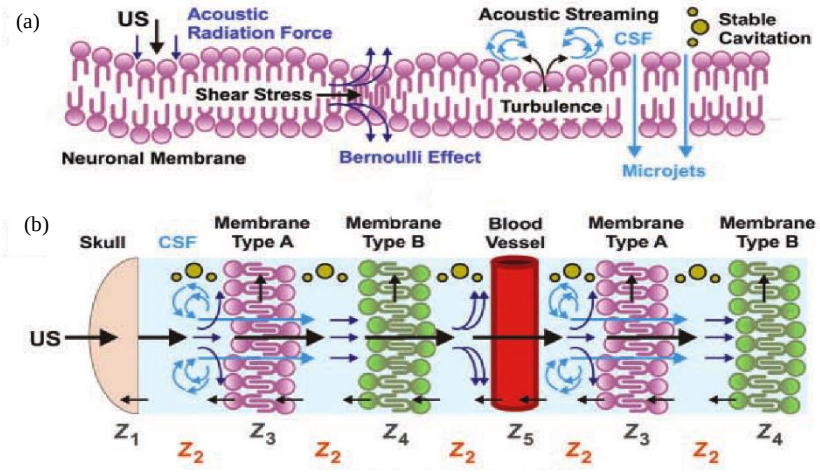

Figure 5.3 Continuum mechanics model proposed to underpin ultrasonic neuromodulation. (a) Some of the proposed fluid mechanical actions by which ultrasound modulates neuronal activity. (b) Similar actions in the model of brain tissue, illustrating different acoustic impedance between boundaries established by cellular interfaces. This figure was modified from REF. [228].

On the other hand, many of the voltage-gated ion channels possess mechanosensitivity so that their gating kinetics are sensitive to mechanical changes in membranes (see **Figure *5.4***) [230–232]. Therefore, it is possible that acoustic radiation forces may lead to the opening of voltage-gated channels sufficient to evoke the action potentials [66][233], thereby mediating neuromodulation. Alternatively, acoustic streaming and stable cavitation occurring near neuronal membranes might change the membrane's ionic conductance [234,235], which is able to produce membrane depolarization. Consequently, these changes could sufficiently activate voltage-gated channels and induce neuromodulation.

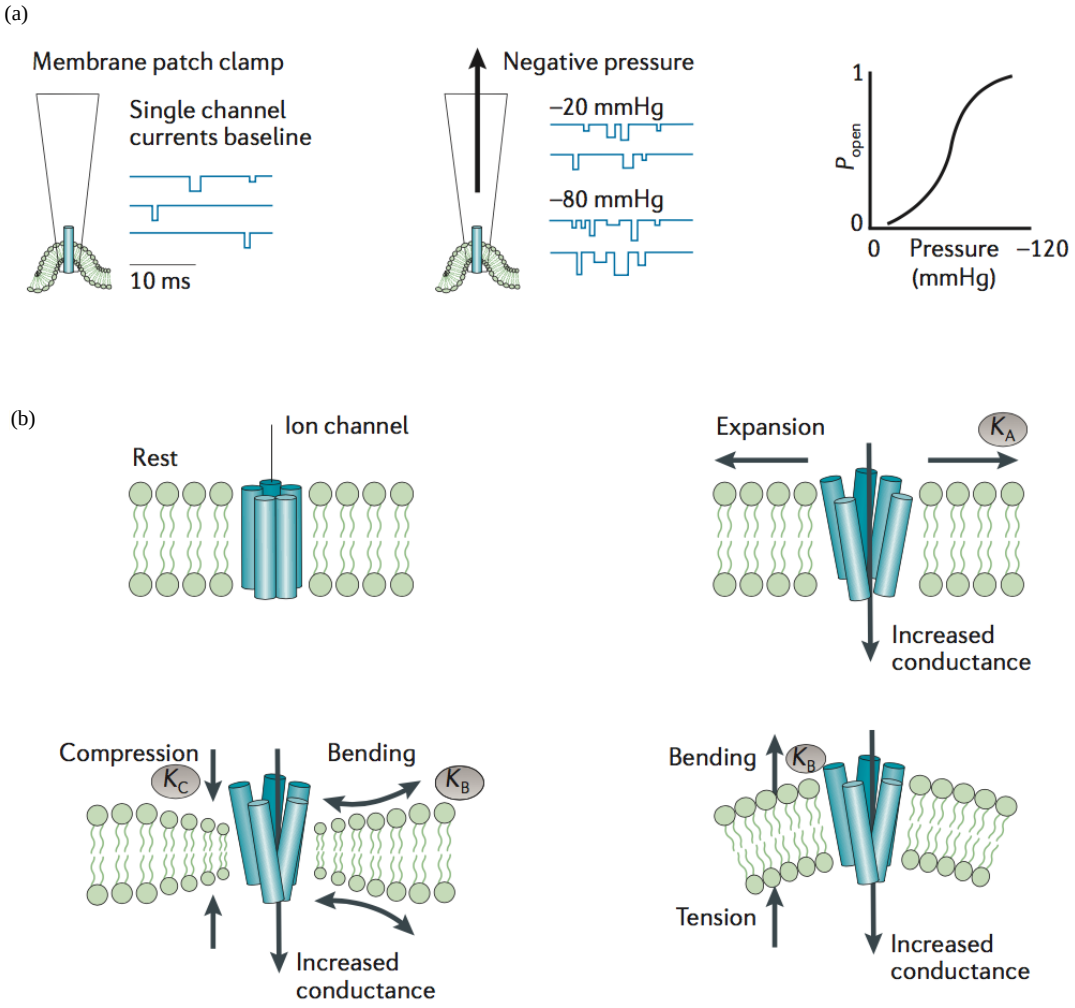

Figure 5.4 Ion channels that are sensitive to membrane mechanics. (a). A modified pressure-clamp experiment showed an increase in mechanosensitive channel activity when the channel is applied with a negative pressure. (b). Membrane expansion, compression, bending and tension change the conformational structure of the ion channel, which modulates the membrane conductance. This figure was modified from REF. [232].

Although continuum mechanics model provides some insights into how ultrasound induces neuromodulation, biophysical models are still required to quantitatively describe and explain the pTUS neuromodulation. Referring to recent reviews [73,236–238], three biophysical models and hypotheses are introduced below. They also provide some explanation on ultrasonic neuromodulation by modeling how mechanical waves might influence action potentials (AP). These models include the soliton model proposed by Heimburg et al. [239], the flexoelectricity hypothesis proposed by Petrov [240] and the

neuronal intramembrane cavitation excitation (NICE) model that developed by Plaksin and Kimmel et al. with a series of studies [112,120,223].

5.2.3 Soliton model

Based on the thermodynamics and phase behavior of the cell membrane lipids, Heimbrug et al. proposed that the AP (action potential) is "a propagating density pulse (soliton), and therefore an electromechanical rather than a purely electrical phenomenon". It is currently accepted that lipids of biological membranes are in both fluid and gel phase (see ***Figure 5.5***) and display reversible phase transitions from one phase to the other [241] due to various factors, including temperature, voltage, chemical potentials and pressure. In addition, gel and fluid phases are associated with different area density ρ_A, which was defined as mass/area. Therefore, the application of an adequate acoustic pressure that decreases the area of a local patch of membrane and increases its thickness can bring the membrane within the phase transition, thereby changing the area density ρ_A.

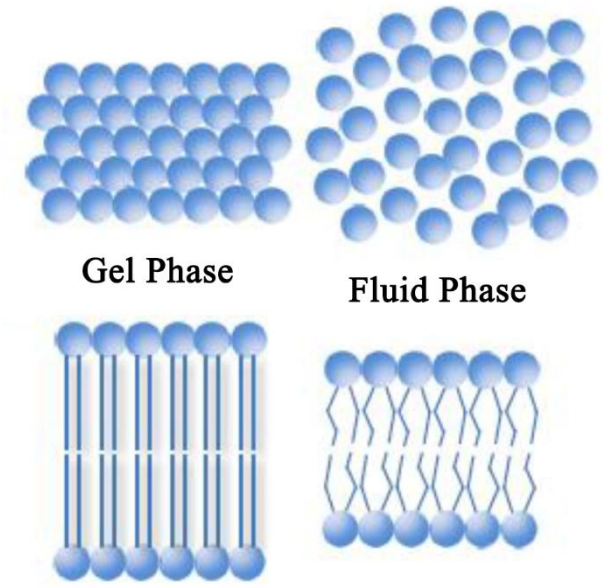

Figure 5.5 Illustration of gel and fluid phases. In the gel phase the area and the volume of the lipid membrane are minimal, while the thickness is maximal. This figure was edited based on the figure cited from REF. [237].

The changes of membrane area density or membrane area induce the membrane potential due to the piezoelectric effect. Piezoelectricity refers to the appearance of an electrical potential (a voltage) across the sides of a piezoelectric material subjected to mechanical stress. Polarization charges are induced on the opposite sides of the membrane when the membrane was compressed/stretched/sheared by ultrasound pressure. Therefore, the electro-mechanical coupling between ultrasound waves and the generation of AP in this model is explained by piezoelectricity of cell membrane as expressed in Eq. (5.3):

$$\mathrm{V}_{\mathrm{piezo}} = f_{\mathrm{piezo}}\mathrm{dA}, \tag{5.3}$$

where f_{piezo} is the piezoelectric coefficient, which is currently not known and dA is the change in membrane area induced by ultrasound waves

There are several limitations in the soliton model. First, it cannot explain the role that voltage-gated ion channels play in the generation and propagation of the AP. Second, it did not well explain why ultrasound could induce phase transition of lipid membrane. Additionally, we still lack evidence supporting the hypothesis that the soliton pulse propagates as piezoelectric waves.

5.2.4 Flexoelectricity model

Similarly to piezoelectricity, flexoelectricity describes the polarization charges across the membrane surface induced by membrane bending. A change in the membrane curvature dC induced by ultrasound waves alters the membrane potential as expressed in Eq. (5.4) [242]:

$$\mathrm{V}_{\mathrm{flexo}} = \frac{f_{flexo}}{\varepsilon_0}\mathrm{dC}, \tag{5.4}$$

where f_{flexo} is the flexoelectric coefficient and has been measured for some membranes [243,244].

Petrov proposed that the propagation of the AP generated by pTUS might arise from the flexoelectrical property of the cell membrane [245]. Unlike the soliton model, the flexoelectricity model suggested that the voltage-gated ion channels play a fundamental role in the generation and propagation of the AP, whereas phase transitions of membrane lipids play no role. Specifically, a membrane depolarization could

be strong enough to induce ionic currents through the voltage-gated ion channels as proposed in the conventional Hodgkin–Huxley (H-H) model.

Flexoelectricity hypothesis proposed electromechanical coupling in membranes based on flexoelectric effects. Such effects have been both proved experimentally in artificial lipid membranes or cells membranes. However, no mathematical model has been developed to describe or predict the generation and propagation of the AP as a result of the changes in membrane curvature through the flexoelectric effect.

Collectively, more work is needed to develop the model for explaining the mechanistic underpinnings of ultrasonic neuromodulation. Elucidation of the mechanisms can facilitate the applications of pTUS to brain disorders as well as the technical development, as ultrasound waveforms can be designed for a specific application with the knowledge of their neuromodulatory effects.

5.3 Mechanisms underlying therapeutic effects of pTUS

Our findings indicated that ultrasound treatment might serve as a neuroprotective preconditioning for patients with high risk of brain ischemia or refractory depression. Nevertheless, additional experiments are desirable to fully elucidate the underlying mechanisms for ultrasound treatment before applying it to humans. As noted earlier, this thesis discussed some possible underlying mechanisms for pTUS, which might directly alter the neuronal activity or indirectly modulate the expression of disease-related factors, such as endothelial nitric oxide and brain derived neurotrophic factor.

5.3.1 Metabolic down-regulation and release of nitric oxide in pTUS preconditioning

The idea of using suppressive pTUS as neuroprotective preconditioning was inspired by clinical practices that used hypoxia and deep hypothermia to protect the brain during surgeries. These practices demonstrated that the brain tissue was more tolerant to subsequent ischemic events by suppressing the metabolic activity, which in turn improved the cell survival. Therefore, the suppressive pTUS parameter was used in this study for preconditioning. As $pTUS_S$ has been shown to down-regulate brain metabolism within a relatively short period of time (about 9 sec) [75], it is conceivable that such neuroprotective pTUS preconditioning could promote ischemic tolerance through metabolic depression of the brain.

In addition, as hemodynamic changes are closely associated with the pathogenesis of stroke, LSCI was integrated into the experimental system to monitor CBF changes. Based on the CBF results (see sections 3.3.1 and 3.3.2), the neuroprotection of pTUS preconditioning was likely to be ascribed to the release of endothelial nitric oxide (NO). Indeed, ultrasound (2.5 MHz, 2 MPa peak pressure in study [177] and 1.05-MHz, 0.35-1.3 MPa in study [178]) was reported to be capable of promoting the formation and release of endothelial nitric oxide (NO) within several (15 and 2 in [177] and [178], respectively) minutes of exposure. Hence, the alleviated hemodynamic compromise and the improved blood supply observed here may be associated with the production of endothelial NO due to its antithrombotic effect [179–182]. More specifically, the promoted production of NO by cerebral endothelial cells could alleviate the development of thrombus by promoting tissue perfusion and preventing the platelet adhesion.

5.3.2 Elevation of BNDF expression in antidepressant-like effects of pTUS

It has been extensively proved that BDNF plays an important role in the survival, differentiation, and proliferation of neurons and the formation of new synapses [213], whereas pTUS could elevate hippocampal BDNF expression in mice [54]. It was therefore speculated that the antidepressant effect of pTUS might operate by promoting the expression of BDNF and thereby protecting neurons from restraint stress.

In addition to the change of BDNF, depression is also associated with decrease in hippocampal neurogenesis. As it has been reported that pTUS as well as BDNF could promote hippocampal neurogenesis [116,218], it is worth investigating whether pTUS alleviated depression via promoting neurogenesis directly or indirectly by boosting BDNF expression. Therefore, more studies are needed to fully elucidate mechanisms underlying the antidepressant effect of pTUS.

5.4 Future work

5.4.1 Individualized pTUS treatment

As reported in Chapter Chapter 2: as well as in previous studies [77,78,132], the neuromodulatory effect of pTUS varies across different rats, especially that of excitatory pTUS. Several reasons might contribute to this inconsistency. For example, the intensity of ultrasound that reaches the target region is

related to the anatomic difference in the skull and brain tissues across subjects. On the other side, the intensity threshold for effective pTUS, especially excitatory effect, might also vary across subjects, as discussed in section 2.4 referring to the theoretical framework proposed by Plaskin et al [112].

Consequently, the variation across subjects might lead to inconsistent efficacy of pTUS when treating neurological and psychiatry disorders. Additionally, it was also suggested that interpretation of experimental outcomes in neuroscience research should be cautious especially when applying $pTUS_E$ due to its subject-dependent effects.

In clinical practices of TMS, clinicians need examine the motor threshold (MT) for each patient, which is a standard protocol to individualize TMS parameters. Therefore, individualized pTUS would be the strategy to obtain more consistent neuromodulatory effect in pTUS, so as to improve the efficacy across subjects. As suggested by the results of Chapter 2, the state-dependency of pTUS-induced neuromodulatory effects is worth further investigation. This might provide a feasible way to individualize the pTUS parameters, i.e., by examining the baseline brain excitability prior to application of pTUS. As a result, it could reduce the amplitude of pTUS to avoid adverse effects.

5.4.2 System improvements

Current pTUS system is not able to work with the optical imaging system simultaneously due to the transducer's interference with the imaging pathway. Consequently, we had to change the stimulated location or give up simultaneous imaging. To solve this problem, we may propose a design (see ***Figure 5.6***) which modified the system in Chapter Chapter 2: using a hollow transducer, enabling simultaneously monitoring the hemodynamic changes when applying the pTUS neuromodulation. A Chinese patent has been filed for this design.

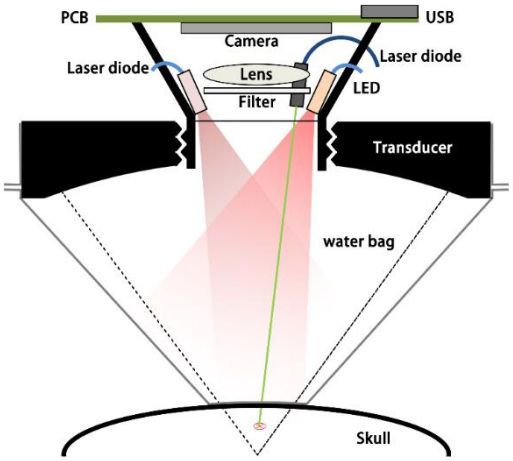

Figure 5.6 Design of the system which enables imaging of the hemodynamic changes when applying pTUS neuromodulation simultaneously.

5.4.3 Future directions

More future work is still required before pTUS could eventually serve as a reliable tool for both basic and therapeutic neurosciences. For example, imaging guidance techniques are needed to accurately target the desired brain regions with high-quality images of brain structures and tracking system to capture relative position of transducer to brain. It is also required to unravel optimal pTUS parameters for excitatory and suppressive pTUS neuromodulation, where the imaging based approach might serve as a promising tool. Additionally, it will require extensive multidisciplinary investigations to understand the mechanisms underlying neuromodulatory and therapeutic effects of pTUS. Continuing examination to identify safe pTUS parameters from different perspectives, such as histological analysis and behavioral tests on animals, is also imperative before its application to humans.

Despite of many challenges, pTUS holds great potential to become a powerful next generation tool for basic neuroscience and therapeutic applications. Combined with non-invasive neuroimaging techniques, pTUS will give researchers new insights into the activities and networks in the brain. More excitingly, pTUS might provide a means of enhancing cognitive performance, such as attention, memory and mood, or an alternative treatment of many other neurological and psychiatric disorders, such as migraine, schizophrenia and anxiety, and etc.

List of References

[1] Olesen J, Gustavsson A, Svensson M, Wittchen HU, Jönsson B. The economic cost of brain disorders in Europe. Eur J Neurol 2012;19:155–62. doi:10.1111/j.1468-1331.2011.03590.x.

[2] Olesen J, Freund TF. European Brain Council: partnership to promote European and national brain research. Trends Neurosci 2006;29:493–5. doi:10.1016/j.tins.2006.07.008.

[3] Olesen J, Baker MG, Freund T, Olesen J, Baker MG, Freund T, et al. Consensus document on European brain research Consensus document on European brain research 2006.

[4] Mega S, Cummings L. Frontal-subcortical circuits and neuropsychiatric disorders. J Neuropsychiatry Clin Neurosci 1994;6:358–70. doi:10.1176/jnp.6.4.358.

[5] Jankovic J. Parkinson's disease: clinical features and diagnosis. J Neurol Neurosurg Psychiatry 2008;79:368–76. doi:10.1136/jnnp.2007.131045.

[6] Olanow CW, Tatton WG. Etiology and pathogenesis of Parkinson's disease. Annu Rev Neurosci 1999;22:123–44.

[7] Engel J. Mesial Temporal Lobe Epilepsy: What Have We Learned? Neurosci 2001;7:340–52. doi:10.1177/107385840100700410.

[8] Sharma AK, Reams RY, Jordan WH, Miller MA, Thacker HL, Snyder PW. Mesial Temporal Lobe Epilepsy: Pathogenesis, Induced Rodent Models and Lesions. Toxicol Pathol 2007;35:984–99. doi:10.1080/01926230701748305.

[9] Fregni F, Pascual-Leone A. Technology Insight: noninvasive brain stimulation in neurology—perspectives on the therapeutic potential of rTMS and tDCS. Nat Clin Pract Neurol 2007;3:383–93. doi:10.1038/ncpneuro0530.

[10] Löscher W, Potschka H. Drug resistance in brain diseases and the role of drug efflux transporters. Nat Rev Neurosci 2005;6:591–602. doi:10.1038/nrn1728.

[11] Hellewell JSE. Treatment-resistant schizophrenia: Reviewing the options and identifying the way forward. J Clin Psychiatry 1999;60:14–9.

[12] Greden JF. Unmet need: what justifies the search for a new antidepressant? J Clin Psychiatry 2002.

[13] Löscher W. Current status and future directions in the pharmacotherapy of epilepsy. Trends Pharmacol Sci 2002;23:113–8.

[14] Lee BH, Scharff L, Sethna NF, McCarthy CF, Scott-Sutherland J, Shea AM, et al. Physical therapy and cognitive-behavioral treatment for complex regional pain syndromes. J Pediatr 2002;141:135–40. doi:10.1067/mpd.2002.124380.

[15] Teasdale JD, Segal Z V., Williams JMG, Ridgeway VA, Soulsby JM, Lau MA. Prevention of relapse/recurrence in major depression by mindfulness-based cognitive therapy. J Consult Clin Psychol 2000;68:615–23. doi:10.1037/0022-006X.68.4.615.

[16] Dayan E, Censor N, Buch ER, Sandrini M, Cohen LG. Noninvasive brain stimulation: from physiology to network dynamics and back. Nat Neurosci 2013;16:838–44. doi:10.1038/nn.3422.

[17] Alexander GE, DeLong MR, Strick PL. Parallel organization of functionally segregated circuits linking basal ganglia and cortex. Annu Rev Neurosci 1986;9:357–81.

[18] Bergman H, Wichmann T, DeLong MR. Reversal of experimental parkinsonism by lesions of the subthalamic nucleus. Science (80-) 1990;249:1436–8.

[19] Benabid A-L, Pollak P, Louveau A, Henry S, De Rougemont J. Combined (thalamotomy and stimulation) stereotactic surgery of the VIM thalamic nucleus for bilateral Parkinson disease. Stereotact Funct Neurosurg 1987;50:344–6.

[20] Krack P, Batir A, Van Blercom N, Chabardes S, Fraix V, Ardouin C, et al. Five-year follow-up of bilateral stimulation of the subthalamic nucleus in advanced Parkinson's disease. N Engl J Med 2003;349:1925–34.

[21] Hubble JP, Busenbark KL, Wilkinson S, Penn RD, Lyons K, Koller WC. Deep brain stimulation for essential tremor. Neurology 1996;46:1150–3.

[22] Vercueil L, Pollak P, Fraix V, Caputo E, Moro E, Benazzouz A, et al. Deep brain stimulation in the treatment of severe dystonia. J Neurol 2001;248:695–700.

[23] Loddenkemper T, Pan A, Neme S, Baker KB, Rezai AR, Dinner DS, et al. Deep brain stimulation in epilepsy. J Clin Neurophysiol 2001;18:514–32.

[24] Abelson JL, Curtis GC, Sagher O, Albucher RC, Harrigan M, Taylor SF, et al. Deep brain stimulation for refractory obsessive-compulsive disorder. Biol Psychiatry 2005;57:510–6.

[25] Mayberg HS, Lozano AM, Voon V, McNeely HE, Seminowicz D, Hamani C, et al. Deep brain stimulation for treatment-resistant depression. Neuron 2005;45:651–60.

[26] Laxton AW, Tang-Wai DF, McAndrews MP, Zumsteg D, Wennberg R, Keren R, et al. A phase I trial of deep brain stimulation of memory circuits in Alzheimer's disease. Ann Neurol 2010;68:521–34.

[27] Houeto J-L, Karachi C, Mallet L, Pillon B, Yelnik J, Mesnage V, et al. Tourette's syndrome and deep brain stimulation. J Neurol Neurosurg Psychiatry 2005;76:992–5.

[28] Oh MY, Abosch A, Kim SH, Lang AE, Lozano AM. Long-term hardware-related complications of deep brain stimulation. Neurosurgery 2002;50:1268–76.

[29] Okun MS. Deep-brain stimulation—entering the era of human neural-network modulation. N Engl J Med 2014;371:1369–73.

[30] Hummel F, Celnik P, Giraux P, Floel A, Wu WH, Gerloff C, et al. Effects of non-invasive cortical stimulation on skilled motor function in chronic stroke. Brain 2005;128:490–9. doi:10.1093/brain/awh369.

[31] Miniussi C, Cappa SF, Cohen LG, Floel A, Fregni F, Nitsche MA, et al. Efficacy of repetitive transcranial magnetic stimulation/transcranial direct current stimulation in cognitive neurorehabilitation. Brain Stimul 2008;1:326–36. doi:10.1016/j.brs.2008.07.002.

[32] Tweney RD. Faraday's discovery of induction: A cognitive approach. Faraday rediscovered,

Springer; 1985, p. 189–209.

[33] Barker AT, Jalinous R, Freeston IL. Non-invasive magnetic stimulation of human motor cortex. Lancet 1985;325:1106–7.

[34] Hallett M. Transcranial magnetic stimulation and the human brain. Nature 2000;406:147.

[35] Pasley BN, Allen EA, Freeman RD. State-Dependent Variability of Neuronal Responses to Transcranial Magnetic Stimulation of the Visual Cortex. Neuron 2009;62:291–303. doi:10.1016/j.neuron.2009.03.012.

[36] Pascual-Leone A, Tarazona F, Keenan J, Tormos J, Hamilton R, Catala M. Transcranial magnetic stimulation and neuroplasticity. Neuropsychologia 1999;37:207–17.

[37] Bindman LJ, Lippold OCJ, Redfearn JWT. The action of brief polarizing currents on the cerebral cortex of the rat (1) during current flow and (2) in the production of long-lasting after-effects. J Physiol 1964;172:369–82.

[38] Purpura DP, McMurtry JG. Intracellular activities and evoked potential changes during polarization of motor cortex. J Neurophysiol 1965;28:166–85.

[39] Utz KS, Dimova V, Oppenländer K, Kerkhoff G. Electrified minds: transcranial direct current stimulation (tDCS) and galvanic vestibular stimulation (GVS) as methods of non-invasive brain stimulation in neuropsychology—a review of current data and future implications. Neuropsychologia 2010;48:2789–810.

[40] Nitsche MA, Paulus W. Excitability changes induced in the human motor cortex by weak transcranial direct current stimulation. J Physiol 2000;527:633–9. doi:10.1111/j.1469-7793.2000.t01-1-00633.x.

[41] Dhuna A, Gates J, Pascual-Leone A. Transcranial magnetic stimulation in patients with epilepsy. Neurology 1991;41:1067.

[42] Khedr EM, Ahmed MA, Fathy N, Rothwell JC. Therapeutic trial of repetitive transcranial magnetic stimulation after acute ischemic stroke. Neurology 2005;65:466–8. doi:10.1212/01.wnl.0000173067.84247.36.

[43] Boggio PS, Alonso-Alonso M, Mansur CG, Rigonatti SP, Schlaug G, Pascual-Leone A, et al. Hand Function Improvement with Low-Frequency Repetitive Transcranial Magnetic Stimulation of the Unaffected Hemisphere in a Severe Case of Stroke. Am J Phys Med Rehabil 2006;85:927–30. doi:10.1097/01.phm.0000242635.88129.38.

[44] Liston C, Chen AC, Zebley BD, Drysdale AT, Gordon R, Leuchter B, et al. Default mode network mechanisms of transcranial magnetic stimulation in depression. Biol Psychiatry 2014;76:517–26. doi:10.1016/j.biopsych.2014.01.023.

[45] Fregni F, Freedman S, Pascual-Leone A. Recent advances in the treatment of chronic pain with non-invasive brain stimulation techniques. Lancet Neurol 2007;6:188–91. doi:10.1016/S1474-4422(07)70032-7.

[46] Andr é-Obadia N, Peyron R, Mertens P, Maugui ère F, Laurent B, Garcia-Larrea L. Transcranial magnetic stimulation for pain control. Double-blind study of different frequencies against placebo, and correlation with motor cortex stimulation efficacy. Clin Neurophysiol 2006;117:1536–44. doi:10.1016/j.clinph.2006.03.025.

[47] Fregni F, Boggio PS, Lima MC, Ferreira MJL, Wagner T, Rigonatti SP, et al. A sham-controlled, phase II trial of transcranial direct current stimulation for the treatment of central pain in traumatic spinal cord injury. Pain 2006;122:197–209. doi:10.1016/j.pain.2006.02.023.

[48] Groves DA, Brown VJ. Vagal nerve stimulation: A review of its applications and potential mechanisms that mediate its clinical effects. Neurosci Biobehav Rev 2005;29:493–500. doi:10.1016/j.neubiorev.2005.01.004.

[49] Ansari S, Chaudhri K, Moutaery K. Vagus nerve stimulation: indications and limitations. Oper Neuromodulation 2007:281–6.

[50] Lefaucheur JP. Methods of therapeutic cortical stimulation. Neurophysiol Clin 2009;39:1–14. doi:10.1016/j.neucli.2008.11.001.

[51] Bystritsky A, Kerwin L, Feusner J. A pilot study of cranial electrotherapy stimulation for generalized anxiety disorder. J Clin Psychiatry 2008;69:412–7.

[52] DeGiorgio CM, Murray D, Markovic D, Whitehurst T. Trigeminal Nerve Stimulation for Epilepsy: Long-Term Feasibility and Efficacy. Neurology 2009;72:936–8. doi:10.1212/01.wnl.0000344181.97126.b4.

[53] Levkovitz Y, Roth Y, Harel EV, Braw Y, Sheer A, Zangen A. A randomized controlled feasibility and safety study of deep transcranial magnetic stimulation. Clin Neurophysiol 2007;118:2730–44. doi:10.1016/j.clinph.2007.09.061.

[54] Tufail Y, Matyushov A, Baldwin N, Tauchmann ML, Georges J, Yoshihiro A, et al. Transcranial pulsed ultrasound stimulates intact brain circuits. Neuron 2010;66:681–94. doi:10.1016/j.neuron.2010.05.008.

[55] Legon W, Sato TF, Opitz A, Mueller J, Barbour A, Williams A, et al. Transcranial focused ultrasound modulates the activity of primary somatosensory cortex in humans. Nat Neurosci 2014;17:322–9. doi:10.1038/nn.3620.

[56] Mayberg HS, Lozano AM, Voon V, McNeely HE, Seminowicz D, Hamani C, et al. Deep brain stimulation for treatment-resistant depression. Neuron 2005;45:651–60. doi:10.1016/j.neuron.2005.02.014.

[57] O'Brien WD. Ultrasound-biophysics mechanisms. Prog Biophys Mol Biol 2007;93:212–55. doi:10.1016/j.pbiomolbio.2006.07.010.

[58] Szabo TL. Diagnostic ultrasound imaging: inside out. Academic Press; 2004.

[59] Hynynen K, Jolesz FA. Demonstration of potential noninvasive ultrasound brain therapy through an intact skull. Ultrasound Med Biol 1998;24:275–83.

[60] White J, Clement GT, Hynynen K. Transcranial ultrasound focus reconstruction with phase and amplitude correction. Ieee Trans Ultrason Ferroelectr Freq Control 2005;52:1518–22.

[61] Martin E, Jeanmonod D, Morel A, Zadicario E, Werner B. High-intensity focused ultrasound for noninvasive functional neurosurgery. Ann Neurol 2009;66:858–61. doi:10.1002/ana.21801.

[62] Fishman PS, Frenkel V. Treatment of Movement Disorders With Focused Ultrasound 2017. doi:10.1177/1179573517705670.

[63] E Konofagou E, Tunga Y-S, Choia J, Deffieuxa T, Baseria B, Vlachosa F. Ultrasound-induced blood-brain barrier opening. Curr Pharm Biotechnol 2012;13:1332–45.

[64] Aryal M, Arvanitis CD, Alexander PM, McDannold N. Ultrasound-mediated blood–brain barrier disruption for targeted drug delivery in the central nervous system. Adv Drug Deliv Rev 2014;72:94–109.

[65] McDannold N, Zhang Y-Z, Power C, Arvanitis C, Vykhodtseva N, Livingstone M. Targeted delivery of GABA via ultrasound-induced blood-brain barrier disruption blocks somatosensory-evoked potentials. J Ther Ultrasound 2015;3:P28.

[66] Tyler WJ, Tufail Y, Finsterwald M, Tauchmann ML, Olson EJ, Majestic C. Remote excitation of neuronal circuits using low-intensity, low-frequency ultrasound. PLoS One 2008;3. doi:10.1371/journal.pone.0003511.

[67] Harvey EN. THE EFFECT OF HIGH FREQUENCY SOUND WAVES ON HEART MUSCLE AND OTHER IRRITABLE TISSUES. Am J Physiol -- Leg Content 1929;91:284–90.

[68] Science S, Series N, Jan N. Production of Reversible Changes in the Central Nervous System by Ultrasound Author (s): F . J . Fry , H . W . Ades and W . J . Fry Stable URL : http://www.jstor.org/stable/1753347 . of Reversible Production Changes in the Central Nervous System by Ultr 1958;127:83–4.

[69] Gavrilov LR, Gersuni G V, Ilyinski OB, Tsirulnikov EM, Shchekanov EE. A study of reception with the use of focused ultrasound. I. Effects on the skin and deep receptor structures in man. Brain Res 1977;135:265–77.

[70] Gavrilov LR, Gersuni G V, Ilyinsky OB, Tsirulnikov EM, Shchekanov EE. A study of reception with the use of focused ultrasound. II. Effects on the animal receptor structures. Brain Res 1977;135:279–85.

[71] Gavrilov LR, Tsirulnikov EM, Davies IA. Application of focused ultrasound for the stimulation of neural structures. Ultrasound Med Biol 1996;22:179–92.

[72] Muratore R, LaManna J, Szulman E, Kalisz A, Lamprecht M, Simon M, et al. Bioeffective ultrasound at very low doses: Reversible manipulation of neuronal cell morphology and function in vitro. AIP Conf Proc 2009;1113:25–9. doi:10.1063/1.3131426.

[73] Fini M, Tyler WJ. Transcranial focused ultrasound: a new tool for non-invasive neuromodulation. Int Rev Psychiatry 2017;29:168–77. doi:10.1080/09540261.2017.1302924.

[74] Min B-K, Bystritsky A, Jung K-I, Fischer K, Zhang Y, Maeng L-S, et al. Focused ultrasound-mediated suppression of chemically-induced acute epileptic EEG activity. BMC Neurosci 2011;12:23. doi:10.1186/1471-2202-12-23.

[75] Yoo S-S, Bystritsky A, Lee J-H, Zhang Y, Fischer K, Min B-K, et al. Focused ultrasound modulates region-specific brain activity. Neuroimage 2011;56:1267–75. doi:10.1016/j.neuroimage.2011.02.058.

[76] Yang PS, Kim H, Lee W, Bohlke M, Park S, Maher TJ, et al. Transcranial focused ultrasound to the thalamus is associated with reduced rxtracellular GABA levels in rats. Neuropsychobiology 2012;65:153–60. doi:10.1159/000336001.

[77] King RL, Brown JR, Newsome WT, Pauly KB. Effective parameters for ultrasound-induced in

vivo neurostimulation. Ultrasound Med Biol 2013;39:312–31. doi:10.1016/j.ultrasmedbio.2012.09.009.

[78] Younan Y, Deffieux T, Larrat B, Fink M, Tanter M, Aubry J-F. Influence of the pressure field distribution in transcranial ultrasonic neurostimulation. Med Phys 2013;40:82902. doi:10.1118/1.4812423.

[79] Mehić E, Xu JM, Caler CJ, Coulson NK, Moritz CT, Mourad PD. Increased Anatomical Specificity of Neuromodulation via Modulated Focused Ultrasound. PLoS One 2014;9:e86939. doi:10.1371/journal.pone.0086939.

[80] Kim H, Chiu A, Lee SD, Fischer K, Yoo S-S. Focused Ultrasound-mediated Non-invasive Brain Stimulation: Examination of Sonication Parameters. Brain Stimul 2014;7:748–56. doi:http://dx.doi.org/10.1016/j.brs.2014.06.011.

[81] Kim H, Park MY, Lee SD, Lee W, Chiu A, Yoo S-S. Suppression of EEG visual-evoked potentials in rats via neuromodulatory focused ultrasound. Neuroreport 2015;26:211.

[82] Naor O, Krupa S, Shoham S, Adrianov O S VNIFVFUNAAVM and GM, W A, Aryal M ACDAPM and MN, et al. Ultrasonic neuromodulation. J Neural Eng 2016;13:31003. doi:10.1088/1741-2560/13/3/031003.

[83] Hameroff S, Trakas M, Duffield C, Annabi E, Gerace MB, Boyle P, et al. Transcranial ultrasound (TUS) effects on mental states: a pilot study. Brain Stimul 2013;6:409–15.

[84] Deffieux T, Younan Y, Wattiez N, Tanter M, Pouget P, Aubry J-F. Low-Intensity Focused Ultrasound Modulates Monkey Visuomotor Behavior. Curr Biol 2013;23:2430–3. doi:http://dx.doi.org/10.1016/j.cub.2013.10.029.

[85] Wattiez N, Constans C, Deffieux T, Daye PM, Tanter M, Aubry J-F, et al. Transcranial ultrasonic stimulation modulates single-neuron discharge in macaques performing an antisaccade task. Brain Stimul 2017.

[86] Legon W, Sato TF, Opitz A, Mueller J, Barbour A, Williams A, et al. Transcranial focused ultrasound modulates the activity of primary somatosensory cortex in humans. Nat Neurosci 2014;74:322.

[87] Mueller J, Legon W, Opitz A, Sato TF, Tyler WJ. Transcranial Focused Ultrasound Modulates Intrinsic and Evoked EEG Dynamics. Brain Stimul n.d. doi:http://dx.doi.org/10.1016/j.brs.2014.08.008.

[88] Lee W, Kim H, Jung Y, Song I-U, Chung YA, Yoo S-S. Image-Guided Transcranial Focused Ultrasound Stimulates Human Primary Somatosensory Cortex. Sci Rep 2015;5:8743. doi:10.1038/srep08743.

[89] Lee W, Chung YA, Jung Y, Song I-U, Yoo S-S. Simultaneous acoustic stimulation of human primary and secondary somatosensory cortices using transcranial focused ultrasound. BMC Neurosci 2016;17:68. doi:10.1186/s12868-016-0303-6.

[90] Lee W, Kim H-C, Jung Y, Chung YA, Song I-U, Lee J-H, et al. Transcranial focused ultrasound stimulation of human primary visual cortex. Sci Rep 2016;6:34026. doi:10.1038/srep34026.

[91] Song K-I, Lee S, Park SE, Hwang D, Kim H, Youn I. Localization of ultrasound waveform for low intensity ultrasound-induced neuromodulation in a mouse model. Eng. Med. Biol. Soc.

(EMBC), 2017 39th Annu. Int. Conf. IEEE, IEEE; 2017, p. 1122–5.

[92] Robertson J, Martin E, Cox B, Treeby BE. Sensitivity of simulated transcranial ultrasound fields to acoustic medium property maps. Phys Med Biol 2017:aa5e98. doi:10.1088/1361-6560/aa5e98.

[93] Robertson JLB, Cox BT, Jaros J, Treeby BE. Accurate simulation of transcranial ultrasound propagation for ultrasonic neuromodulation and stimulation. J Acoust Soc Am 2017;141:1726–38.

[94] Jung YJ, Kim R, Ham H-J, Park SI, Lee MY, Kim J, et al. Focused Low-Intensity Pulsed Ultrasound Enhances Bone Regeneration in Rat Calvarial Bone Defect through Enhancement of Cell Proliferation. Ultrasound Med Biol 2015;41:999–1007. doi:10.1016/j.ultrasmedbio.2014.11.008.

[95] Lee W, Lee SD, Park MY, Foley L, Purcell-Estabrook E, Kim H, et al. Image-Guided Focused Ultrasound-Mediated Regional Brain Stimulation in Sheep. Ultrasound Med Biol 2016;42:459–70. doi:10.1016/j.ultrasmedbio.2015.10.001.

[96] Liu D, Schaible K, Low W, Ebbini ES. Three-dimensional image guidance for transcranial focused ultrasound therapy. Biomed. Imaging (ISBI 2017), 2017 IEEE 14th Int. Symp., IEEE; 2017, p. 916–9.

[97] Kim H, Chiu A, Park S, Yoo SS. Image-guided navigation of single-element focused ultrasound transducer. Int J Imaging Syst Technol 2012;22:177–84. doi:10.1002/ima.22020.

[98] Kamimura HAS, Wang S, Chen H, Wang Q, Aurup C, Acosta C, et al. Focused ultrasound neuromodulation of cortical and subcortical brain structures using 1.9 MHz. Med Phys 2016;43:5730–5.

[99] Constans C, Deffieux T, Pouget P, Tanter M, Aubry J-F. A 200 - 1380 kHz Quadrifrequency Focused Ultrasound Transducer For Neurostimulation In Rodents And Primates: Transcranial In Vitro Calibration And Numerical Study Of The Influence Of Skull Cavity. IEEE Trans Ultrason Ferroelectr Freq Control 2017:1–1. doi:10.1109/TUFFC.2017.2651648.

[100] Oh S, Kim DH, Youn I. Low-intensity focused ultrasound stimulator using focal depth controller for improved targeting in neuromuscular rehabilitation. Eng. Med. Biol. Soc. (EMBC), 2017 39th Annu. Int. Conf. IEEE, IEEE; 2017, p. 209–12.

[101] Li G-F, Zhao H-X, Zhou H, Yan F, Wang J-Y, Xu C-X, et al. Improved Anatomical Specificity of Non-invasive Neuro-stimulation by High Frequency (5 MHz) Ultrasound. Sci Rep 2016;6:24738. doi:10.1038/srep24738.

[102] Mueller JK, Ai L, Bansal P, Legon W. Numerical evaluation of the skull for human neuromodulation with transcranial focused ultrasound. J Neural Eng 2017.

[103] Dallapiazza RF, Timbie KF, Holmberg S, Gatesman J, Lopes MB, Price RJ, et al. Noninvasive neuromodulation and thalamic mapping with low-intensity focused ultrasound 2017:1–10. doi:10.3171/2016.11.JNS16976.

[104] Downs ME, Teichert T, Buch A, Karakatsani ME, Sierra C, Chen S, et al. Focused ultrasound enhances sensorimotor decision-making in monkeys 2016:1–29. doi:http://dx.doi.org/10.1101/041152.

[105] Lee W, Kim S, Kim B, Lee C, Chung YA, Kim L, et al. Non-invasive transmission of

sensorimotor information in humans using an EEG/focused ultrasound brain-to-brain interface. PLoS One 2017;12:e0178476.

[106] Yulug B, Hanoglu L, Kilic E. The neuroprotective effect of focused ultrasound : New perspectives on an old tool 2017. doi:10.1016/j.brainresbull.2017.04.015.

[107] Hakimova H, Kim S, Chu K, Lee SK, Jeong B, Jeon D. Ultrasound stimulation inhibits recurrent seizures and improves behavioral outcome in an experimental model of mesial temporal lobe epilepsy. Epilepsy Behav 2015. doi:10.1016/j.yebeh.2015.04.008.

[108] Leinenga G, Gotz J. Scanning ultrasound removes amyloid- and restores memory in an Alzheimer's disease mouse model. Sci Transl Med 2015;7:278ra33-278ra33. doi:10.1126/scitranslmed.aaa2512.

[109] Guo T, Li H, Lv Y, Lu H, Niu J, Sun J, et al. Pulsed transcranial ultrasound stimulation immediately after the ischemic brain injury is neuroprotective. IEEE Trans Biomed Eng 2015;62:2352–7. doi:10.1109/TBME.2015.2427339.

[110] Yenari M, Kitagawa K, Lyden P, Perez-Pinzon M. Metabolic downregulation: a key to successful neuroprotection? Stroke 2008;39:2910–7. doi:10.1161/STROKEAHA.108.514471.

[111] Sakata K, Woo NH, Martinowich K, Greene JS, Schloesser RJ, Shen L, et al. Critical role of promoter IV-driven BDNF transcription in GABAergic transmission and synaptic plasticity in the prefrontal cortex. Proc Natl Acad Sci 2009;106:5942–7.

[112] Plaksin M, Kimmel E, Shoham S. Cell-Type-Selective Effects of Intramembrane Cavitation as a Unifying Theoretical Framework for Ultrasonic Neuromodulation. eNeuro 2016;3:ENEURO.0136-15.2016. doi:10.1523/ENEURO.0136-15.2016.

[113] Li H, Li Y, Yuan L, Wu C, Lu H, Tong S. Intraoperative cerebral blood flow imaging of rodents. Rev Sci Instrum 2014;85. doi:10.1063/1.4895657.

[114] Duman RS, Monteggia LM. A Neurotrophic Model for Stress-Related Mood Disorders. Biol Psychiatry 2006;59:1116–27. doi:10.1016/j.biopsych.2006.02.013.

[115] Castren E. Is mood chemistry? Nat Rev Neurosci 2005;6:241–6.

[116] Scarcelli T, Jordão JF, O'Reilly M a, Ellens N, Hynynen K, Aubert I. Stimulation of hippocampal neurogenesis by transcranial focused ultrasound and microbubbles in adult mice. Brain Stimul 2014;7:304–7. doi:10.1016/j.brs.2013.12.012.

[117] Devor A, Sakadžić S, Srinivasan VJ, Yaseen M a, Nizar K, Saisan P a, et al. Frontiers in optical imaging of cerebral blood flow and metabolism. J Cereb Blood Flow Metab 2012;32:1259–76. doi:10.1038/jcbfm.2011.195.

[118] Li H, Sun J, Zhang D, Omire-Mayor D, Lewin PA, Tong S. Low-intensity (400 mW/cm 2 , 500 kHz) pulsed transcranial ultrasound preconditioning may mitigate focal cerebral ischemia in rats. Brain Stimul 2017. doi:10.1016/j.brs.2017.02.008.

[119] Kim H, Chiu A, Lee SD, Fischer K, Yoo SS. Focused ultrasound-mediated non-invasive brain stimulation: Examination of sonication parameters. Brain Stimul 2014;7:748–56. doi:10.1016/j.brs.2014.06.011.

[120] Plaksin M, Shoham S, Kimmel E. Intramembrane cavitation as a predictive bio-piezoelectric

mechanism for ultrasonic brain stimulation. Phys Rev X 2014;4:11004. doi:10.1103/PhysRevX.4.011004.

[121] Dunn AK, Devor A, Dale AM, Boas DA. Spatial extent of oxygen metabolism and hemodynamic changes during functional activation of the rat somatosensory cortex. Neuroimage 2005;27:279–90. doi:S1053-8119(05)00269-7 [pii] 10.1016/j.neuroimage.2005.04.024.

[122] Guo X, He Y, Lu H, Li Y, Su X, Jiang Y, et al. Plastic change along the intact crossed pathway in acute phase of cerebral ischemia revealed byoptical intrinsic signal imaging. Neural Plast 2016;2016. doi:10.1155/2016/1923160.

[123] Briers JD, Webster S. Laser speckle contrast analysis (LASCA): a nonscanning, full-field technique for monitoring capillary blood flow. J Biomed Opt 1996;1:174. doi:10.1117/12.231359.

[124] Jones PB, Shin HK, Boas D a, Hyman BT, Moskowitz M a, Ayata C, et al. Simultaneous multispectral reflectance imaging and laser speckle flowmetry of cerebral blood flow and oxygen metabolism in focal cerebral ischemia. J Biomed Opt 2008;13:44007. doi:10.1117/1.2950312.

[125] Cheng H, Luo Q, Zeng S, Chen S, Cen J, Gong H. Modified laser speckle imaging method with improved spatial resolution. J Biomed Opt 2003;8:559–64. doi:10.1117/1.1578089.

[126] Miao P, Rege A, Li N, Thakor N V, Tong S. High resolution cerebral blood flow imaging by registered laser speckle contrast analysis. IEEE Trans Biomed Eng 2010;57:1152–7. doi:10.1109/TBME.2009.2037434.

[127] Boas DA, Dunn AK. Laser speckle contrast imaging in biomedical optics. J Biomed Opt 2010;15:11109. doi:10.1117/1.3285504.

[128] Lu H, Li Y, Li H, Yuan L, Liu Q, Sun Y, et al. Single-trial estimation of the cerebral metabolic rate of oxygen with imaging photoplethysmography and laser speckle contrast imaging. Opt Lett 2015;40:1193. doi:10.1364/OL.40.001193.

[129] Charan J, Kantharia ND. How to calculate sample size in animal studies? J Pharmacol Pharmacother 2013;4:303–6. doi:10.4103/0976-500X.119726.

[130] Guo X, He Y, Lu H, Li Y, Su X, Jiang Y, et al. Plastic change along the Intact Crossed Pathway in Acute Phase of Cerebral Ischemia Revealed by Optical Intrinsic Signal Imaging. Neural Plast 2016;2016.

[131] Haigh SM, Cooper NR, Wilkins AJ. Cortical excitability and the shape of the haemodynamic response. Neuroimage 2015;111:379–84. doi:10.1016/j.neuroimage.2015.02.034.

[132] Kim H, Lee SD, Chiu A, Yoo S-S, Park S. Estimation of the spatial profile of neuromodulation and the temporal latency in motor responses induced by focused ultrasound brain stimulation. Neuroreport 2014;25:475–9. doi:10.1097/WNR.0000000000000118.

[133] Plaksin M, Kimmel E, Shoham S. Cell-type-selective effects of intramembrane cavitation as a unifying theoretical framework for ultrasonic neuromodulation. eNeuro 2016;3:ENEURO-0136. doi:10.1523/ENEURO.0136-15.2016.

[134] Belousov AB. Novel model for the mechanisms of glutamate-dependent excitotoxicity: Role of neuronal gap junctions. Brain Res 2012;1487:123–30. doi:10.1016/j.brainres.2012.05.063.

[135] Lindauer U, Dirnagl U, Füchtemeier M, Böttiger C, Offenhauser N, Leithner C, et al.

Pathophysiological interference with neurovascular coupling–when imaging based on hemoglobin might go blind. Front Neuroenergetics 2010;2:25.

[136] Krause B, Cohen Kadosh R. Not all brains are created equal: the relevance of individual differences in responsiveness to transcranial electrical stimulation. Front Syst Neurosci 2014;8:25.

[137] Weigand A, Richtermeier A, Feeser M, Guo JS, Briesemeister BB, Grimm S, et al. State-dependent effects of prefrontal repetitive transcranial magnetic stimulation on emotional working memory. Brain Stimul 2013;6:905–12.

[138] Mazzoni N, Jacobs C, Venuti P, Silvanto J, Cattaneo L. State-dependent TMS reveals representation of affective body movements in the anterior intraparietal cortex. J Neurosci 2017;37:7231–9.

[139] Wiegert JS, Mahn M, Prigge M, Printz Y, Yizhar O. Silencing neurons: tools, applications, and experimental constraints. Neuron 2017;95:504–29. doi:10.1016/j.neuron.2017.06.050.

[140] Vierling-Claassen D, Cardin JA, Moore CI, Jones SR. Computational modeling of distinct neocortical oscillations driven by cell-type selective optogenetic drive: separable resonant circuits controlled by low-threshold spiking and fast-spiking interneurons. Front Hum Neurosci 2010;4:198. doi:10.3389/fnhum.2010.00198.

[141] Klooster DCW, de Louw AJA, Aldenkamp AP, Besseling RMH, Mestrom RMC, Carrette S, et al. Technical aspects of neurostimulation: Focus on equipment, electric field modeling, and stimulation protocols. Neurosci Biobehav Rev 2016;65:113–41. doi:10.1016/j.neubiorev.2016.02.016.

[142] Kelley RE. Stroke in the postoperative period. Med Clin North Am 2001;85:1263–76. doi:10.1016/S0025-7125(05)70377-1.

[143] Dacey LJ, Likosky DS, Leavitt BJ, Lahey SJ, Quinn RD, Hernandez F, et al. Perioperative stroke and long-term survival after coronary bypass graft surgery. Ann Thorac Surg 2005;79:532–6. doi:10.1016/j.athoracsur.2004.07.027.

[144] Wilson P V., Ammar AD. The incidence of ischemic stroke versus intracerebral hemorrhage after carotid endarterectomy: a review of 2452 cases. Ann Vasc Surg 2005;19:1–4. doi:10.1007/s10016-004-0131-5.

[145] McKhann GM, Grega MA, Borowicz LM, Baumgartner WA, Selnes OA. Stroke and encephalopathy after cardiac surgery: an update. Stroke 2006;37:562–71. doi:10.1161/01.STR.0000199032.78782.6c.

[146] Gidday JM. Cerebral preconditioning and ischaemic tolerance. Nat Rev Neurosci 2006;7:437–48. doi:10.1038/nrn1927.

[147] Stevens SL, Vartanian KB, Stenzel-Poore MP. Reprogramming the response to stroke by preconditioning. Stroke 2014;45:2527–31. doi:10.1161/STROKEAHA.114.002879.

[148] Otori T, Greenberg JH, Welsh FA. Cortical spreading depression causes a long-lasting decrease in cerebral blood flow and induces tolerance to permanent focal ischemia in rat brain. J Cereb Blood Flow Metab 2003;23:43–50. doi:10.1097/01.WCB.0000035180.38851.38.

[149] Matsushima K, Hogan MJ, Hakim AM. Cortical spreading depression protects against subsequent focal cerebral ischemia in rats. J Cereb Blood Flow Metab 1996;16:221–6.

[150] Kobayashi S, Harris VA, Welsh FA. Spreading depression induces tolerance of cortical neurons to ischemia in rat brain. J Cereb Blood Flow Metab 1995;15:721–7. doi:10.1038/jcbfm.1995.93.

[151] Pérez-Pinzón MA, Xu G-P, Dietrich WD, Rosenthal M, Sick TJ. Rapid preconditioning protects rats against ischemic neuronal damage after 3 but not 7 days of reperfusion following global cerebral ischemia. J Cereb Blood Flow Metab 1997;17:175–82. doi:10.1097/00004647-199702000-00007.

[152] DAHL NA, BALFOUR WM. Prolonged anoxic survival due to anoxia pre-exposure: brain ATP, lactate, and pyruvate. Am J Physiol 1964;207:452–6.

[153] Gesuete R, Kohama SG, Stenzel-Poore MP. Toll-like receptors and ischemic brain injury. J Neuropathol Exp Neurol 2014;73:378–86. doi:10.1097/NEN.0000000000000068.

[154] Plaschke K, Weigand MA, Michel A, Martin E, Bardenheuer HJ. Permanent cerebral hypoperfusion: "preconditioning-like" effects on rat energy metabolism towards acute systemic hypotension. Brain Res 2000;858:363–70. doi:10.1016/S0006-8993(00)01950-8.

[155] Chopp M, Chen H, Ho K-L, Dereski MO, Brown E, Hetzel FW, et al. Transient hyperthermia protects against subsequent forebrain ischemic cell damage in the rat. Neurology 1989;39:1396–1396. doi:10.1212/WNL.39.10.1396.

[156] Wang L, Traystman RJ, Murphy SJ. Inhalational anesthetics as preconditioning agents in ischemic brain. Curr Opin Pharmacol 2008;8:104–10. doi:10.1016/j.coph.2007.09.005.

[157] Dirnagl U, Becker K, Meisel A. Preconditioning and tolerance against cerebral ischaemia: from experimental strategies to clinical use. Lancet Neurol 2009;8:398–412. doi:10.1016/S1474-4422(09)70054-7.

[158] Bracko O, Di Pietro V, Lazzarino G, Amorini AM, Tavazzi B, Artmann J, et al. 3-Nitropropionic acid-induced ischemia tolerance in the rat brain is mediated by reduced metabolic activity and cerebral blood flow. J Cereb Blood Flow Metab 2014;34:1522–30. doi:10.1038/jcbfm.2014.112.

[159] Wiegand F, Liao W, Busch C, Castell S, Knapp F, Lindauer U, et al. Respiratory chain inhibition induces tolerance to focal cerebral ischemia. J Cereb Blood Flow Metab 1999;19:1229–37. doi:10.1097/00004647-199911000-00007.

[160] Sun M, Deng B, Zhao X, Gao C, Yang L, Zhao H, et al. Isoflurane preconditioning provides neuroprotection against stroke by regulating the expression of the TLR4 signalling pathway to alleviate microglial activation. Sci Rep 2015;5:11445. doi:10.1038/srep11445.

[161] Nawashiro H, Tasaki K, Ruetzler CA, Hallenbeck JM. TNF-a pretreatment induces protective effects against focal cerebral ischemia in mice. J Cereb Blood Flow Metab 1997;17:483–90. doi:10.1097/00004647-199705000-00001.

[162] Pasley BN, Inglis BA, Freeman RD. Analysis of oxygen metabolism implies a neural origin for the negative BOLD response in human visual cortex. Neuroimage 2007;36:269–76. doi:10.1016/j.neuroimage.2006.09.015.

[163] Elhag M, Coghlan K, Christmas P, Harvey W, Harris M. The anti-inflammatory effects of dexamethasone and therapeutic ultrasound in oral surgery. Br J Oral Maxillofac Surg 1985;23:17–23. doi:10.1016/0266-4356(85)90074-9.

[164] Gigliotti JC, Huang L, Ye H, Bajwa A, Chattrabhuti K, Lee S, et al. Ultrasound prevents renal

ischemia-reperfusion injury by stimulating the splenic cholinergic anti-inflammatory pathway. J Am Soc Nephrol 2013;24:1451–60. doi:10.1681/ASN.2013010084.

[165] Chung JI, Barua S, Choi BH, Min BH, Han HC, Baik EJ. Anti-inflammatory effect of low intensity ultrasound (LIUS) on complete Freund's adjuvant-induced arthritis synovium. Osteoarthr Cartil 2012;20:314–22. doi:10.1016/j.joca.2012.01.005.

[166] Kravchenko IA, Kobernik AA, Aleksandrova AI, Prystupa B V., Lepikh YI, Snegur PA. Anti-inflammatory action of therapeutic and low-frequency ultrasound on the inflammatory process model on rats. Biophysics (Oxf) 2013;58:423–7. doi:10.1134/S0006350913030081.

[167] Watson BD, Dietrich WD, Busto R, Wachtel MS, Ginsberg MD. Induction of reproducible brain infarction by photochemically initiated thrombosis. Ann Neurol 1985;17:497–504. doi:10.1002/ana.410170513.

[168] Li Y, Zhu S, Yuan L, Lu H, Li H, Tong S. Predicting the ischemic infarct volume at the first minute after occlusion in rodent stroke model by laser speckle imaging of cerebral blood flow. J Biomed Opt 2013;18:76024. doi:10.1117/1.JBO.18.7.076024.

[169] Paul JS, Luft AR, Yew E, Sheu FS. Imaging the development of an ischemic core following photochemically induced cortical infarction in rats using Laser Speckle Contrast Analysis (LASCA). Neuroimage 2006;29:38–45. doi:S1053-8119(05)00535-5 [pii]10.1016/j.neuroimage.2005.07.019.

[170] Watson C, George P. The rat brain in stereotaxic coordinates. 6th ed. San Diego: Academic Press; 2007.

[171] Sun Z, Baker W, Hiraki T, Greenberg JH. The effect of right vagus nerve stimulation on focal cerebral ischemia: an experimental study in the rat. Brain Stimul 2012;5:1–10. doi:10.1016/j.brs.2011.01.009.

[172] McBride DW, Klebe D, Tang J, Zhang JH. Correcting for brain swelling's effects on infarct volume calculation after middle cerebral artery occlusion in rats. Transl Stroke Res 2015;6:323–38. doi:10.1007/s12975-015-0400-3.

[173] Mcbride DW, Donovan V, Hsu MS, Obenaus A, Rodgers VGJ, Binder DK. Reduction of cerebral edema via an osmotic transport device improves functional outcome after traumatic brain injury in mice 2016;121:285–9. doi:10.1007/978-3-319-18497-5.

[174] Hakim AM. Ischemic penumbra: The therapeutic window. Neurology 1998;51:S44–6. doi:10.1212/WNL.51.3_Suppl_3.S44.

[175] Hanawa K, Ito K, Aizawa K, Shindo T, Nishimiya K, Hasebe Y, et al. Low-intensity pulsed ultrasound induces angiogenesis and ameliorates aeft ventricular dysfunction in a porcine model of chronic myocardial ischemia. PLoS One 2014;9:e104863. doi:10.1371/journal.pone.0104863.

[176] Huang J-J, Shi Y-Q, Li R-L, Hu A, Zhou H-S, Cheng Q, et al. Angiogenesis effect of therapeutic ultrasound on ischemic hind limb in mice. Am J Transl Res 2014;6:703–13.

[177] Bertuglia S, Giusti A, Picano E. Effects of diagnostic cardiac ultrasound on oxygen free radical production and microvascular perfusion during ischemia reperfusion. Ultrasound Med Biol 2004;30:549–57. doi:10.1016/j.ultrasmedbio.2003.12.008.

[178] Davis CM, Ammi AY, Alkayed NJ, Kaul S, Ahmad A, Yun Y, et al. Ultrasound stimulates

formation and release of vasoactive compounds in brain endothelial cells. Am J Physiol Heart Circ Physiol 2015;309:H583-91. doi:10.1152/ajpheart.00690.2014.

[179] Radomski M., Palmer RM., Moncada S. Endogenous nitric oxide inhibits human platelet adhesion to vascular endothelium. Lancet 1987;330:1057–8. doi:10.1016/S0140-6736(87)91481-4.

[180] Laufs U, Gertz K, Huang P, Nickenig G, Böhm M, Dirnagl U, et al. Atorvastatin upregulates type III nitric oxide synthase in thrombocytes, decreases platelet activation, and protects from cerebral ischemia in normocholesterolemic mice. Stroke 2000;31:2442–9. doi:10.1161/01.STR.31.10.2442.

[181] Loscalzo J. Nitric oxide insufficiency, platelet activation, and arterial thrombosis 2012:756–62. doi:10.1161/hh0801.089861.

[182] Gidday JM, Shah a R, Maceren RG, Wang Q, Pelligrino D a, Holtzman DM, et al. Nitric oxide mediates cerebral ischemic tolerance in a neonatal rat model of hypoxic preconditioning. J Cereb Blood Flow Metab 1999;19:331–40. doi:10.1097/00004647-199903000-00011.

[183] WHO. http://www.who.int/mental_health/management/depression/en/ 2009.

[184] Vos T, Barber RM, Bell B, Bertozzi-Villa A, Biryukov S, Bolliger I, et al. Global, regional, and national incidence, prevalence, and years lived with disability for 301 acute and chronic diseases and injuries in 188 countries, 1990-2013: A systematic analysis for the Global Burden of Disease Study 2013. Lancet 2015;386:743–800. doi:10.1016/S0140-6736(15)60692-4.

[185] WHO. Depression fact sheet 2017. http://www.who.int/mediacentre/factsheets/fs369/en/.

[186] Al-harbi KS. Treatment-resistant depression : therapeutic trends , challenges , and future directions 2012:369–88.

[187] Fava M. Diagnosis and definition of treatment-resistant depression. Biol Psychiatry 2003;53:649–59. doi:http://dx.doi.org/10.1016/S0006-3223(03)00231-2.

[188] Lisanby SH. Electroconvulsive Therapy for Depression. N Engl J Med 2007;19357:1939–45. doi:10.1056/NEJMct075234.

[189] Rush AJ, Marangell LB, Sackeim HA, George MS, Brannan SK, Davis SM, et al. Vagus nerve stimulation for treatment-resistant depression: A randomized, controlled acute phase trial. Biol Psychiatry 2005;58:347–54. doi:10.1016/j.biopsych.2005.05.025.

[190] Kennedy SH, Giacobbe P, Rizvi SJ, Placenza FM, Nishikawa Y, Mayberg HS, et al. Deep brain stimulation for treatment-resistant depression: follow-up after 3 to 6 years. Am J Psychiatry 2011;168:502–10.

[191] Pascual-Leone A, Rubio B, Pallardó F, Catalá MD. Rapid-rate transcranial magnetic stimulation of left dorsolateral prefrontal cortex in drug-resistant depression. Lancet 1996;348:233–7.

[192] Sackeim HA, Prudic J, Fuller R, Keilp J, Lavori PW, Olfson M. The Cognitive Effects of Electroconvulsive Therapy in Community Settings. Neuropsychopharmacology 2007;32:244–54. doi:10.1038/sj.npp.1301180.

[193] Bystritsky A, Korb AS, Douglas PK, Cohen MS, Melega WP, Mulgaonkar AP, et al. A review of low-intensity focused ultrasound pulsation. Brain Stimul 2011;4:125–36.

doi:10.1016/j.brs.2011.03.007.

[194] Guo T, Li H, Lv Y, Lu H, Niu J, Sun J, et al. Neuroprotective pulsed transcranial ultrasound stimulation in ischemic brain injury after distal middle cerebral artery occlusion. IEEE Trans Biomed Eng 2015:1.

[195] Li H, Sun J, Zhang D, Omire-Mayor D, Lewin PA, Tong S. Low-intensity (400 mW/cm 2 , 500 kHz) pulsed transcranial ultrasound preconditioning may mitigate focal cerebral ischemia in rats. Brain Stimul 2017;10:695–702. doi:10.1016/j.brs.2017.02.008.

[196] Hakimova H, Kim S, Chu K, Sang KL, Jeong B, Jeon D. Ultrasound stimulation inhibits recurrent seizures and improves behavioral outcome in an experimental model of mesial temporal lobe epilepsy. Epilepsy Behav 2015;49:26–32.

[197] Lin W-T, Chen R-C, Lu W-W, Liu S-H, Yang F-Y. Protective effects of low-intensity pulsed ultrasound on aluminum-induced cerebral damage in Alzheimer's disease rat model. Sci Rep 2015;5:9671. doi:10.1038/srep09671.

[198] Tsai S-J. Transcranial focused ultrasound as a possible treatment for major depression. Med Hypotheses 2015;84:381–3. doi:10.1016/j.mehy.2015.01.030.

[199] Nestler EJ, Barrot M, DiLeone RJ, Eisch AJ, Gold SJ, Monteggia LM. Neurobiology of depression. Neuron 2002;34:13–25.

[200] Guilloux J-P, Douillard-Guilloux G, Kota R, Wang X, Gardier A, Martinowich K, et al. Molecular evidence for BDNF-and GABA-related dysfunctions in the amygdala of female subjects with major depression. Mol Psychiatry 2012;17:1130.

[201] Dwivedi Y, Rizavi HS, Conley RR, Roberts RC, Tamminga CA, Pandey GN. Altered gene expression of brain-derived neurotrophic factor and receptor tyrosine kinase B in postmortem brain of suicide subjects. Arch Gen Psychiatry 2003;60:804–15.

[202] Sen S, Duman R, Sanacora G. Serum brain-derived neurotrophic factor, depression, and antidepressant medications: meta-analyses and implications. Biol Psychiatry 2008;64:527–32.

[203] Sakata K, Jin L, Jha S. Lack of promoter IV-driven BDNF transcription results in depression-like behavior. Genes, Brain Behav 2010;9:712–21.

[204] Sakata K. Brain-Derived Neurotrophic Factor for Depression Therapeutics. Austin J Pharmacol Ther 2014;2:1–10.

[205] Sakata K. Brain-Derived Neurotrophic Factor and Major Depression. Neurobiol Depress 2011:391.

[206] Nestler EJ, Carlezon WA. The Mesolimbic Dopamine Reward Circuit in Depression. Biol Psychiatry 2006;59:1151–9. doi:10.1016/j.biopsych.2005.09.018.

[207] Solvason HB, Husain M, Fitzgerald PB, Rosenquist P, Mccall W V, Kimball J, et al. Improvement in quality of life with left prefrontal transcranial magnetic stimulation in patients with pharmacoresistant major depression: acute and six month outcomes. Brain Stimul 2014;7:219.

[208] Dalley JW, Cardinal RN, Robbins TW. Prefrontal executive and cognitive functions in rodents: Neural and neurochemical substrates. Neurosci. Biobehav. Rev., vol. 28, 2004, p. 771–84. doi:10.1016/j.neubiorev.2004.09.006.

[209] Chu X, Zhou Y, Hu Z, Lou J, Song W, Li J, et al. 24-Hour-Restraint Stress Induces Long-Term Depressive-Like Phenotypes in Mice. Sci Rep 2016;6:32935. doi:10.1038/srep32935.

[210] Paxinos G, Watson C. The Rat Brain in Stereotaxic Coordinates Sixth Edition by. Acad Press 2006;170:547612. doi:10.1016/0143-4179(83)90049-5.

[211] Pizzagalli DA. Depression, stress, and anhedonia: toward a synthesis and integrated model. Annu Rev Clin Psychol 2014;10:393–423. doi:10.1146/annurev-clinpsy-050212-185606.

[212] Choleris E. A detailed ethological analysis of the mouse open field test: effects of diazepam, chlordiazepoxide and an extremely low frequency pulsed magnetic field. Neurosci Biobehav Rev 2001;25:235–60. doi:10.1016/S0149-7634(01)00011-2.

[213] Castrén E, Kojima M. Brain-derived neurotrophic factor in mood disorders and antidepressant treatments. Neurobiol Dis 2017;97:119–26. doi:10.1016/j.nbd.2016.07.010.

[214] Godsil BP, Kiss JP, Spedding M, Jay TM. The hippocampal-prefrontal pathway: The weak link in psychiatric disorders? Eur Neuropsychopharmacol 2013;23:1165–81. doi:10.1016/j.euroneuro.2012.10.018.

[215] Takita M, Izaki Y, Jay TM, Kaneko H, Suzuki SS. Induction of stable long-term depression in vivo in the hippocampal-prefrontal cortex pathway. Eur J Neurosci 1999;11:4145–8. doi:10.1046/j.1460-9568.1999.00870.x.

[216] Adhikari A, Topiwala MA, Gordon JA. Synchronized Activity between the Ventral Hippocampus and the Medial Prefrontal Cortex during Anxiety. Neuron 2010;65:257–69. doi:10.1016/j.neuron.2009.12.002.

[217] Gersner R, Toth E, Isserles M, Zangen A. Site-specific antidepressant effects of repeated subconvulsive electrical stimulation: potential role of brain-derived neurotrophic factor. Biol Psychiatry 2010;67:125–32.

[218] Mattson MP, Maudsley S, Martin B. BDNF and 5-HT: A dynamic duo in age-related neuronal plasticity and neurodegenerative disorders. Trends Neurosci 2004;27:589–94. doi:10.1016/j.tins.2004.08.001.

[219] Tyler WJ, Tufail Y, Finsterwald M, Tauchmann ML, Olson EJ, Majestic C. Remote Excitation of Neuronal Circuits Using Low- Intensity, Low-Frequency Ultrasound. PLoS One 2008;3:e3511. doi:10.1371/journal.pone.0003511.

[220] Okamoto K, Aoki K. Development of a strain of spontaneously hypertensive rats. Jpn Circ J 1963;27:282–93.

[221] Paré WP. The performance of WKY rats on three tests of emotional behavior. Physiol Behav 1992;51:1051–6.

[222] Overstreet DH. Modeling depression in animal models. Psychiatr Disord Methods Protoc 2012:125–44.

[223] Krasovitski B, Frenkel V, Shoham S, Kimmel E. Intramembrane cavitation as a unifying mechanism for ultrasound-induced bioeffects. Proc Natl Acad Sci 2011;108:3258–63. doi:10.1073/pnas.1015771108.

[224] Wu J, Nyborg WL. Ultrasound, cavitation bubbles and their interaction with cells. Adv Drug

Deliv Rev 2008;60:1103–16. doi:10.1016/j.addr.2008.03.009.

[225] Pospischil M, Toledo-Rodriguez M, Monier C, Piwkowska Z, Bal T, Frégnac Y, et al. Minimal Hodgkin–Huxley type models for different classes of cortical and thalamic neurons. Biol Cybern 2008;99:427–41. doi:10.1007/s00422-008-0263-8.

[226] Chung TJ. General continuum mechanics. Cambridge University Press; 1988.

[227] Bloomfield IG, Johnston IH, Bilston LE. Effects of proteins, blood cells and glucose on the viscosity of cerebrospinal fluid. Pediatr Neurosurg 1998;28:246–51.

[228] Tyler WJ. Noninvasive neuromodulation with ultrasound? A continuum mechanics hypothesis. Neuroscientist 2011;17:25–36. doi:10.1177/1073858409348066.

[229] Ahmadi F, McLoughlin I V, Chauhan S, ter-Haar G. Bio-effects and safety of low-intensity, low-frequency ultrasonic exposure. Prog Biophys Mol Biol 2012;108:119–38.

[230] Morris CE, Juranka PF. Lipid stress at play: mechanosensitivity of voltage-gated channels. Curr Top Membr 2007;59:297–338.

[231] Sukharev S, Corey DP. Mechanosensitive channels: multiplicity of families and gating paradigms. Sci STKE 2004;2004:re4-re4.

[232] Tyler WJ. The mechanobiology of brain function. Nat Rev Neurosci 2012;13:867–78. doi:10.1038/nrn3383.

[233] Kubanek J, Shi J, Marsh J, Chen D, Deng C, Cui J, et al. Ultrasound modulates ion channel currents. Sci Rep 2016;6:24170. doi:10.1038/srep24170.

[234] Dinno MA, Dyson M, Young SR, Mortimer AJ, Hart J, Crum LA. The significance of membrane changes in the safe and effective use of therapeutic and diagnostic ultrasound. Phys Med Biol 1989;34:1543.

[235] Sundaram J, Mellein BR, Mitragotri S. An experimental and theoretical analysis of ultrasound-induced permeabilization of cell membranes. Biophys J 2003;84:3087–101.

[236] Mueller JK, Tyler WJ. A quantitative overview of biophysical forces impinging on neural function. Phys Biol 2014;11:51001. doi:10.1088/1478-3975/11/5/051001.

[237] Sassaroli E, Vykhodtseva N. Acoustic neuromodulation from a basic science prospective. J Ther Ultrasound 2016;4:17. doi:10.1186/s40349-016-0061-z.

[238] Naor O, Krupa S, Shoham S, Adrianov O S, Vykhodtseva N I, Fokin V F, Uranova N A AVM and GM, W A, Aryal M, Arvanitis C D APM and MN, et al. Ultrasonic neuromodulation. J Neural Eng 2016;13:31003. doi:10.1088/1741-2560/13/3/031003.

[239] Heimburg T, Jackson AD. On soliton propagation in biomembranes and nerves. Proc Natl Acad Sci U S A 2005;102:9790–5. doi:10.1073/pnas.0503823102.

[240] Petrov AG. Flexoelectric model for active transport. Phys. Chem. Bases Biol. Inf. Transf., Springer; 1975, p. 111–25.

[241] Heimburg T. Thermal biophysics of membranes. John Wiley & Sons; 2008.

[242] Petrov AG, Sokolov VS. Curvature-electric effect in black lipid membranes. Eur Biophys J 1986;13:139–55.

[243] Petrov AG. The lyotropic state of matter: molecular physics and living matter physics. CRC Press; 1999.

[244] Petrov AG. Electricity and mechanics of biomembrane systems: flexoelectricity in living membranes. Anal Chim Acta 2006;568:70–83.

[245] Petrov AG. Flexoelectricity in lyotropics and in living liquid crystals. Flexoelectricity Liq. Cryst. theory, Exp. Appl., Imperial College Press; 2013, p. 177–210.

Vita

Name: Hangdao Li

Education:

Shanghai Jiao Tong University, Shanghai, China, Sept 2013 – Mar 2018 (PhD)

Drexel University, Philadelphia, PA, United States, Sept 2015 – Jun 2018 (PhD)

Shanghai Jiao Tong University, Shanghai, China, Sept 2011 - Jun 2013 (M.S.)

Shanghai Jiao Tong University, Shanghai, China, Sept 2011 - Jun 2013 (B.S.)

Publications:

Journal Articles

1. **Li, H.**, et al. (2017). Low-intensity (400 mW/cm2, 500 kHz) pulsed transcranial ultrasound preconditioning may mitigate focal cerebral ischemia in rats. Brain Stimulation, vol. 10, no. 3, pp. 695–702. **(IF 6.078, JCR journal ranking Clinical Neurology Top 10%)**
2. **Li, H**., et al. (2014). Intraoperative cerebral blood flow imaging of rodents. Review of Scientific Instruments, 85(9), 094301.
3. **Li, H.**, et al. Pulsed transcranial ultrasound modulates the cortical response to the functional electrical stimulation: in vivo animal study using optical neurovascular imaging. Brain Stimulation. **(Under review)**
4. Zhang, D., **Li, H.**, et al. Antidepressant-like effect of low-intensity transcranial ultrasound stimulation. IEEE Trans. Biomed. Eng. **(Co-first author, under review)**
5. Guo, T., **Li, H.**, et al. (2015). Neuroprotective pulsed transcranial ultrasound stimulation in ischemic brain injury after distal middle cerebral artery occlusion. IEEE Trans. Biomed. Eng.
6. Yuan, L., Li, Y., **Li, H.**, et al. (2015). Intraoperative laser speckle contrast imaging improves the stability of rodent middle cerebral artery occlusion model. Journal of Biomedical Optics, 20(9), 096012-096012.
7. Lu, H., Li, Y., **Li, H.**, et al. (2015). Single-trial estimation of the cerebral metabolic rate of oxygen with imaging photoplethysmography and laser speckle contrast imaging. Optics Letters, 40(7), 1193-1196.
8. Lu, H., Li, Y., Bo, B., Yuan, L., Lu, X., **Li, H.**, et al. (2017). Hemodynamic effects of intraoperative anesthetics administration in photothrombotic stroke model: a study using laser speckle imaging.

BMC neuroscience, 18(1), 10.

9. Lu, H., Li, Y., Yuan, L., **Li, H.**, Lu, X., & Tong, S. (2014). Induction and imaging of photothrombotic stroke in conscious and freely moving rats. Journal of biomedical optics, 19(9), 096013-096013.

10. Li, Y., Zhu, S., Yuan, L., Lu, H., **Li, H.**, et al. (2013). Predicting the ischemic infarct volume at the first minute after occlusion in rodent stroke model by laser speckle imaging of cerebral blood flow. Journal of biomedical optics, 18(7), 076024-076024.

Conference Articles

11. Zhao, L., Li, Y., **Li, H.**, et al. (2015, August). The cerebral blood flow response dependency on stimulus pulse width is affected by stimulus current amplitude-a study of activation flow coupling. In Engineering in Medicine and Biology Society (EMBC), 2015 37th Annual International Conference of the IEEE (pp. 5888-5891).

12. Li, Y., Li, Y., Omire-Mayor, D., Bo, B., **Li, H.**, et al. (2018, July). Cortical functional reorganization in response to intact forelimb stimulation from acute to chronic stage in rodent amputation model. In Engineering in Medicine and Biology Society (EMBC), 2018 40th Annual International Conference of the IEEE (Under review).

Patents

13. Tong, S., **Li, H.** et al. Animal operation and experiment table. Patent. ZL 201210272208.X. Granted on 01/07/2015

14. Tong, S., Lu, H., Li, Y., **Li, H.**, et al. Miniature stroke induction system for free-moving animals. Patent. ZL 2015204145584. Granted on 04/22/2015

15. **Li, H.**, Sun, J., Tong, S. Multi-modal animal cerebral blood flow monitoring device and method. ZL 2017110091975. Filed on 02/16/2018

16. Yang, J., Sun, J., Tong, S., Wang, J., Tang, Y., **Li, H.** A system for human transcranial ultrasound stimulation synchronized with EEG recording. ZL 2017105481711. Filed on 11/21/2017

17. Zhang, D., Sun, J., **Li, H.,** Tong, S. Device and method to increase the expression of neurotrophic factor using transcranial ultrasound stimulation. ZL 2017109868511. Filed on 12/26/2017

18. Tong, S., Wen, X., **Li, H.** Laser speckle blood flow imaging device. Utility model patent. ZL 201310473522.9 Granted on 11/18/2015